Domain Decomposition Methods for Problems in $\boldsymbol{H}(\mathbf{curl})$

by

Juan Gabriel Calvo

A dissertation submitted in partial fulfillment

of the requirements for the degree of

Doctor of Philosophy

Department of Mathematics

New York University

September 2015

Professor Olof B. Widlund

Dedication

To my family.

Acknowledgements

First, my deepest gratitude goes to my advisor Olof Widlund. I thank him profoundly for his direction, guidance, support and advice during four years.

I would also like to thank the rest of my committee: Professors Berger, Goodman, O'Neil and Stadler. In addition, I also thank Dr. Clark Dohrmann of the SANDIA-Albuquerque laboratories for his help and comments throughout my research.

Finally I thank my Alma Mater, Universidad de Costa Rica, for the support during my academic education at NYU.

Abstract

Two domain decomposition methods for solving vector field problems posed in $H(\text{curl})$ and discretized with Nédélec finite elements are considered. These finite elements are conforming in $H(\text{curl})$.

A two-level overlapping Schwarz algorithm in two dimensions is analyzed, where the subdomains are only assumed to be uniform in the sense of Peter Jones. The coarse space is based on energy minimization and its dimension equals the number of interior subdomain edges. Local direct solvers are based on the overlapping subdomains. The bound for the condition number depends only on a few geometric parameters of the decomposition. This bound is independent of jumps in the coefficients across the interface between the subdomains for most of the different cases considered.

A bound is also obtained for the condition number of a balancing domain decomposition by constraints (BDDC) algorithm in two dimensions, with Jones subdomains. For the primal variable space, a continuity constraint for the tangential average over each interior subdomain edge is imposed. For the averaging operator, a new technique named deluxe scaling is used. The optimal bound is independent of jumps in the coefficients across the interface between the subdomains.

Furthermore, a new coarse function for problems in three dimensions is introduced, with only one degree of freedom per subdomain edge. In all the cases, it is established that the algorithms are scalable. Numerical results that verify the results are provided, including some with subdomains with fractal edges and others obtained by a mesh partitioner.

Contents

List of Figures

List of Tables

Chapter 1

Introduction

1.1 An overview

We are interested in solving linear systems that arise from the discretizations of Partial Differential Equations (PDEs). There are different means to obtain an approximate solution for a PDE numerically, such as finite elements and finite differences, which end up with large and ill-conditioned linear systems of algebraic equations.

Solving these linear systems is often a hard problem: direct methods require much time and memory, and many iterative methods will converge slowly, because of the large condition numbers of the matrices; see Section 1.2. The main goal in this dissertation will be to construct preconditioners for such linear systems.

Domain decomposition refers to the process of subdividing the solution of a large linear system into smaller problems whose solutions can be used to produce a good and scalable preconditioner for the system of equations that results from discretizing the PDE on the entire domain. They are typically used as precondi-

tioners for Krylov space iterative methods, such as the Conjugate Gradient (CG) method or the Generalized Minimal Residual (GMRES) method.

These algorithms typically involve the solution of a global coarse problem (of modest dimension) and many local subproblems. The coarse problem prevents the condition number of the preconditioned system to grow as the number of subdomains increases. These resulting problems usually can be handled with exact solvers, due to their smaller size, but inexact solvers can also be used. Geometrically, a coarse grid is often used to define the coarse problem, and the original domain is often divided into subdomains to obtain local subproblems related to these subdomains.

The problems on the subdomains are independent, which makes domain decomposition methods suitable for parallel computing. These algorithms can also be used for complicated geometries. Thus, the fundamental idea of domain decomposition methods is to reduce the solution of a problem to the solution of problems of a similar form on parts of the domain and an easier lower-dimensional problem on the entire domain.

There exist two main families of domain decomposition methods: overlapping Schwarz methods (with overlapping subdomains) and iterative substructuring methods (with non-overlapping subdomains).

The earliest known domain decomposition method was proposed by Hermann A. Schwarz in 1870 as a theoretical device to deduce the existence and uniqueness of the boundary value problem for Poisson's equation in the union of two overlapping subdomains, given that existence of the solution was known for the subdomains. This method is known as the classical alternating Schwarz method; see e.g., [60] and [13, Chapter 2.7.2]. These methods have been widely extended to different

problems.

With a different approach, iterative substructuring methods reduce the linear system to a Schur complement system, by eliminating the interior unknowns of the subdomains. Then, a preconditioner is build for this new system. Two main classes of iterative substructuring methods are the Balancing Neumann Neumann (BNN) type and the Finite Element Tearing and Interconnecting (FETI) type algorithms; see [22, 24] respectively. There are many variants, e.g., Dual-Primal Finite Element Tearing and Interconnecting (FETI-DP) [23], and Balancing Domain Decomposition by Constraints (BDDC). The latter was introduced by Clark Dohrmann in [15], and is currently very important. Other methods, such as multigrid and multilevel methods, have also been considered for these problems; see e.g. [32, 1, 33].

In this dissertation, we will mainly consider two-level overlapping Schwarz methods and BDDC methods for solving vector-valued problems posed in $H(\text{curl})$ and discretized with Nédélec finite elements, which are conforming in $H(\text{curl})$ and were considered first by Jean-Claude Nédélec in [52]. The results from Chapters 6 and 7 have already appeared as technical reports [9, 10] and have been submitted for publication.

We will use John and Jones subdomains in two dimensions, in order to obtain a theory that applies to quite general types of subdomains; see Chapter 4. We will also allow discontinuities across the interface in our analysis.

1.2 Iterative methods for solving linear systems

As already noted, there are two different approaches to solve linear systems: direct methods, where a factorization of the matrix is fully obtained, and iterative methods, where an approximation for the solution is obtained after a number of iterations. Direct methods include LU decomposition (Gauss Elimination), QR factorization, and Cholesky factorization (for symmetric positive definite matrices), among others. For these algorithms, execution time and storage can impose serious constraints.

Of particular importance is the nested dissection algorithm, originally proposed by Alan George in [26], which provides a more efficient algorithm by finding an elimination ordering, based on a divide and conquer strategy. If applied to a $k \times k$ two-dimensional mesh, nested dissection leads to an asymptotically optimal ordering, requiring $\mathcal{O}(n^{3/2})$ floating-point operations and $\mathcal{O}(n \log n)$ storage (non-zero entries in the Cholesky factorization), where $n = k^2$ is the dimension of the matrix. For a $k \times k$ mesh in 3D, the work is $\mathcal{O}(n^2)$ and the storage $\mathcal{O}(n^{4/3})$, with $n = k^3$; see e.g., [14]. For additional pioneering work, see [46, 28, 27].

Two of the best known iterative methods are the Generalized Minimal Residual method (GMRES, [59]) and for symmetric matrices the Conjugate Gradient method (CG, [31]). Both belong to the Krylov space methods. In this thesis, we almost always will use CG, since most of the matrices considered are symmetric and positive definite, but GMRES will be used for certain non-symmetric problems, when hybrid and multiplicative Schwarz operators are considered.

The rate of convergence of the CG method is determined by the condition number of the linear system. Hence, we can approximate the solution in a few iterations if the problem is very well-conditioned. If the arithmetic is exact, after

n iterations we obtain the exact solution but given that n is very large, the goal is to obtain an accurate solution with just a few iterations. We present the basic algorithm and a lemma for CG; see, e.g., [68, Chapter 38]. For a description of the GMRES method, we refer to [59, 68].

Data: A, b, tolerance ϵ, initial guess u^0

Result: Approximation for the solution of $Au = b$

Initialize $r^0 = b - Au^0$;

while $\|r^k\| > \epsilon$ **do**

$\beta^k = (r^{k-1}, r^{k-1})/(r^{k-2}, r^{k-2})$ $(\beta^1 = 0)$;

$p^k = r^{k-1} + \beta^k p^{k-1}$;

$\alpha^k = (r^{k-1}, r^{k-1})/(p^k, Ap^k)$;

$u^k = u^{k-1} + \alpha^k p^k$;

$r^k = r^{k-1} - \alpha^k Ap^k$;

end

Algorithm 1: Conjugate Gradient

Lemma 1.2.1. *Let A be symmetric positive definite. Then, the iterate u^k of the Conjugate Gradient method minimizes $\|u^k - u\|_A$ over the space*

$$u^0 + \text{ span}\{r^0, Ar^0, \ldots, A^{k-1}r^0\},$$

where u is the solution of $Au = b$, $r^0 = b - A^0u^0$ and $\|u\|_A := u^TAu$. We have the error bound

$$\frac{\|e^k\|_A}{\|e^0\|_A} \leq 2\left(\frac{\sqrt{\kappa_2(A)} - 1}{\sqrt{\kappa_2(A)} + 1}\right)^k.$$

Proof. See [68, Th. 38.5]. □

Lemma 1.2.1 suggests that if the condition number of the matrix is large, the

convergence can be slow. We therefore will build a preconditioner and modify the previous algorithm, and use the Preconditioned Conjugate Gradient (PCG). Given a symmetric, positive definite matrix M, we consider the modified linear system

$$M^{-1/2}AM^{-1/2}v = M^{-1/2}b,\ v = M^{1/2}u.$$

We note that $M^{-1/2}AM^{-1/2}$ is symmetric and positive definite, and reduces to the identity in case $M = A$. We consider M a preconditioner and apply Algorithm 1 to this modified system to obtain the PCG; see Algorithm 2, were we have returned to the original variables.

Data: A, b, tolerance ϵ, initial guess u^0

Result: Approximation for the solution of $Au = b$

Initialize $r^0 = b - Au^0$;

while $\|r^k\| > \epsilon$ **do**

Precondition: $z^{k-1} = M^{-1}r^{k-1}$;

$\beta^k = (z^{k-1}, r^{k-1})/(z^{k-2}, r^{k-2})$ $(\beta^1 = 0)$;

$p^k = z^{k-1} + \beta^k p^{k-1}$;

$\alpha^k = (z^{k-1}, r^{k-1})/(p^k, Ap^k)$;

$u^k = u^{k-1} + \alpha^k p^k$;

$r^k = r^{k-1} - \alpha^k Ap^k$;

end

Algorithm 2: Preconditioned Conjugate Gradient

In this case, the rate of convergence depends on the condition number of $M^{-1}A$. We also note that the algorithm additionally only involves the application of M^{-1}. We will focus on the construction of preconditioners, such that $\kappa_2(M^{-1}A)$ is small. This allows us to obtain a good approximation for the solution of the linear system

in a few iterations.

It is usually hard to obtain exact spectral information on a matrix. However, we can obtain approximate information on the eigenvalues by using a tridiagonal matrix that can be derived from the coefficients of the conjugate gradient algorithm. This information then can be used to estimate the condition number. Thus, we construct a tridiagonal matrix $J^{(m)}$ as follows:

$$J^{(m)} := \begin{pmatrix} \frac{1}{\alpha_0} & \frac{\sqrt{\beta_0}}{\alpha_0} & & & \\ \frac{\sqrt{\beta_0}}{\alpha_0} & \frac{1}{\alpha_1} + \frac{\beta_0}{\alpha_0} & \frac{\sqrt{\beta_1}}{\alpha_1} & & \\ & \frac{\sqrt{\beta_1}}{\alpha_1} & \ddots & \ddots & \\ & & \ddots & \ddots & \frac{\sqrt{\beta_{m-2}}}{\alpha_{m-2}} \\ & & & \frac{\sqrt{\beta_{m-2}}}{\alpha_{m-2}} & \frac{1}{\alpha_{m-1}} + \frac{\beta_{m-2}}{\alpha_{m-2}} \end{pmatrix}.$$

By considering the spectral information of $J^{(m)}$, we can estimate the eigenvalues of the preconditioned system. We note that extreme eigenvalues of $J^{(m)}$ converge rapidly after a few iterations. For more details, see [55, Section 4.4] and [58, Section 6.7].

1.3 Organization of the dissertation

This thesis is organized as follows. In Chapter 2, we introduce the required Sobolev and finite element spaces. In Chapter 3, we describe the model problem that we will discuss throughout this thesis. For two dimensional problems we will consider Jones subdomains, for which some new tools have been developed and are included in Chapter 4. A background on Domain Decomposition methods is given in Chapter 5. In Chapters 6 and 7, an overlapping Schwarz algorithm

and a BDDC deluxe method are described for problems in two dimensions and irregular subdomains, respectively. Finally, in Chapter 8, we introduce a new coarse function for 3D problems and provide some numerical results for a two-level overlapping Schwarz algorithm.

Chapter 2

Finite Element spaces

In this chapter, we introduce the Sobolev spaces and the finite element spaces that we will use throughout our thesis. The finite element methods are based on a variational formulation of elliptic PDEs. This variational problem has a solution in certain function spaces called Sobolev spaces. By introducing a finite-dimensional subspace, we discretize the equation and obtain a linear system of equations. By solving this system, we obtain an approximate solution for the PDE.

In this study, a suitable choice for these finite element spaces are the usual nodal Lagrange elements and the edge Nédélec elements, that will be introduced in Sections 2.3 and 2.4. We refer to [5, 6] for general introductions to these topics.

2.1 Sobolev spaces

We consider the Sobolev space $H(\mathrm{grad}, \Omega)$, denoted also by $H^1(\Omega)$, as the subspace of $L^2(\Omega)$ with a gradient with finite L^2-norm, and with a scaled norm

$$\|u\|^2_{H^1(\Omega)} := |u|^2_{H^1(\Omega)} + \frac{1}{H^2}\|u\|^2_{L^2(\Omega)},$$

where $H := \mathrm{diam}(\Omega)$, and the seminorm $|\cdot|_{H^1(\Omega)}$ is defined by

$$|u|^2_{H^1(\Omega)} := \int_\Omega |\nabla u|^2 \, d\boldsymbol{x}.$$

We also consider the space $H(\mathrm{curl}, \Omega)$, the subspace of $(L^2(\Omega))^d$, $d = 2$ or 3, with a finite L^2-norm of its curl. This is a Hilbert space with the scalar product and graph norm defined by

$$(\boldsymbol{u}, \boldsymbol{v})_{H(\mathrm{curl},\Omega)} := \int_\Omega \boldsymbol{u} \cdot \boldsymbol{v} \, d\boldsymbol{x} + \int_\Omega \nabla \times \boldsymbol{u} \cdot \nabla \times \boldsymbol{v} \, d\boldsymbol{x}, \ \|\boldsymbol{u}\|^2_{H(\mathrm{curl},\Omega)} := (\boldsymbol{u}, \boldsymbol{u})_{H(\mathrm{curl},\Omega)}.$$

For two dimensions, given a scalar function p and a vector $\boldsymbol{u}$, the vector and scalar curl operators are defined, respectively, by

$$\boldsymbol{\nabla} \times p := \left(\frac{\partial p}{\partial x_2}, -\frac{\partial p}{\partial x_1} \right)^T,$$

and

$$\nabla \times \boldsymbol{u} := \frac{\partial u_2}{\partial x_1} - \frac{\partial u_1}{\partial x_2}.$$

We define the unit tangent vector $\boldsymbol{t}$ on the boundary of Ω by

$$\boldsymbol{t} := (-n_2, n_1)^T,$$

where $\boldsymbol{n} = (n_1, n_2)^T$ is the unit outer normal vector. For a generic vector $\boldsymbol{u}$, its tangential component on the boundary is $\boldsymbol{u} \cdot \boldsymbol{t} = |\boldsymbol{n} \times \boldsymbol{u}|$.

In three dimensions, given a vector $\boldsymbol{u}$, the curl operator is defined by

$$\nabla \times \boldsymbol{u} := \left(\frac{\partial u_3}{\partial x_2} - \frac{\partial u_2}{\partial x_3}, \frac{\partial u_1}{\partial x_3} - \frac{\partial u_3}{\partial x_1}, \frac{\partial u_2}{\partial x_1} - \frac{\partial u_1}{\partial x_2} \right)^T.$$

The tangential component of a vector $\boldsymbol{u}$ on the boundary of Ω is defined by

$$\boldsymbol{u}_t := \boldsymbol{u} - (\boldsymbol{u} \cdot \boldsymbol{n})\boldsymbol{n} = (\boldsymbol{n} \times \boldsymbol{u}) \times \boldsymbol{n}.$$

Since $|\boldsymbol{u}_t| = |\boldsymbol{n} \times \boldsymbol{u}|$, the vector $\boldsymbol{u}$ has a vanishing tangential component if and only if $\boldsymbol{n} \times \boldsymbol{u} = 0$. With an abuse of notation, we will refer to $\boldsymbol{n} \times \boldsymbol{u}$ as the tangential component of $\boldsymbol{u}$.

2.2 Triangulations

We will define finite element spaces over a triangulation of our domain in the following sections. Given a domain Ω, we will use a triangulation $\mathcal{T}_h$, which is a subdivision of Ω consisting of elements (triangles in 2D or tetrahedra in 3D). We denote by K a generic (closed) element of the triangulation and by h_K its diameter. The following properties should hold:

1. $\overline{\Omega} = \bigcup K_i$
2. If $K_i \cap K_j$ $(i \neq j)$ consists of one point, then it is a common vertex of K_i and K_j.
3. If $K_i \cap K_j$ $(i \neq j)$ consists of more than one point, then $K_i \cap K_j$ is a common edge or face of K_i and K_j.

A family of partitions $\{\mathcal{T}_h\}$ is called shape regular provided that there exists a constant $C > 0$ such that every $K \in \mathcal{T}_h$ contains a circular disk or a spherical ball of radius ρ_K with $\rho_K \geq h_K/C$.

Finally, a family of partitions $\{\mathcal{T}_h\}$ is called uniform provided that there exits a constant $C > 0$ such that every $K \in \mathcal{T}_h$ contains a circular disk or a spherical ball of radius ρ_K with $\rho_K \geq h/C$, where $h := \max_K h_K$.

2.3 Nodal finite elements

We consider the finite element spaces

$$W^h_{\text{grad}}(\Omega) := \{p \in C^0(\Omega) : p_{|K} \in \mathbb{P}_k(K)\},$$

where $\mathbb{P}_k(K)$ is the space of polynomials of degree k defined on a triangle or tetrahedron K. This is a conforming space, i.e., $W^h_{\text{grad}}(\Omega) \subset H^1(\Omega)$.

For a fixed polynomial degree k, the set of Lagrangian basis functions $\{\phi^h_i\}$ associated to a set of nodes $\{P_i\}$ of the triangulation can be introduced. The basis functions are uniquely defined by $\phi^h_i(P_j) = \delta_{ij}$, and $p(x) = \sum_i p(P_i)\phi^h_i(x)$, for $p \in W^h_{\text{grad}}(\Omega)$.

We will use linear polynomials defined over each element. The three degrees of freedom for each triangle are the values of the function at each vertex. A nodal function associated to a vertex in 2D is depicted in Figure 2.1.

The nodal finite element interpolant of a sufficiently smooth $p \in H(\text{grad}, \Omega)$ is defined as

$$I^h(p) := \sum_{\boldsymbol{v} \in \mathcal{N}^h} p(\boldsymbol{v})\phi_{\boldsymbol{v}}, \tag{2.3.1}$$

where $\mathcal{N}^h$ is the set of nodes of $\mathcal{T}_h$, $\phi_{\boldsymbol{v}} \in W^h_{\text{grad}}(\Omega)$ is the shape function for node $\boldsymbol{v}$, and $p(\boldsymbol{v})$ is the value of p at node $\boldsymbol{v}$. We will need the following auxiliary result:

Lemma 2.3.1. *Let p be a continuous piecewise quadratic function defined on $\mathcal{T}_h$*

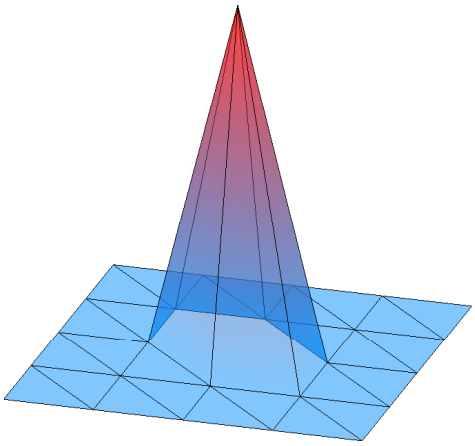

Figure 2.1: Nodal basis function for nodal elements.

and let $I^h p$ be its piecewise linear interpolant defined by (2.3.1) *on the same mesh. Then, there exists a constant C, depending only on the aspect ratio of K, such that*

$$\left|I^h p\right|_{H^1(K)} \leq C \left|p\right|_{H^1(K)} \text{ for } K \in \mathcal{T}_h.$$

Proof. See [66, Lemma 3.9]. □

2.4 Nédeléc finite elements

Nédélec elements are finite elements that are conforming in $H(\text{curl})$. Associated with the triangulation $\mathcal{T}_h$, we will consider the space $W^h_{\text{curl}}(\Omega) \subset H(\text{curl}, \Omega)$, based on linear triangular or tetrahedral Nédélec edge elements in Ω with zero tangential component on $\partial\Omega$; see [52].

2.4.1 Nédélec elements in two dimensions

In two dimensions with triangular elements, the restrictions to an element K are defined by

$$\mathcal{R}_k(K) := \{\boldsymbol{u} + \boldsymbol{v} : \boldsymbol{u} \in \mathbb{P}_{k-1}(K)^2, \boldsymbol{v} \in \tilde{\mathbb{P}}_k(K)^2, \boldsymbol{v} \cdot \boldsymbol{x} = 0\}, k \geq 1,$$

where $\mathbb{P}_{k-1}(K)$ is the space of polynomials of degree $k-1$ on K, $\tilde{\mathbb{P}}_k(K)$ is the space of homogeneous polynomials of degree k on K, and a function $\boldsymbol{u}(\boldsymbol{x}) \in \mathcal{R}_k(K)$ is uniquely defined by the following degrees of freedom:

$$\int_e \boldsymbol{u} \cdot \boldsymbol{t}_e \; p \; ds, \; p \in \mathbb{P}_{k-1}(e),$$

for each edge $e \in \partial K$, and, in addition, for $k > 1$,

$$\int_K \boldsymbol{u} \cdot \boldsymbol{p} \; d\boldsymbol{x}, \; \boldsymbol{p} \in \mathbb{P}_{k-2}(K)^2.$$

Here $\boldsymbol{t}_e$ is a unit vector in the direction of e.

Those of lowest order are defined by

$$W^h_{\text{curl}}(\Omega) := \{\boldsymbol{u} : \boldsymbol{u}_{|K} \in \mathcal{N}_1(K), K \in \mathcal{T}_h \text{ and } \boldsymbol{u} \in H(\text{curl}, \Omega)\},$$

where any function in $\mathcal{N}_1(K)$ has the form

$$\boldsymbol{u}(x_1, x_2) = (a_1 + bx_2, a_2 - bx_1)^T,$$

with $a_1, a_2, b \in \mathbb{R}$. The degrees of freedom for an element $K \in \mathcal{T}_h$ are given by the

average values of the tangential component over the edges of the elements, i.e.,

$$\lambda_e(\boldsymbol{u}) := \frac{1}{|e|}\int_e \boldsymbol{u}\cdot\boldsymbol{t}_e\, ds, \tag{2.4.1}$$

with $e \in \partial K$. We recall that a function in $W^h_{\text{curl}}(\Omega)$ has a continuous tangential component across all the fine edges; see e.g., [52]. A Nédélec function associated to an edge in 2D is depicted in Figure 2.2.

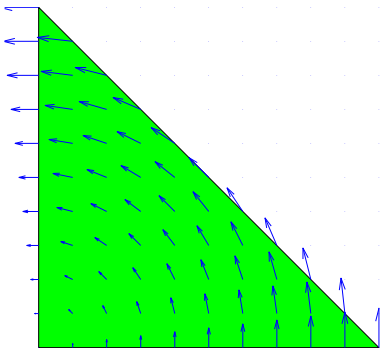

Figure 2.2: Nédélec basis function for edge elements.

2.4.2 Nédélec elements in three dimensions

For triangulations into tetrahedra, the local spaces on a generic tetrahedron K are defined as

$$\mathcal{R}_k(K) := \{\boldsymbol{u}+\boldsymbol{v} : \boldsymbol{u} \in \mathbb{P}_{k-1}(K)^3, \boldsymbol{v} \in \tilde{\mathbb{P}}_k(K)^3, \boldsymbol{v}\cdot\boldsymbol{x} = 0\}, k \geq 1.$$

A vector $\boldsymbol{u} \in \mathcal{R}_k(K)$ is uniquely defined by the following degrees of freedom:

First, for the six edges e of K,

$$\int_e \boldsymbol{u} \cdot \boldsymbol{t}_e \; p \; ds, \;\; p \in \mathbb{P}_{k-1}(e),$$

for $k > 1$ and the four faces f of K,

$$\int_f (\boldsymbol{u} \times \boldsymbol{n}) \cdot \boldsymbol{p} \; dS, \;\; \boldsymbol{p} \in \mathbb{P}_{k-2}(f)^3,$$

and, additionally for $k > 2$,

$$\int_K \boldsymbol{u} \cdot \boldsymbol{p} \; d\boldsymbol{x}, \;\; \boldsymbol{p} \in \mathbb{P}_{k-3}(K)^3.$$

In the case $k = 1$, the elements of the local space $\mathcal{R}_1(K)$ have the simple form

$$\mathcal{R}_1(K) = \{\boldsymbol{u} = \boldsymbol{a} + \boldsymbol{b} \times \boldsymbol{x}, \boldsymbol{a}, \boldsymbol{b} \in \mathbb{P}_0(K)^3\}.$$

It is immediate to see that the tangential components of a vector in $\mathcal{R}_1(K)$ are constant on the six edges e of K. These values, $\lambda_e(\boldsymbol{u})$, can be taken as the degrees of freedom, as in the two-dimensional case.

We will work with the lowest order Nédélec elements in two and three dimensions. Let $\boldsymbol{N}_e \in W^h_{\text{curl}}(\Omega)$ denote the finite element shape function for an edge e of the finite element mesh $\mathcal{T}_h$. We assume that $\boldsymbol{N}_e$ is scaled such that $\boldsymbol{N}_e \cdot \boldsymbol{t}_e = 1$ along e and $\boldsymbol{N}_{e'} \cdot \boldsymbol{t}_e = 0$ for $e \neq e'$. The edge finite element interpolant of a sufficiently smooth vector function $\boldsymbol{u} \in H(\text{curl}, \Omega)$ is then defined as

$$\Pi^h(\boldsymbol{u}) := \sum_{e \in \mathcal{M}^h} u_e \boldsymbol{N}_e, \;\; u_e := \frac{1}{|e|} \int_e \boldsymbol{u} \cdot \boldsymbol{t}_e ds,$$

where $\mathcal{M}^h$ is the set of element edges of $\overline{\Omega}$ and $|e|$ is the length of e. We will also need the following auxiliary result:

Lemma 2.4.1. *Let $\boldsymbol{u} \in W^h_{\text{curl}}(\Omega)$, and let θ be a continuous, piecewise linear, scalar function on Ω. Then, there exists a constant C, depending only on the aspect ratio of K, such that for $K \in \mathcal{T}_h$,*

$$\left\|\Pi^h(\theta \boldsymbol{u})\right\|_{L^2(K)} \leq C \left\|\theta \boldsymbol{u}\right\|_{L^2(K)},$$

$$\left\|\nabla \times \left(\Pi^h(\theta \boldsymbol{u})\right)\right\|_{L^2(K)} \leq C \left\|\nabla \times (\theta \boldsymbol{u})\right\|_{L^2(K)},$$

Proof. See [66, Lemma 10.8]. □

2.5 An inverse inequality

We present an inverse inequality for elements in the space $W^h_{\text{curl}}(\Omega)$ which will be used in our discussion. First, we have the following elementary estimates for a function in $W^h_{\text{curl}}(\Omega)$ in terms of its degrees of freedom defined in (2.4.1).

Lemma 2.5.1. *Let $K \in \mathcal{T}_h$. Then, there exist positive constants c and C, depending only on the aspect ratio of K, such that for all $\boldsymbol{u} \in W^h_{\text{curl}}(\Omega)$, $\Omega \subset \mathbb{R}^d$,*

$$c \sum_{e \in \partial K} h_e^d \lambda_e^2(\boldsymbol{u}) \leq \|\boldsymbol{u}\|^2_{L^2(K)} \leq C \sum_{e \in \partial K} h_e^d \lambda_e^2(\boldsymbol{u}), \text{ and}$$

$$\|\nabla \times \boldsymbol{u}\|^2_{L^2(K)} \leq C \sum_{e \in \partial K} h_e^{d-2} \lambda_e^2(\boldsymbol{u}).$$

Proof. See [57, Proposition 6.3.1] or [67, Lemma 3.1] for the elementary proofs. □

Combining these two inequalities, we find an inverse inequality:

Corollary 2.5.2 (Inverse inequality)**.** *For $\boldsymbol{u} \in W^h_{\mathrm{curl}}(\Omega)$, there exists a constant C that depends only on the aspect ratio of K, such that*

$$\|\nabla \times \boldsymbol{u}\|^2_{L^2(K)} \leq C h_K^{-2} \|\boldsymbol{u}\|^2_{L^2(K)}. \tag{2.5.1}$$

2.6 A discrete Helmholtz decomposition

The following lemma will allow us to obtain a stable decomposition for functions in $W^h_{\mathrm{curl}}(\Omega)$. The HX-preconditioner, due to Hiptmair and Xu, is based on the following decomposition, see [34, 71].

Lemma 2.6.1. *Given Ω homotopy equivalent to a ball, and $\boldsymbol{u} \in W^h_{\mathrm{curl}}(\Omega)$, there exist $\boldsymbol{q} \in W^h_{\mathrm{curl}}(\Omega)$, $\boldsymbol{\Psi} \in \left(W^h_{\mathrm{grad}}(\Omega)\right)^d$, $p \in W^h_{\mathrm{grad}}(\Omega)$, and a constant C, such that*

$$\boldsymbol{u} = \boldsymbol{q} + \Pi^h(\boldsymbol{\Psi}) + \nabla p, \tag{2.6.1}$$

where

$$\|\nabla p\|^2_{L^2(\Omega)} \leq C \left(\|\boldsymbol{u}\|^2_{L^2(\Omega)} + H^2 \|\nabla \times \boldsymbol{u}\|^2_{L^2(\Omega)} \right), \tag{2.6.2a}$$

$$\|h^{-1}\boldsymbol{q}\|^2_{L^2(\Omega)} + \|\boldsymbol{\Psi}\|^2_{H^1(\Omega)} \leq C \|\nabla \times \boldsymbol{u}\|^2_{L^2(\Omega)}. \tag{2.6.2b}$$

The constant C depends on Ω and the shape regularity of the mesh.

Proof. See [34, Lemma 5.1]. □

If the domain Ω is convex, we can improve the bounds given in (2.6.2a) and (2.6.2b):

Lemma 2.6.2. *If the domain Ω is convex, the splitting* (2.6.1) *from Lemma 2.6.1*

can be chosen such that, in addition to the estimates of Lemma 2.6.1, we have

$$\|\nabla p\|^2_{L^2(\Omega)} \leq C\|\boldsymbol{u}\|^2_{L^2(\Omega)}, \quad \|\boldsymbol{\Psi}\|^2_{L^2(\Omega)} \leq C\|\boldsymbol{u}\|^2_{L^2(\Omega)},$$

with C a constant depending on the quasi-uniformity of the mesh.

Proof. See [34, Lemma 5.2]. □

We have also the following decomposition for John domains in two dimensions; see Section 4 for the definition of John domains.

Lemma 2.6.3. *Given a John domain $D \subset \mathbb{R}^2$ of diameter H and $\boldsymbol{u} \in W^h_{\mathrm{curl}}(D)$, there exist $p \in W^h_{\mathrm{grad}}(D)$, $\boldsymbol{r} \in W^h_{\mathrm{curl}}(D)$ and a constant C such that*

$$\boldsymbol{u} = \nabla p + \boldsymbol{r},$$

$$\|\nabla p\|^2_{L^2(D)} \leq C\left(\|\boldsymbol{u}\|^2_{L^2(D)} + H^2\|\nabla \times \boldsymbol{u}\|^2_{L^2(D)}\right), \text{ and} \tag{2.6.3a}$$

$$\|\boldsymbol{r}\|^2_{L^\infty(D)} \leq C\left(1 + \log\frac{H}{h}\right)\|\nabla \times \boldsymbol{u}\|^2_{L^2(D)}. \tag{2.6.3b}$$

The constant C depends on D and the shape regularity of the mesh.

Proof. See [19, Lemma 3.14]. □

Chapter 3

A model problem

3.1 Introduction

The space $H(\mathrm{curl})$ is used for electromagnetism and some formulations of Navier-Stokes equations. We will consider a model problem that arises, for example, from implicit time integration or the eddy current model of Maxwell's equation; see, e.g., [4, Chapter 8]. It is also considered in [2, 29, 30, 32, 34, 62, 67].

When time-dependent equations are considered, the electric field $\boldsymbol{u}$ satisfies the equation

$$\nabla \times \left(\mu^{-1}\nabla \times \boldsymbol{u}\right) + \epsilon\frac{\partial^2 \boldsymbol{u}}{\partial t^2} + \sigma\frac{\partial \boldsymbol{t}}{\partial t} = -\frac{\partial \boldsymbol{J}}{\partial t}, \text{ in } \Omega \times (0,T), \tag{3.1.1}$$

where $\boldsymbol{J}(\boldsymbol{x},t)$ is the current density, and ϵ, μ, σ are positive definite tensors that, in general, describe the electromagnetic properties of the medium. For their meaning and a general discussion of Maxwell's equations, see [51, 43, 12]. A similar equation holds for the magnetic field. For a conducting medium and low-frequency fields, σ is large, and the term in (3.1.1) involving the second derivative in time can be

neglected, giving rise to a parabolic equation.

We will consider the boundary value problem in $\mathbb{R}^d$, $d = 2$ or 3, with a perfect conducting boundary, given by

$$\nabla \times (\alpha \nabla \times \boldsymbol{u}) + B\boldsymbol{u} = \boldsymbol{f} \text{ in } \Omega, \tag{3.1.2a}$$

$$\boldsymbol{u} \times \boldsymbol{n} = 0 \text{ on } \partial\Omega, \tag{3.1.2b}$$

where $\alpha(\boldsymbol{x}) \geq 0$, B is a $d \times d$ strictly positive definite symmetric matrix. This PDE is obtained from (3.1.1) by a discretization in time with an implicit finite difference time scheme, and (3.1.2) has to be solved at each time step. We could equally well consider cases where the boundary condition (3.1.2b) is imposed only on one or several subdomain edges or faces which form part of $\partial\Omega$, with a natural boundary condition over the rest of the boundary.

3.2 Weak form and discretization

In order to formulate an appropriate weak form for problem (3.1.2), we will use the Hilbert space $H(\text{curl}, \Omega)$, see Section 2.1. By integration by parts, we then obtain a weak formulation: Find $\boldsymbol{u} \in H_0(\text{curl}, \Omega)$ such that

$$a(\boldsymbol{u}, \boldsymbol{v}) = (\boldsymbol{f}, \boldsymbol{v}) \qquad \forall\ \boldsymbol{v} \in H_0(\text{curl}, \Omega), \tag{3.2.1}$$

with

$$a(\boldsymbol{u}, \boldsymbol{v}) := \int_\Omega \left[\alpha(\nabla \times \boldsymbol{u}) \cdot (\nabla \times \boldsymbol{v}) + B\boldsymbol{u} \cdot \boldsymbol{v}\right]\ d\boldsymbol{x}, \qquad (\boldsymbol{f}, \boldsymbol{v}) := \int_\Omega \boldsymbol{f} \cdot \boldsymbol{v}\ d\boldsymbol{x}. \tag{3.2.2}$$

Here, $H_0(\mathrm{curl}, \Omega)$ is the subspace of $H(\mathrm{curl}, \Omega)$ with a vanishing tangential component on $\partial\Omega$.

In order to discretize equation (3.2.1), we introduce a triangulation $\mathcal{T}_h$ as in Section 2.2. By considering the basis $\{\boldsymbol{N}_{e_i}\}_{i=1}^n$ for the finite-dimensional space $W^h_{\mathrm{curl}}(\Omega)$ described in Section 2.4, we obtain the problem: Find $\boldsymbol{u}_h \in W^h_{\mathrm{curl}}(\Omega)$ such that

$$a(\boldsymbol{u}_h, \boldsymbol{v}_h) = (\boldsymbol{f}, \boldsymbol{v}_h) \qquad \forall\ \boldsymbol{v}_h \in W^h_{\mathrm{curl}}(\Omega),$$

and the associated sparse, symmetric linear system

$$A\boldsymbol{u} = \boldsymbol{g},$$

where $A_{i,j} = a(\boldsymbol{N}_{e_j}, \boldsymbol{N}_{e_i})$, $\boldsymbol{g}_i = (\boldsymbol{f}, \boldsymbol{N}_{e_i})$, and $\boldsymbol{u}$ is the vector of coordinates of $\boldsymbol{u}_h$ with respect to the basis $\{\boldsymbol{N}_{e_i}\}_{i=1}^n$. We are interested in building preconditioners for this ill-conditioned system of equations, given that the condition number of the matrix A satisfies $\kappa(A) = \mathcal{O}(h^{-2})$.

3.3 Notation

We next introduce some notation that we will use throughout our thesis. We will decompose the domain Ω into N non-overlapping subdomains $\{\Omega_i\}_{i=1}^N$, each of which is the union of elements of the triangulation $\mathcal{T}_h$ of Ω. Each Ω_i will be simply connected and will have a connected boundary $\partial\Omega_i$. We denote by H_i the diameter of Ω_i, by h_i the smallest element diameter of the shape-regular triangulation $\mathcal{T}_{h_i}$ of Ω_i, and by H/h the maximum of the ratios H_i/h_i.

In the case that we consider overlapping subdomains, we will construct Ω_i' by

adding layers of fine elements to Ω_i, and will denote by δ_i the minimal distance from $\partial\Omega_j' \cap \Omega_i$ to $\overline{\Omega}_i \cap \overline{\Omega}_j$, for all indices $j \neq i$ such that $\Omega_i \cap \Omega_j' \neq \varnothing$. The maximum of the ratios H_i/δ_i and δ_i/h_i are denoted by H/δ and δ/h.

The interface of the decomposition $\{\Omega_i\}_{i=1}^N$ is given by

$$\Gamma := \left(\bigcup_{i=1}^{N} \partial\Omega_i \right) \setminus \partial\Omega,$$

and the contribution to Γ from $\partial\Omega_i$ by $\Gamma_i := \partial\Omega_i \setminus \partial\Omega$. These sets are unions of subdomain faces, edges and vertices in 3D, and subdomain edges and vertices in 2D. We recall that there are no degrees of freedom associated with the subdomain vertices, and that the interface does not include edges and faces that lie on the boundary of Ω. We will denote by $\mathcal{M}_G$ the set of finite element edges on G, and by $\mathcal{N}_G$ the set of nodes on G.

In our analysis, we will replace B by βI, and assume that α, β are constants α_i, β_i in each subdomain Ω_i. We denote by $a_i(\boldsymbol{u}, \boldsymbol{v})$ the bilinear form $a(\cdot, \cdot)$ defined in (3.2.2) restricted to Ω_i, and by $E_D(\boldsymbol{v})$ the energy of $\boldsymbol{v}$ over a set D, i.e.

$$E_D(\boldsymbol{v}) := \int_D \alpha |\nabla \times \boldsymbol{v}|^2 + \beta |\boldsymbol{v}|^2 \, d\boldsymbol{x}.$$

We can also rewrite the bilinear form (3.2.2) as

$$a(\boldsymbol{u}, \boldsymbol{v}) = \sum_{i=1}^{N} \alpha_i \int_{\Omega_i} (\nabla \times \boldsymbol{u}) \cdot (\nabla \times \boldsymbol{v}) \, d\boldsymbol{x} + \beta_i \int_{\Omega_i} \boldsymbol{u} \cdot \boldsymbol{v} \, d\boldsymbol{x}.$$

For the 2D problems, we will denote the subdomain edges of Ω_i by $\mathcal{E}^{ij}$, given by the intersection of the closure of Ω_i and Ω_j, excluding the two vertices at their endpoints. We note that the intersection of the closure of two subdomains might

have several components; in such a case, each component will be regarded as an edge. We will write $\mathcal{E}$ instead of $\mathcal{E}^{ij}$ when there is no ambiguity.

The set of all subdomain edges is defined as

$$S_{\mathcal{E}} := \{\mathcal{E}^{ij} : i < j, \mathcal{E}^{ij} \neq \varnothing\}$$

and $S_{\mathcal{E}_i}$ is the subset of subdomain edges which belong to Γ_i. When there is a need to uniquely define the unit tangential vector $\boldsymbol{t}_{\mathcal{E}}$ over a subdomain edge, we will select the subdomain with the smallest index and use the counterclockwise direction over the boundary of the relevant subdomain. The unit vector in the direction from one endpoint of a subdomain edge $\mathcal{E}$ to the other (with the same sense of direction as $\boldsymbol{t}_{\mathcal{E}}$) is denoted by $\boldsymbol{d}_{\mathcal{E}}$, and the distance between the two endpoints is $d_{\mathcal{E}}$.

Finally, we will consider subdomain edges that can be quite irregular. In two dimensions we will consider a covering by disks of a subdomain edge, and we will denote by $\chi_{\mathcal{E}}(d)(d_{\mathcal{E}}/d)$ the number of closed circular disks of diameter d that are required to cover it. We note that $\chi_{\mathcal{E}}(d) = 1$ if the edge is straight and that it can be proved that for a prefractal Koch snowflake curve, which is a polygon with side length h_i and diameter H_i, $\chi_{\mathcal{E}}(h_i) \leq (H_i/h_i)^{\log(4/3)} < (H_i/h_i)^{1/8}$; see [19, Section 3.2]. This is not a large factor, being less than 10 even in the extreme case of $H_i/h_i = 10^8$.

In three dimensions, the subdomain face common to Ω_i and Ω_j will be denoted by $\mathcal{F}^{ij}$, regarded as an open set, and the subdomain edges of Ω_i by $\mathcal{E}^{ij}$. We note that the intersection of the closure of two subdomains might have several components. In such a case, each component will be regarded as a face. We will

write $\mathcal{F}$ and $\mathcal{E}$ instead of $\mathcal{F}^{ij}$ and $\mathcal{E}^{ij}$ when there is no ambiguity. The wire-basket of the decomposition is the union of the subdomain edges, and will be denote by $\mathcal{W}$. The local contribution from Ω_i to the wire-basket will be denoted by $\mathcal{W}_i$.

We will also consider unit vectors tangential to $\partial\mathcal{F}$ and $\mathcal{E}$, denoted by $\boldsymbol{t}_{\partial\mathcal{F}}$ and $\boldsymbol{t}_{\mathcal{E}}$, respectively. The union of the closed triangles that have one edge on $\partial\mathcal{F}$ will be denoted by $\mathcal{F}_b$, and we then define

$$\Delta_i := \bigcup_{\mathcal{F}\in\partial\Omega_i} \mathcal{F}_b.$$

We also define

$$\Xi_{ij} := \left(\Omega_i \cup \mathcal{F}^{ij} \cup \Omega_j\right) \cap \left(\Omega_i' \cap \Omega_j'\right), \text{ and}$$

$$\Upsilon_{jl} := \bigcap_{m\in\mathcal{I}_{jl}} \Omega_m',$$

which is the intersection of the extensions Ω_m' of all subdomains Ω_m which have the edge $\mathcal{E}^{jl}$ in common with Ω_i. Here, $\mathcal{I}_{jl}$ also includes i.

3.4 Some implementation details

We recall that the edge element basis functions $\boldsymbol{N}_e$ satisfy

$$\lambda_{e'}(\boldsymbol{N}_e) = \begin{cases} 1 & \text{if } e' = e \\ 0 & \text{if } e' \neq e \end{cases}.$$

They have the representation

$$\boldsymbol{N}_e = c_e \left(\lambda_1^e \nabla \lambda_2^e - \lambda_2^e \nabla \lambda_1^e\right), \tag{3.4.1}$$

where c_e is a constant independent of h such that $\boldsymbol{N}_e \cdot \boldsymbol{t}_e = 1$, and λ_1^e, λ_2^e are the two barycentric basis functions for the two endpoints of e.

In order to compute the entries of the matrix A, we need to evaluate the integrals

$$\int_K \nabla \times \boldsymbol{N}_{e_i} \cdot \nabla \times \boldsymbol{N}_{e_j} \, d\boldsymbol{x} \text{ and } \int_K \boldsymbol{N}_{e_i} \cdot \boldsymbol{N}_{e_j} \, d\boldsymbol{x}, \; K \in \mathcal{T}_h.$$

For the linear edge elements, $\nabla \times \boldsymbol{N}_e$ is piecewise constant, and it is easy to compute them from the gradient of the corresponding barycentric basis functions. Hence, the curl-contribution for the assembled matrix is trivial. For the mass-contribution, we use the formula

$$\int_K \lambda_i \lambda_j \, d\boldsymbol{x} = \frac{1 + \delta_{ij}}{C} |K|,$$

where δ_{ij} is the usual Kronecker delta function, and $C = 12$ or $C = 20$ for two or three dimensional problems, respectively. In order to obtain the right-hand side $\boldsymbol{g}$, we also use (3.4.1) with a quadrature formula.

We present in Table 3.1 the assembling time (in seconds) for the matrix A for different values of the number of degrees of freedom and the corresponding storage (number on non-zero entries), for the problem on the unit cube partitioned into tetrahedral elements, with a sequential code implemented in Matlab, and a 2.4GHz Intel Core i5 processor.

Table 3.1: Assembling time for the stiffness matrix A in 3D.

Size	Time (s)	$nnz(A)$
795 024	8	12 167 520
1 872 064	20	29 163 664
3 641 840	46	57 340 352
6 276 384	93	99 523 824

3.5 Some previous work on vector-valued problems

Work on vector-valued problems include [33], where overlapping Schwarz methods are analyzed for elliptic problems in $H(\text{curl})$ and $H(\text{div})$ in three dimensions. With the assumption that Ω is a convex polyhedral domain and $B = I$, the condition number is bounded by $C(1 + H/\delta)^2$, where subdomains are tetrahedra and constant coefficients are considered. In a previous study related to $H(\text{curl})$, the same estimate is given in [62] for an overlapping Schwarz algorithm in three dimensions, where the coarse space consists of standard edge finite element functions for coarse tetrahedral elements, the domain is assumed convex and $\alpha \equiv 1$, $B \equiv I$ over the whole domain. The coarse triangulation is shape-regular and quasi-uniform.

Also in [70, 67], the bound $C(1 + \log(H/h))^2$ is found for $H(\text{div})$ and $H(\text{curl})$ problems for bounded polygonal domains in $\mathbb{R}^3$ and $\mathbb{R}^2$ respectively, where an iterative substructuring algorithm is used with shape regular hexahedral and triangular subdomains. In [53], a two-level overlapping Schwarz method for Raviart-Thomas vector fields is developed. Here the bilinear form is

$$a(\boldsymbol{u}, \boldsymbol{v}) = \int_\Omega [\alpha \text{div } \boldsymbol{u} \text{div } \boldsymbol{v} + B\boldsymbol{u} \cdot \boldsymbol{v}] d\boldsymbol{x}$$

and the condition number is bounded by $C(1+H/\delta)(1+\log(H/h))$, where the domain is a bounded polyhedron in $\mathbb{R}^3$ and discontinuous coefficients and hexahedral elements are considered. A BDDC algorithm with deluxe averaging is studied in [54] for the space $H(\mathrm{div})$, with Raviart-Thomas elements, where convex polyhedral subdomains are assumed. The condition number is bounded by $C(1+\log(H/h))^2$, where the constant is independent of the values and jumps of the coefficients across the interface.

Studies based on FETI algorithms for our problem include [64, 65] for problems posed in 2D, and [63] in 3D. The subdomains are bounded convex polyhedra and the bounds depend on the coefficients α_i, β_i and H_i. In addition, a BDDC algorithm with deluxe scaling is considered in [21] for 3D.

There are also some related studies with Algebraic Multigrid Methods (AMG). A parallel implementation of different preconditioners based on the Hiptmair-Xu decomposition (derived in [34]) is analyzed in [40]. Also, different coarse spaces are constructed for problems in 3D with unstructured meshes in [41]. More studies on multigrid and multilevel methods include [32, 1, 33].

Chapter 4

John and Jones domains

4.1 Introduction

Previous studies on domain decomposition algorithms for our model problem include different methods, but usually with certain restrictions such as the convexity of the subdomains and the continuity of the coefficients.

As for the geometry of the substructures in two dimensions, we will consider John domains and Jones domains; see Definitions 4.2.1 and 4.2.6. John domains where first considered by Fritz John in work on elasticity [36], and were named after him by Martio and Sarvas in [49]. Jones domains were introduced as (ϵ, δ) domains by Peter Jones [37], and we will consider the case of $\delta = \infty$. These domains form the largest family of domains for which a bounded extension of $H(\text{grad}, \Omega)$ to $H(\text{grad}, \mathbb{R}^2)$ is possible.

In domain decomposition theory, it is typically assumed that each subdomain is quite regular, e.g., the union of a small set of coarse triangles or tetrahedra. But, it is unrealistic in general to assume that the subdomains are regular. Thus,

subdomain boundaries that arise from mesh partitioners might not even be Lipschitz continuous, i.e., the number of patches required to cover the boundary of the region in each of which the boundary is the graph of a Lipschitz continuous function, might not be uniformly bounded independently of the finite element mesh size. We also note that the shape of the subdomains are likely to change if the mesh size is altered and a mesh partitioner is used several times.

Some recent work and technical tools have been developed for irregular subdomains, cf. [69]. Scalar elliptic problems in the plane are analyzed in [16, 18]; [39] includes a FETI-DP algorithm for scalar elliptic and elasticity problems, [17] an overlapping Shwarz algorithm for almost incompressible elasticity, and [19] concerns an iterative substructuring method, different from ours, for problems in $H(\text{curl})$ in 2D. In this dissertation we will consider a two-level overlapping Schwarz algorithm and a BDDC deluxe method for irregular subdomains in two dimensions.

4.2 Definitions and properties

We start this section by defining the type of subdomains that we will consider for the partition of the domain of our model problem in 2D. We also collect some well-known tools for these particular domains.

Definition 4.2.1 (John domain)**.** A domain $\Omega \subset \mathbb{R}^n$ — an open, bounded, and connected set — is a John domain if there exists a constant $C_J \geq 1$ and a distinguished central point $\boldsymbol{x}_0 \in \Omega$, such that each $\boldsymbol{x} \in \Omega$ can be joined to $\boldsymbol{x}_0$ by a rectifiable curve $\gamma : [0,1] \to \Omega$, with $\gamma(0) = \boldsymbol{x}_0$, $\gamma(1) = \boldsymbol{x}$, and

$$|\boldsymbol{x} - \gamma(t)| \leq C_J \cdot \operatorname{dist}\left(\gamma(t), \partial\Omega\right), \ \forall t \in [0,1].$$

This condition can be viewed as a twisted cone condition. We note that certain snowflake curves with fractal boundaries are John domains, and that the length of the boundary of a John domain can be arbitrary much greater than its diameter. John domains may possess internal cusps while external cusps are excluded. It is also easy to see that $\mathrm{diam}(\Omega) \leq 2C_J r_\Omega$, where r_Ω is the radius of the largest ball inscribed in Ω and centered at x_0.

Remark 4.2.2. For a rectangular domain, $C_J \geq L_1/L_2$, where L_1, L_2 are the height and width of the domain, respectively. Thus, the constant C_J can be large if the subdomain has a large aspect ratio.

For domain decomposition methods with a coarse level, a Poincaré inequality is necessary, which is closely related to an isoperimetric inequality. We have the following result; see [50, 25].

Lemma 4.2.3 (Isoperimetric inequality)**.** *Let $\Omega \subset \mathbb{R}^n$ be a domain and let u be sufficiently smooth. Then,*

$$\inf_{c\in\mathbb{R}} \left(\int_\Omega |u-c|^{n/(n-1)} dx \right)^{(n-1)/n} \leq \gamma(\Omega, n) \int_\Omega |\nabla u| dx, \tag{4.2.1}$$

if and only if,

$$\left(\min\left(|A|, |B|\right)\right)^{1-1/n} \leq \gamma(\Omega, n) |\partial A \cap \partial B|.$$

Here, $A \subset \Omega$ is an arbitrary open set, and $B = \Omega \setminus \overline{A}$; $\gamma(\Omega, n)$ is the best possible constant and $|A|$ is the measure of the set A, etc.

A simply connected plane domain of finite area satisfies (4.2.1) if and only if Ω is a John domain; see [8]. Furthermore, the parameter $\gamma(\Omega, 2)$ can be expressed in terms of the John constant C_J; see [3].

For two dimensions, we immediately obtain a standard Poincaré inequality from (4.2.1) by using the Cauchy-Schwarz inequality. We note that the best choice of c is $\overline{u}_\Omega$, the average of u over the domain. For three dimensions, we use Hölder inequality several times.

Lemma 4.2.4 (Poincaré's inequality)**.** *Consider a John domain $\Omega \subset \mathbb{R}^d$, $d = 2, 3$. Then*

$$\|u - \bar{u}_\Omega\|^2_{L^2(\Omega)} \leq C|\Omega|^{2/d}\|\nabla u\|^2_{L^2(\Omega)} \ \forall \ u \in H(grad, \Omega),$$

where the constant C depends on the John constant $C_J(\Omega)$.

Finally, we need the following discrete Sobolev inequality, proved in [16, Lemma 3.2] for John domains in 2D:

Lemma 4.2.5. *Consider a John domain $\Omega \subset \mathbb{R}^2$. For $u \in W^h_{grad}(\Omega)$, there exists a constant C such that*

$$\|u\|^2_{L^\infty(\Omega)} \leq C\left(1 + \log\frac{H}{h}\right)\|u\|^2_{H^1(\Omega)},$$

$$\|u - \bar{u}_\Omega\|^2_{L^\infty(\Omega)} \leq C\left(1 + \log\frac{H}{h}\right)|u|^2_{H^1(\Omega)},$$

where $H := diam(\Omega)$. The constant C depends on the John constant $C_J(\Omega)$ and the shape regularity of the elements.

We will also consider Jones domains, also known as (ϵ, ∞) or uniform domains:

Definition 4.2.6 (Jones domain)**.** A bounded domain $\Omega \subset \mathbb{R}^2$ is uniform if there exists a constant $C_U(\Omega) > 0$ such that for any pair of points $\boldsymbol{a}$, $\boldsymbol{b}$ in the closure of Ω, there is a curve $\gamma(t) : [0, l] \to \Omega$, parametrized by arc length, with $\gamma(0) = \boldsymbol{a}$,

$\gamma(l) = \boldsymbol{b}$, and with

$$l \leq C_U |\boldsymbol{a} - \boldsymbol{b}|,$$

$$\min(|\gamma(t) - \boldsymbol{a}|, |\gamma(t) - \boldsymbol{b}|) \leq C_U \text{dist}(\gamma(t), \partial\Omega).$$

Remark 4.2.7. The left-hand side of the second condition can be replaced by

$$\min_t(t, l - t) \text{ or by } \frac{|\gamma(t) - \boldsymbol{x}||\gamma(t) - \boldsymbol{y}|}{|\boldsymbol{x} - \boldsymbol{y}|}.$$

It is easy to see that any Jones domain is a John domain, and therefore Lemmas 4.2.4 and 4.2.5 are valid for Jones domains. The Jones domains form the largest class of finitely connected domains for which an extension theorem holds in two dimensions; see [37, Theorem 4].

Related to the curve γ in Definition 4.2.6, we define the following region:

Definition 4.2.8. Let $\boldsymbol{a}$ and $\boldsymbol{b}$ denote the endpoints of $\mathcal{E} = \mathcal{E}^{ij} \in S_{\mathcal{E}_i}$. The region $\mathcal{R}_\mathcal{E}$ is defined as the open set with boundary $\partial\mathcal{R}_\mathcal{E} = \gamma_{\boldsymbol{ab}} \cup \mathcal{E}$, where $\gamma_{\boldsymbol{ab}}$ is the curve γ in Definition 4.2.6.

By simple geometric considerations, it is easy to prove that $\mathcal{R}_\mathcal{E}$ satisfies the following lemma; see [19, Lemma 3.4].

Lemma 4.2.9. *Given a uniform subdomain Ω_i and a connected subset $\mathcal{E} \subset \partial\Omega_i$, the region $\mathcal{R}_\mathcal{E}$ satisfies*

$$|\mathcal{R}_\mathcal{E}| \leq (C_U^2/\pi) d_\mathcal{E}^2,$$

$$diam(\mathcal{R}_\mathcal{E}) \leq (2C_U - 1) d_\mathcal{E}.$$

Finally, we introduce a modified region $\widehat{\mathcal{R}}_\mathcal{E}$ related to $\mathcal{R}_\mathcal{E}$, that will be used as the support of functions constructed for each subdomain:

Lemma 4.2.10. *Given a uniform domain Ω_i and a connected subset $\mathcal{E} \subset \partial\Omega_i$, there exist a constant C, depending on $C_U(\Omega_i)$, and a uniform domain $\widehat{\mathcal{R}}_{\mathcal{E}}$, which is a union of finite elements of Ω_i, such that $\mathcal{R}_{\mathcal{E}} \subset \widehat{\mathcal{R}}_{\mathcal{E}}$, $\partial\widehat{\mathcal{R}}_{\mathcal{E}} \cap \partial\Omega_i = \mathcal{E}$, and*

$$|\widehat{\mathcal{R}}_{\mathcal{E}}| \leq C d_{\mathcal{E}}^2,$$

$$diam(\widehat{\mathcal{R}}_{\mathcal{E}}) \leq C d_{\mathcal{E}}.$$

Proof. See [19, Lemma 3.5]. □

Chapter 5

Domain Decomposition methods

Domain decomposition methods have been studied widely for different problems. We refer to [61, 56, 66] for general introductions to these topics.

5.1 Abstract Schwarz theory

We introduce the abstract Schwarz analysis in this section, which is useful in the design and analysis of different iterative methods.

5.1.1 Schwarz methods

Consider a finite dimensional Hilbert space V. Given a symmetric, positive definite bilinear form,

$$a(\cdot,\cdot) : V \times V \to \mathbb{R},$$

and an element $f \in V'$, we consider the problem: Find $u \in V$, such that

$$a(u, v) = f(v), \ \forall v \in V.$$

Given a basis for V, denote by A the corresponding stiffness matrix relative to the bilinear form $a(\cdot,\cdot)$. Then, the problem is equivalent to the linear system

$$Au = f,$$

with A a symmetric, positive definite matrix.

We next consider a family of spaces $\{V_i,\ i = 0,\dots,N\}$, and suppose that there exist extension operators

$$R_i^T : V_i \to V.$$

We assume that V admits the (not necessarily a direct sum) decomposition

$$V = R_0^T V_0 + \sum_{i=1}^{N} R_i^T V_i.$$

The $V_i,\ i \geq 1$, do not need to be subspaces of V, but they are often called subspaces or local spaces, and V_0 is named the coarse space, and is usually related to a coarse lower-dimensional problem.

We introduce local symmetric positive definite bilinear forms on the subspaces,

$$\tilde{a}_i(\cdot,\cdot) : V_i \times V_i \to \mathbb{R},\ i = 0,\dots,N,$$

and the associated local stiffness matrices

$$\tilde{A}_i : V_i \to V_i.$$

We can use the original bilinear form on the subspaces by choosing

$$\tilde{a}_i(u_i, v_i) = a(R_i^T u_i, R_i^T v_i),\ u_i, v_i \in V_i,$$

and then

$$\tilde{A}_i = R_i A R_i^T.$$

In this case, we say that we use exact local solvers.

Schwarz operators are defined in terms of projection-like operators

$$P_i := R_i^T \tilde{P}_i : V \to R_i^T V_i \subset V,\ i = 0, \ldots, N,$$

where $\tilde{P}_i : V \to V_i$ is defined by

$$\tilde{a}_i(\tilde{P}_i u, v_i) = a(u, R_i^T v_i),\ v_i \in V_i.$$

We note that $\tilde{P}_i$ is well-defined since the local bilinear forms are coercive. In the case of exact solvers, we have

$$a(P_i u, R_i^T v_i) = a(u, R_i^T v_i),\ v_i \in V_i.$$

It can be proven easily that the P_i can be written as

$$P_i = R_i^T \tilde{A}_i^{-1} R_i A,\ 0 \leq i \leq N,$$

and that in the case of exact solvers, P_i is a projection; see [66, Lemma 2.1].

We can now define a number of different Schwarz operators. The additive

operator is defined by

$$P_{ad} := \sum_{i=0}^{N} P_i. \tag{5.1.1}$$

A multiplicative operator is defined by

$$P_{mu} := I - E_{mu}, \tag{5.1.2}$$

where the error propagation operator E_{mu} is defined by

$$E_{mu} := (I - P_N)(I - P_{N-1}) \dots (I - P_0).$$

A hybrid operator is defined by

$$P_{hy1} = I - E_{hy1}, \;\; E_{hy1} := (I - P_0) \left(I - \sum_{i=1}^{N} P_i \right) (I - P_0), \tag{5.1.3}$$

which is additive with respect to the local components and multiplicative with respect to the levels. In the case of exact solvers, we can rewrite this operator as

$$P_{hy1} = P_0 + (I - P_0) \sum_{i=0}^{N} P_i (I - P_0).$$

All these Schwarz operators provide preconditioned operators for the original operator A and can be written as the product of a suitable preconditioner and A, where the former only involves extensions R_i^T, restrictions R_i, local operators $\tilde{A}_i^{-1}$, and A. For example,

$$P_{ad} = A_{ad}^{-1} A, \;\; A_{ad}^{-1} = \sum_{i=0}^{N} R_i^T \tilde{A}_i^{-1} R_i.$$

5.1.2 Convergence theory

We consider the solution of $P_{ad}u = g_{ad}$, where $g_{ad} := A_{ad}^{-1}f$. In an abstract setting, we need to consider the following assumptions:

Assumption 5.1.1. There exists a constant C_0, such that every $u \in V$ admits a decomposition

$$u = \sum_{i=0}^{N} R_i^T u_i,\ \{u_i \in V_i,\ 0 \le i \le N\},$$

that satisfies

$$\sum_{i=0}^{N} \tilde{a}_i(u_i, u_i) \le C_0^2 a(u, u).$$

Assumption 5.1.2. There exist constants $0 \le \epsilon_{ij} \le 1$, $1 \le i, j \le N$, such that

$$\left|a(R_i^T u_i, R_j^T u_j)\right| \le \epsilon_{ij} a(R_i^T u_i, R_i^T u_i)^{1/2} a(R_j^T u_j, R_j^T u_j)^{1/2},$$

for $u_i \in V_i$, $u_j \in V_j$. We will denote the spectral radius of $\mathcal{E} = (\epsilon_{ij})$ by $\rho(\mathcal{E})$.

Assumption 5.1.3. There exists $\omega > 0$ such that

$$a(R_i^T u_i, R_i^T u_i) \le \omega\ \tilde{a}_i(u_i, u_i),\ u_i \in\ \text{range}(\tilde{P}_i) \subset V_i,\ 0 \le i \le N.$$

We then have the following lemmas:

Lemma 5.1.4. *Let Assumption 5.1.1 be satisfied. Then,*

$$a(P_{ad}u, u) \ge C_0^{-2} a(u, u), u \in V.$$

Proof. See [66, Lemma 2.5] □

Lemma 5.1.5. *Let Assumptions 5.1.2 and 5.1.3 be satisfied. Then,*

$$\|P_i\|_a \leq \omega, \text{ for } i = 0, \ldots, N.$$

In addition,

$$a(P_{ad}u, u) \leq \omega\,(\rho(\mathcal{E}) + 1)\,a(u, u).$$

Proof. See [66, Lemma 2.6] □

Combining the previous two lemmas, we obtain the following bound for the condition number of the preconditioned system; see [66, Theorem 2.7].

Theorem 5.1.6. *The condition number of the additive Schwarz operator* (5.1.1) *satisfies*

$$\kappa(P_{ad}) \leq C_0^2\omega\,(\rho(\mathcal{E}) + 1)\,.$$

Remark 5.1.7. We can bound $\rho(\mathcal{E})$ by N^c, the minimum number of colors needed to color the subdomains associated with the local subproblems such that no pair of subdomains of the same color intersect; see [66, Section 3.6]. Also, if exact solvers are used, it is clear that $\omega = 1$.

We also have the following bounds for the multiplicative and hybrid operators defined in (5.1.2) and (5.1.3), respectively; see [66, Theorems 2.9 and 2.13].

Lemma 5.1.8. *Let Assumptions 5.1.1, 5.1.2 and 5.1.3 be satisfied and suppose that* $\omega \in (0, 2)$. *Then, the error propagation operator of the multiplicative Schwarz algorithm satisfies*

$$\|E_{mu}\|_a^2 \leq 1 - \frac{2 - \omega}{(2\hat{\omega}^2\rho(\mathcal{E})^2 + 1)C_0^2} < 1,$$

where $\hat{\omega} = \max\{1, \omega\}$.

Lemma 5.1.9. *Let Assumptions 5.1.1, 5.1.2 and 5.1.3 be satisfied, where Assumption 5.1.1 holds for any* $u \in \text{range}(\text{I} - \text{P}_0)$. *Then,*

$$\max\{1, C_0^2\}^{-1} a(u,u) \leq a(P_{hy1}u, u) \leq \max\{1, \omega\rho(\mathcal{E})\} a(u,u).$$

5.2 Overlapping Schwarz methods

We will consider an additive two-level Schwarz algorithm for problems in 2D and 3D in Chapters 6 and 8, respectively. The need of a coarse level arises from the fact that the condition number estimate deteriorates as the number of subdomain increases. As we will see, our overlapping Schwarz methods will be scalable, meaning that its rate of convergence does not deteriorate when the number of subdomains grows.

We will consider a particular coarse space for each problem V_0 (see Sections 6.2.1 and 8.2), and the local spaces

$$V_i := \Big\{ \boldsymbol{w}_i \in W^{h_i}_{\text{curl}}(\Omega_i') : \boldsymbol{w}_i = \sum_{e \in \mathcal{M}_{\Omega_i'}} \alpha_e \boldsymbol{N}_e \Big\},$$

where $\mathcal{M}_{\Omega_i'}$ is the set of element edges in Ω_i', $1 \leq i \leq N$.

We will use exact local solvers in the overlapping domains Ω_i'; see Section 5.1.1. Therefore, in order to estimate $\kappa(P_{ad})$, our problem reduces to obtaining a constant C_0^2 such that

$$a(\boldsymbol{u}_0, \boldsymbol{u}_0) + \sum_{i=1}^{N} a_i'(\boldsymbol{u}_i, \boldsymbol{u}_i) \leq C_0^2 a(\boldsymbol{u}, \boldsymbol{u}),$$

where

$$\boldsymbol{u} = R_0^T \boldsymbol{u}_0 + \sum_{i=1}^{N} R_i^T \boldsymbol{u}_i, \ \boldsymbol{u} \in W_{\text{curl}}^h(\Omega),$$

and the local bilinear forms are defined by

$$a_i'(\boldsymbol{u}, \boldsymbol{u}) := \int_{\Omega_i'} \left(\alpha |\nabla \times \boldsymbol{u}|^2 + \beta |\boldsymbol{u}|^2 \right) d\boldsymbol{x}.$$

By Theorem 5.1.6, the condition number of the additive operator (5.1.1) is bounded by

$$\kappa(P_{ad}) \leq (N^C + 1) C_0^2, \tag{5.2.1}$$

where N^C is the minimum number of colors needed to color the overlapping subdomains Ω_i' such that no pair of subdomains of the same color intersect. Clearly, as the overlap increases, the number of colors required can become larger.

In order to use the preconditioned conjugate gradient, we need a subroutine that applies the preconditioner to a vector; see Algorithm 2. This is trivial if we want to compute the action of the additive preconditioner A_{ad}^{-1}. For the multiplicative preconditioner

$$P_{mu} = A_{mu}^{-1} A,$$

we use the following subroutine in order to compute $A_{mu}^{-1} \boldsymbol{r}$. A similar subroutine can be written for the hybrid preconditioner A_{hy1}^{-1}.

Result: Compute $A_{mu}^{-1}\boldsymbol{r}$

$\boldsymbol{y} = R_0^T \tilde{A}_0^{-1} R_0 \boldsymbol{r}$;

for $i = 1, \ldots, N$ **do**

  $\boldsymbol{y} = \boldsymbol{y} + R_i^T \tilde{A}_i^{-1} R_i (\boldsymbol{r} - A\boldsymbol{y})$;

end

Algorithm 3: Applying A_{mu}^{-1} to a vector $\boldsymbol{r}$

5.3 BDDC methods

In this section, we describe the BDDC algorithms. For simplicity, we write $W^{(i)} := W^{h_i}_{\text{curl}}(\Omega_i)$. We decompose this space into two, $W^{(i)} := W_I^{(i)} \oplus W_\Gamma^{(i)}$, where $W_I^{(i)}$ represents the interior space and $W_\Gamma^{(i)}$ the interface space, associated to the interior and interface degrees of freedom, respectively. We decompose the space $W_\Gamma^{(i)}$ as the sum of a dual and a primal space, $W_\Gamma^{(i)} := W_\Delta^{(i)} \oplus W_\Pi^{(i)}$.

We make a change of variables in order to work explicitly with these primal variables, similar to what is done in [45, Section 3.3]. The complementary dual space will then be represented by elements with zero values at the primal degrees of freedom.

We will also use the following product spaces, which allow discontinuities across the interface:

$$W := \prod_{i=1}^{N} W^{(i)},\ W_I := \prod_{i=1}^{N} W_I^{(i)},\ W_\Gamma := \prod_{i=1}^{N} W_\Gamma^{(i)},$$

and

$$W_\Delta := \prod_{i=1}^{N} W_\Delta^{(i)},\ W_\Pi := \prod_{i=1}^{N} W_\Pi^{(i)}.$$

We then have

$$W = W_I \oplus W_\Gamma = W_I \oplus W_\Delta \oplus W_\Pi.$$

The finite element solutions have a continuous tangential component across the interface and we denote the corresponding subspace of W_Γ by $\widehat{W}_\Gamma$; generally, functions in W_Γ do not satisfy this condition. We also introduce a subspace $\widetilde{W}_\Gamma$, intermediate between $\widehat{W}_\Gamma$ and W_Γ, for which all the primal constraints are enforced. We can then decompose

$$\widehat{W}_\Gamma := \widehat{W}_\Delta \oplus \widehat{W}_\Pi, \ \widetilde{W}_\Gamma := W_\Delta \oplus \widehat{W}_\Pi,$$

where $\widehat{W}_\Delta$ is the continuous dual variable subspace and $\widehat{W}_\Pi$ is the continuous primal variable subspace.

The contribution of our problem to the subdomain Ω_i can be written in terms of the local stiffness matrix $A^{(i)}$ and the local right hand side $\boldsymbol{f}^{(i)}$,

$$A^{(i)} = \begin{pmatrix} A_{II}^{(i)} & A_{I\Delta}^{(i)} & A_{I\Pi}^{(i)} \\ A_{\Delta I}^{(i)} & A_{\Delta\Delta}^{(i)} & A_{\Delta\Pi}^{(i)} \\ A_{\Pi I}^{(i)} & A_{\Pi\Delta}^{(i)} & A_{\Pi\Pi}^{(i)} \end{pmatrix}, \ \boldsymbol{f}^{(i)} = \begin{pmatrix} \boldsymbol{f}_I^{(i)} \\ \boldsymbol{f}_\Delta^{(i)} \\ \boldsymbol{f}_\Pi^{(i)} \end{pmatrix}. \tag{5.3.1}$$

We can express the global linear system by assembling the local subdomain problems as

$$A \begin{pmatrix} \boldsymbol{u}_I \\ \boldsymbol{u}_\Delta \\ \boldsymbol{u}_\Pi \end{pmatrix} = \begin{pmatrix} A_{II} & A_{I\Delta} & A_{I\Pi} \\ A_{\Delta I} & A_{\Delta\Delta} & A_{\Delta\Pi} \\ A_{\Pi I} & A_{\Pi\Delta} & A_{\Pi\Pi} \end{pmatrix} \begin{pmatrix} \boldsymbol{u}_I \\ \boldsymbol{u}_\Delta \\ \boldsymbol{u}_\Pi \end{pmatrix} = \begin{pmatrix} \boldsymbol{f}_I \\ \boldsymbol{f}_\Delta \\ \boldsymbol{f}_\Pi \end{pmatrix}, \tag{5.3.2}$$

with $\boldsymbol{u}_I \in W_I$, $\boldsymbol{u}_\Delta \in \widehat{W}_\Delta$, $\boldsymbol{u}_\Pi \in \widehat{W}_\Pi$.

We now define some operators that we will also use in our analysis. We first introduce restriction operators. Let

$$\widehat{R}_\Gamma^{(i)} : \widehat{W}_\Gamma \to W_\Gamma^{(i)}, \ \widetilde{R}_\Gamma^{(i)} : \widetilde{W}_\Gamma \to W_\Gamma^{(i)}$$

be the operators that map global interface vectors defined on Γ to their components on Γ_i. Similarly, we define

$$R_\Delta^{(i)} : W_\Delta \to W_\Delta^{(i)}, \ R_\Pi^{(i)} : \widehat{W}_\Pi \to W_\Pi^{(i)}, \ \widetilde{R}_{\Gamma\Delta} : \widetilde{W}_\Gamma \to W_\Delta,$$

$$\widetilde{R}_{\Gamma\Pi} : \widetilde{W}_\Gamma \to \widehat{W}_\Pi \ \text{ and } \ R_{\Gamma\Delta}^{(i)} : W_\Gamma^{(i)} \to W_\Delta^{(i)}.$$

We also will use the direct sums

$$\widehat{R}_\Gamma := \bigoplus_{i=1}^{N} \widehat{R}_\Gamma^{(i)} \text{ and } \overline{R}_\Gamma := \bigoplus_{i=1}^{N} \widetilde{R}_\Gamma^{(i)}.$$

Furthermore, $\widetilde{R}_\Gamma : \widetilde{W}_\Gamma \to \widetilde{W}_\Gamma$ will be the direct sum of $\widehat{R}_\Pi$ and the $\widehat{R}_\Delta^{(i)}$, where $\widehat{R}_\Pi : \widehat{W}_\Gamma \to \widehat{W}_\Pi$ and $\widehat{R}_\Delta^{(i)} : \widehat{W}_\Gamma \to W_\Delta^{(i)}$ are the corresponding restriction operators.

We next introduce scaling matrices $D^{(i)}$, acting on the degrees of freedom associated with Γ_i. They are combined into a block diagonal matrix and should provide a discrete partition of unity, i.e.,

$$\widehat{R}_\Gamma^T \begin{pmatrix} D^{(1)} & & & \\ & D^{(2)} & & \\ & & \ddots & \\ & & & D^{(N)} \end{pmatrix} \widehat{R}_\Gamma = I. \tag{5.3.3}$$

We then define the scaled operators $R^{(i)}_{D,\Gamma} := D^{(i)}\widehat{R}^{(i)}_{\Gamma}$, $\widetilde{R}^{(i)}_{D,\Delta} := R^{(i)}_{\Gamma\Delta}R^{(i)}_{D,\Gamma}$. We next consider a globally scaled operator $\widetilde{R}_{D,\Gamma} : \widetilde{W}_{\Gamma} \rightarrow \widetilde{W}_{\Gamma}$ defined by

$$\widetilde{R}_{D,\Gamma} := \widehat{R}_{\Pi} \oplus \left(\bigoplus_{i=1}^{N} \widetilde{R}^{(i)}_{D,\Delta} \right).$$

From (5.3.3), it follows that

$$\widetilde{R}^{T}_{\Gamma}\widetilde{R}_{D,\Gamma} = \widetilde{R}^{T}_{D,\Gamma}\widetilde{R}_{\Gamma} = I. \tag{5.3.4}$$

Finally, we introduce an averaging operator $E_D : \widetilde{W}_{\Gamma} \rightarrow \widehat{W}_{\Gamma}$ by

$$E_D := \widetilde{R}_{\Gamma}\widetilde{R}^{T}_{D,\Gamma}. \tag{5.3.5}$$

This operator is a projection, i.e., $E^2_D = E_D$; this follows from (5.3.4) and therefore E_D provides a weighted average across the interface Γ.

We will consider the subdomain Schur complements

$$S^{(i)}_{\Gamma} := A^{(i)}_{\Gamma\Gamma} - A^{(i)}_{\Gamma I}A^{(i)^{-1}}_{II}A^{(i)}_{I\Gamma}, \tag{5.3.6}$$

where

$$A^{(i)}_{\Gamma\Gamma} := \begin{pmatrix} A^{(i)}_{\Delta\Delta} & A^{(i)}_{\Delta\Pi} \\ A^{(i)}_{\Pi\Delta} & A^{(i)}_{\Pi\Pi} \end{pmatrix}$$

is the block matrix corresponding to the interface degrees of freedom in (5.3.1). From (5.3.6), we note that we can compute $S^{(i)}_{\Gamma}$ times a vector by a local computation involving Ω_i; the application of the inverse of $A^{(i)}_{II}$ to a vector corresponds to the solution of a Dirichlet problem in Ω_i. Similarly, we can find $S^{(i)^{-1}}_{\Gamma}\boldsymbol{u}^{(i)}_{\Gamma}$ by

solving a linear system with the matrix $A^{(i)}$ and right hand side $(\mathbf{0}, \boldsymbol{u}_\Gamma^{(i)})^T$. Hence, we do not need to compute the elements of the Schur complements.

We denote the global Schur complement by S_Γ, given by the direct sum of the local Schur complements $S_\Gamma^{(i)}$. By using the local Schur complements, we can build a global interface problem. By eliminating the interior variables, the global problem (5.3.2) can thus be reduced to

$$\widehat{S}_\Gamma \boldsymbol{u}_\Gamma = \boldsymbol{g}_\Gamma, \tag{5.3.7}$$

with

$$\widehat{S}_\Gamma := \sum_{i=1}^{N} \widehat{R}_\Gamma^{(i)^T} S_\Gamma^{(i)} \widehat{R}_\Gamma^{(i)} = \widehat{R}_\Gamma^T S_\Gamma \widehat{R}_\Gamma,$$

and

$$\boldsymbol{g}_\Gamma := \sum_{i=1}^{N} \widehat{R}_\Gamma^{(i)^T} \left[\begin{pmatrix} \boldsymbol{f}_\Delta^{(i)} \\ \boldsymbol{f}_\Pi^{(i)} \end{pmatrix} - \begin{pmatrix} A_{\Delta I}^{(i)} \\ A_{\Pi I}^{(i)} \end{pmatrix} A_{II}^{(i)^{-1}} \boldsymbol{f}_I^{(i)} \right].$$

We will build a preconditioner for (5.3.7). Once $\boldsymbol{u}_\Gamma^{(i)}$ has been found, $\boldsymbol{u}_I^{(i)}$ is found by solving

$$A_{II}^{(i)} \boldsymbol{u}_I^{(i)} = \boldsymbol{f}_I^{(i)} - \left(A_{I\Delta}^{(i)} A_{I\Pi}^{(i)} \right) \boldsymbol{u}_\Gamma^{(i)}.$$

We now consider a partially subassembled Schur complement $\widetilde{S}_\Gamma$ on the space

$\widetilde{W}_\Gamma$: given $\boldsymbol{u}_\Gamma \in \widetilde{W}_\Gamma$, $\widetilde{S}_\Gamma \boldsymbol{u}_\Gamma \in \widetilde{W}_\Gamma$ is determined such that

$$\begin{pmatrix} A_{II}^{(1)} & A_{\Delta I}^{(1)^T} & & & & A_{\Pi I}^{(1)^T} \\ A_{\Delta I}^{(1)} & A_{\Delta\Delta}^{(1)} & & & & A_{\Pi\Delta}^{(1)^T} \\ & & \ddots & & & \vdots \\ & & & A_{II}^{(N)} & A_{\Delta I}^{(N)^T} & A_{\Pi I}^{(N)^T} \\ & & & A_{\Delta I}^{(N)} & A_{\Delta\Delta}^{(N)} & A_{\Pi\Delta}^{(N)^T} \\ A_{\Pi I}^{(1)} & A_{\Pi\Delta}^{(1)} & \cdots & A_{\Pi I}^{(N)} & A_{\Pi\Delta}^{(N)} & \widehat{A}_{\Pi\Pi} \end{pmatrix} \begin{pmatrix} \boldsymbol{u}_I^{(1)} \\ \boldsymbol{u}_\Delta^{(1)} \\ \vdots \\ \boldsymbol{u}_I^{(N)} \\ \boldsymbol{u}_\Delta^{(N)} \\ \boldsymbol{u}_\Pi \end{pmatrix} = \begin{pmatrix} 0 \\ R_\Delta^{(1)} \widetilde{R}_{\Gamma\Delta} \widetilde{S}_\Gamma \boldsymbol{u}_\Gamma \\ \vdots \\ 0 \\ R_\Delta^{(N)} \widetilde{R}_{\Gamma\Delta} \widetilde{S}_\Gamma \boldsymbol{u}_\Gamma \\ \widetilde{R}_{\Gamma\Pi} \widetilde{S}_\Gamma \boldsymbol{u}_\Gamma \end{pmatrix}.$$

Here,

$$\widehat{A}_{\Pi\Pi} := \sum_{i=1}^{N} R_\Pi^{(i)^T} A_{\Pi\Pi}^{(i)} R_\Pi^{(i)} \text{ and } \widetilde{R}^i := R_\Delta^{(i)} \widetilde{R}_{\Gamma\Delta} \widetilde{S}_\Gamma \boldsymbol{u}_\Gamma.$$

We note that $\widetilde{S}_\Gamma = \overline{R}_\Gamma^T S_\Gamma \overline{R}_\Gamma$, and by using restriction and extension operators, we also find that $\widehat{S}_\Gamma = \widetilde{R}_\Gamma^T \widetilde{S}_\Gamma \widetilde{R}_\Gamma$. Then, (5.3.7) can be rewritten as

$$\widetilde{R}_\Gamma^T \widetilde{S}_\Gamma \widetilde{R}_\Gamma \boldsymbol{u}_\Gamma = \boldsymbol{g}_\Gamma. \tag{5.3.8}$$

A linear system with the matrix $\widetilde{S}_\Gamma$ can be solved by using the fact that

$$\widetilde{S}_\Gamma^{-1} = \widetilde{R}_{\Gamma\Delta}^T \left(\sum_{i=1}^{N} \begin{pmatrix} 0 & R_\Delta^{(i)^T} \end{pmatrix} \begin{pmatrix} A_{II}^{(i)} & A_{I\Delta}^{(i)} \\ A_{\Delta I}^{(i)} & A_{\Delta\Delta}^{(i)} \end{pmatrix}^{-1} \begin{pmatrix} 0 \\ R_\Delta^{(i)} \end{pmatrix} \right) \widetilde{R}_{\Gamma\Delta} + \Phi S_{\Pi\Pi}^{-1} \Phi^T,$$

with

$$\Phi := \widetilde{R}_{\Gamma\Pi}^T - \widetilde{R}_{\Gamma\Delta}^T \sum_{i=1}^{N} \begin{pmatrix} 0 & R_\Delta^{(i)^T} \end{pmatrix} \begin{pmatrix} A_{II}^{(i)} & A_{I\Delta}^{(i)} \\ A_{\Delta I}^{(i)} & A_{\Delta\Delta}^{(i)} \end{pmatrix}^{-1} \begin{pmatrix} A_{\Pi I}^{(i)^T} \\ A_{\Pi\Delta}^{(i)^T} \end{pmatrix} R_\Pi^{(i)}$$

and where

$$S_{\Pi\Pi} := \sum_{i=1}^{N} R_{\Pi}^{(i)^T} \left(A_{\Pi\Pi}^{(i)} - \begin{pmatrix} A_{\Pi I}^{(i)} & A_{\Pi\Delta}^{(i)} \end{pmatrix} \begin{pmatrix} A_{II}^{(i)} & A_{I\Delta}^{(i)} \\ A_{\Delta I}^{(i)} & A_{\Delta\Delta}^{(i)} \end{pmatrix}^{-1} \begin{pmatrix} A_{\Pi I}^{(i)^T} \\ A_{\Pi\Delta}^{(i)^T} \end{pmatrix} \right) R_{\Pi}^{(i)};$$

see, e.g., [45].

In order to define a particular BDDC method, all that is left is to define the primal constraints and the average on the interface; see Chapter 7 for the description of our algorithm. With these operators, we define the BDDC preconditioner as

$$M_{BDDC}^{-1} := \widetilde{R}_{D,\Gamma}^T \widetilde{S}_{\Gamma}^{-1} \widetilde{R}_{D,\Gamma}, \tag{5.3.9}$$

and, from (5.3.8), the preconditioned linear system is given by

$$M_{BDDC}^{-1} \widehat{S}_{\Gamma} \boldsymbol{u}_{\Gamma} = \widetilde{R}_{D,\Gamma}^T \widetilde{S}_{\Gamma}^{-1} \widetilde{R}_{D,\Gamma} \widetilde{R}_{\Gamma}^T \widetilde{S}_{\Gamma} \widetilde{R}_{\Gamma} \boldsymbol{u}_{\Gamma} = \widetilde{R}_{D,\Gamma}^T \widetilde{S}_{\Gamma}^{-1} \widetilde{R}_{D,\Gamma} \boldsymbol{g}_{\Gamma}.$$

We next define norms related to the Schur complements. The S_Γ-norm is given by $\|\boldsymbol{u}_\Gamma\|_{S_\Gamma}^2 := \boldsymbol{u}_\Gamma^T S_\Gamma \boldsymbol{u}_\Gamma$ for $\boldsymbol{u}_\Gamma \in W_\Gamma$. Similar expressions can be written for $\|\boldsymbol{u}_\Gamma^{(i)}\|_{S_\Gamma^{(i)}}^2$, $\|\boldsymbol{u}_\mathcal{E}^{(i)}\|_{S_\mathcal{E}^{(i)}}^2$ and $\|\tilde{\boldsymbol{u}}_\Gamma\|_{\widetilde{S}_\Gamma}^2$. It is easy to see that $\|\tilde{\boldsymbol{u}}_\Gamma\|_{\widetilde{S}_\Gamma}^2 = \|\overline{R}_\Gamma \tilde{\boldsymbol{u}}_\Gamma\|_{S_\Gamma}^2$.

Finally, the condition number of the BDDC algorithm satisfies (see Lemmas 7.5.1 and 7.5.2):

$$\kappa(M_{BDDC}^{-1} \widehat{S}_\Gamma) \leq \|E_D\|_{\widetilde{S}_\Gamma}^2.$$

Chapter 6

An overlapping Schwarz algorithm for Nédélec vector fields in 2D

6.1 Introduction

In this chapter, we analyze a two-level overlapping Schwarz method for our problem in two dimensions, with Jones subdomains. Our study applies to a much broader range of material properties and subdomain geometries than previous studies. We obtain the bound

$$\kappa \leq C|\Xi|\chi\eta\left(1+\log\frac{\delta}{h}\right)\left(1+\frac{H}{\delta}\right)\left(1+\log\frac{H}{h}\right),$$

where C is independent of the jumps of the coefficients between the subdomains. The parameter χ is related to the geometry of the subdomains and it is quite close

to 1 even for fractal edges and large values of H/h (see Section 3.3), $|\Xi|$ represents the maximum number of neighbors for any subdomain, and

$$\eta = \max_i \left\{ \min \left\{ \frac{H_i^2}{h_i^2}, 1 + \frac{\beta_i H_i^2}{\alpha_i} \right\} \right\},$$

where the maximum is taken over all the subdomains; see Section 6.3. We observe that in many cases we can obtain a bound independent of η; see Theorem 6.3.2.

The standard way of constructing the local components involves a partition of unity for all of Ω. This is a decomposition of functions in the sense of the Schwarz theory as in Section 5.1. In our study, we adopt a different strategy, creating a partition of unity for the interface and we then split the corresponding functions supported in the different overlapping regions, in a way similar to what is done in [17].

We also introduce a new type of cutoff function for overlapping regions with John subdomains. We recall that certain snowflake curves with fractal boundaries are John domains, and that the length of the boundary of a John domain can be arbitrary greater that its diameter. This cutoff function will allow us to define local decompositions, and can be used in different overlapping Scharwz algorithms for problems with discontinuities in the coefficients across the interface, reducing the problem to obtaining local bounds. This idea is used in Section 6.2.3, where we analyze a stability result for our coarse space.

6.2 Technical tools

The auxiliary results presented in this section will be used in the proof of our main results, Theorems 6.3.1 and 6.3.2.

6.2.1 Coarse functions

We will consider the same coarse space functions as introduced in [19]. For $\mathcal{E} \in S_{\mathcal{E}}$, we define the coarse function $\boldsymbol{c}_{\mathcal{E}}$ with tangential data given by $\boldsymbol{c}_{\mathcal{E}} \cdot \boldsymbol{t}_e = \boldsymbol{d}_{\mathcal{E}} \cdot \boldsymbol{t}_e$ along $\mathcal{E}$ and with $\boldsymbol{c}_{\mathcal{E}} \cdot \boldsymbol{t}_e = 0$ on $\Gamma \cup \partial\Omega \setminus \mathcal{E}$. We obtain $\boldsymbol{c}_{\mathcal{E}}$ by the energy minimizing extension of this tangential data into the interiors of the two subdomains sharing $\mathcal{E}$. We note that the construction of $\boldsymbol{c}_{\mathcal{E}^{ij}}$ involves the solution of a Dirichlet problem with inhomogeneous boundary data for Ω_i and Ω_j. We then define the coarse interpolant for $\boldsymbol{u} \in H(\text{curl}, \Omega)$ by

$$\boldsymbol{u_0} := \sum_{\mathcal{E} \in S_{\mathcal{E}}} \overline{u}_{\mathcal{E}} \boldsymbol{c}_{\boldsymbol{\mathcal{E}}}, \text{ with } \overline{u}_{\mathcal{E}} := \frac{1}{d_{\mathcal{E}}} \int_{\mathcal{E}} \boldsymbol{u} \cdot \boldsymbol{t}_{\mathcal{E}} ds. \tag{6.2.1}$$

6.2.2 Cutoff functions

We introduce a new cutoff function that will provide a partition of unity on the interface of the domain and which will be used later for the local decomposition. The following result is valid for John subdomains.

Lemma 6.2.1. *Let $\mathcal{E} \in S_{\mathcal{E}_i}$ with endpoints $\boldsymbol{a}$ and $\boldsymbol{b}$. Then there exists an edge function $\theta^{\delta}_{\mathcal{E}} \in W^{h_i}_{grad}(\Omega_i)$ that takes the value 1 at the nodes on $\mathcal{E}$, vanishes in $\Omega_i \setminus \Omega'_j$, and such that*

$$\|\nabla \theta^{\delta}_{\mathcal{E}}\|^2_{L^2(\Omega_i \cap \Omega'_j)} \leq C \chi_{\mathcal{E}}(\delta_i) \left(1 + \frac{d_{\mathcal{E}}}{\delta_i}\right) \left(1 + \log \frac{\delta_i}{h_i}\right), \tag{6.2.2}$$

for some constant C depending on C_J and the shape regularity of the elements.

Proof. For the proof of this lemma, we use similar ideas as in [18, Lemma 2.7] and [19, Lemma 3.6]. Rename $\mathcal{E}_1 := \mathcal{E}$ and let $\mathcal{E}_2 := \partial\left(\Omega_i \cap \Omega'_j\right) \setminus \mathcal{E}$. Split $\mathcal{E}_2$ into two

subsets, $\mathcal{E}_3 := \mathcal{E}_2 \cap \partial\Omega_j'$ and $\mathcal{E}_4 := \mathcal{E}_2 \setminus \mathcal{E}_3$. Note that $\mathcal{E}_4$ is a subset of $\partial\Omega_i$ with two components, one with $\boldsymbol{a}$ and the other with $\boldsymbol{b}$ as endpoints. Denote by $d_i(\boldsymbol{x})$ the distance of $\boldsymbol{x}$ to the edge $\mathcal{E}_i$ and consider the function $\tilde{\theta}_{\mathcal{E}}$ given by

$$\tilde{\theta}_{\mathcal{E}}(\boldsymbol{x}) := \frac{1/d_1(\boldsymbol{x})}{1/d_1(\boldsymbol{x}) + 1/d_2(\boldsymbol{x})}$$

for $\boldsymbol{x} \in \Omega_i \cap \Omega_j'$ and by zero everywhere else in Ω_i. At the endpoints $\boldsymbol{a}$ and $\boldsymbol{b}$, we set this function to zero. Note that this function vanishes on $\mathcal{E}_2$ and takes the required values on $\mathcal{E}$. We then define $\theta_{\mathcal{E}}^{\delta} := I^h(\tilde{\theta}_{\mathcal{E}})$.

We first note that the contribution from any element with $\boldsymbol{a}$ or $\boldsymbol{b}$ as an vertex is bounded, because the gradient of the interpolant is bounded by $1/h_i$, since all the nodal values are between 0 and 1.

We next estimate the energy over all the elements that do not intersect the endpoints and lie inside $\Omega_i \cap \Omega_j'$. We denote this region by $\mathcal{R}$. It is easy to prove that

$$|\nabla\tilde{\theta}_{\mathcal{E}}(\boldsymbol{x})| \leq \frac{1}{d_1(\boldsymbol{x}) + d_2(\boldsymbol{x})}.$$

We divide $\mathcal{R}$ into two disjoint sets, $\mathcal{R}_1 := \{\boldsymbol{x} \in \mathcal{R} : d_3(\boldsymbol{x}) \leq d_4(\boldsymbol{x})\}$, and $\mathcal{R}_2$, its complement.

First, for $\boldsymbol{x} \in \mathcal{R}_1$, we note that $d_2(\boldsymbol{x}) = d_3(\boldsymbol{x})$. Let $\boldsymbol{x}_1$ and $\boldsymbol{x}_3$ be the points on $\mathcal{E}_1$ and $\mathcal{E}_3$ closest to $\boldsymbol{x}$. We have $\delta_i \leq d(\boldsymbol{x}_1, \mathcal{E}_3) \leq |x_1 - x_3| \leq d_1(\boldsymbol{x}) + d_3(\boldsymbol{x})$ and then $|\nabla\tilde{\theta}_{\mathcal{E}}(\boldsymbol{x})| \leq 1/\delta_i$. As in [16, Section 4], we cover the set with square patches with diameters of the order of δ_i and note that on the order of $\chi_{\mathcal{E}}(\delta_i)d_{\mathcal{E}}/\delta_i$ of them will suffice. The contribution of each square is bounded, and therefore

$$\int_{\mathcal{R}_1} |\nabla\tilde{\theta}_{\mathcal{E}}(\boldsymbol{x})|^2 d\boldsymbol{x} \leq C\chi_{\mathcal{E}}(\delta_i)\frac{d_{\mathcal{E}}}{\delta_i}.$$

Second, for $\boldsymbol{x} \in \mathcal{R}_2$, we note that $d_2(\boldsymbol{x}) = d_4(\boldsymbol{x})$. Denote by $r(\boldsymbol{x})$ the minimal distance of $\boldsymbol{x}$ to $\boldsymbol{a}$ and $\boldsymbol{b}$. We claim that $d_1(\boldsymbol{x}) + d_4(\boldsymbol{x}) \geq Cr(\boldsymbol{x})$. This implies that

$$\int_{\mathcal{R}_2} |\nabla \tilde{\theta}_{\mathcal{E}}(\boldsymbol{x})|^2 d\boldsymbol{x} \leq C \int_{\mathcal{R}_2} \frac{1}{r^2(\boldsymbol{x})} d\boldsymbol{x} \leq C \log \frac{\delta_i}{h_i},$$

by using polar coordinates centered at $\boldsymbol{a}$ and $\boldsymbol{b}$. From the last two inequalities, and the fact that $|\nabla \theta^{\delta}_{\mathcal{E}}| = |\nabla I^h(\tilde{\theta}_{\mathcal{E}})| \leq C \max_{x \in K} |\nabla \tilde{\theta}_{\mathcal{E}}|$, we obtain (6.2.2).

All that is left is to show that $d_1(\boldsymbol{x}) + d_4(\boldsymbol{x}) \geq Cr(\boldsymbol{x})$ for some constant C. Without loss of generality, assume that $|\boldsymbol{x} - \boldsymbol{a}| \leq |\boldsymbol{x} - \boldsymbol{b}|$. Consider the curve $\gamma(t)$ in the Definition 4.2.1 between $\boldsymbol{x}_0$ and $\boldsymbol{a}$, and let $\boldsymbol{x}_\gamma$ be the point on γ which is closest to $\boldsymbol{x}$. By the triangle inequality and the definition of a John domain, we have that

$$r(\boldsymbol{x}) = |\boldsymbol{x} - \boldsymbol{a}| \leq |\boldsymbol{x} - \boldsymbol{x}_\gamma| + C_J dist(\boldsymbol{x}_\gamma, \mathcal{E}_1).$$

Again by the triangle inequality and the fact that $dist(\boldsymbol{x}_\gamma, \mathcal{E}_1) \leq |\boldsymbol{x}_\gamma - \boldsymbol{x}_1|$, where $\boldsymbol{x}_1$ is the point on $\mathcal{E}_1$ closest to $\boldsymbol{x}$, we obtain

$$r(\boldsymbol{x}) \leq (C_J + 1) |\boldsymbol{x} - \boldsymbol{x}_\gamma| + C_J |\boldsymbol{x} - \boldsymbol{x}_1|.$$

We notice that if $\boldsymbol{x}$ lies in the region between γ and $\mathcal{E}$, then $|\boldsymbol{x} - \boldsymbol{x}_\gamma| \leq d_4(\boldsymbol{x})$ and if not, then $|\boldsymbol{x} - \boldsymbol{x}_\gamma| \leq d_1(\boldsymbol{x})$. In both cases we can deduce that $|\boldsymbol{x} - \boldsymbol{x}_\gamma| \leq d_1(\boldsymbol{x}) + d_4(\boldsymbol{x})$. This concludes the proof of the lemma. □

From the proof of Lemma 6.2.1, we can estimate the diameter and area of $\Omega_i \cap \Omega'_j$:

Lemma 6.2.2. *For each coarse edge $\mathcal{E}^{ij} \in S_{\mathcal{E}_i}$, we have that*

$$diam(\Omega_i \cap \Omega_j') \leq C\chi_{\mathcal{E}}(\delta_i)d_{\mathcal{E}}, \text{ and}$$

$$|\Omega_i \cap \Omega_j'| \leq C\chi_{\mathcal{E}}(\delta_i)d_{\mathcal{E}}\delta_i.$$

Proof. Consider the covering by squares at the end of the proof of Lemma 6.2.1. Given two points $x, y \in \Omega_i \cap \Omega_j'$, we can join them by segments that lie in the interior of a certain number of squares. Each of these segments have a length less than $\sqrt{2}\delta_i$ and since the total number of squares is on the order of $\chi_{\mathcal{E}}(\delta_i)d_{\mathcal{E}}/\delta_i$, we can conclude that the diameter of $\Omega_i \cap \Omega_j'$ is bounded by $C\chi_{\mathcal{E}}(\delta_i)d_{\mathcal{E}}$. The second inequality follows by adding the area of all the squares that cover $\Omega_i \cap \Omega_j'$. □

6.2.3 Estimates for auxiliary functions

We start by introducing a linear interpolant for functions in $W^{h_i}_{\text{grad}}(\Omega_i)$. Consider an edge $\mathcal{E} \in S_{\mathcal{E}_i}$ with endpoints $\boldsymbol{a}$ and $\boldsymbol{b}$, and moving from $\boldsymbol{a}$ past $\boldsymbol{b}$, pick a point $\boldsymbol{c}$ on $\partial\Omega_i$, such that $|\boldsymbol{c} - \boldsymbol{b}|$ is of order $d_{\mathcal{E}}$. Consider the function $\theta_{\boldsymbol{b}\ell} \in W^{h_i}_{\text{grad}}(\Omega_i)$ constructed in [18, Lemma 2.7] for the points $\boldsymbol{a}, \boldsymbol{b}$ and $\boldsymbol{c}$. This function is uniformly bounded in Ω_i, $\theta_{\boldsymbol{b}\ell}(\boldsymbol{a}) = 0$, $\theta_{\boldsymbol{b}\ell}(\boldsymbol{b}) = 1$, and also satisfies

$$\|\nabla\theta_{\boldsymbol{b}\ell}\|^2_{L^2(\Omega_i)} \leq C, \text{ and } \nabla\theta_{\boldsymbol{b}\ell} \cdot \boldsymbol{t}_e = \frac{1}{d_{\mathcal{E}}}\boldsymbol{d}_{\mathcal{E}} \cdot \boldsymbol{t}_e$$

along $\mathcal{E}$. Using this function, we introduce our linear interpolant:

Definition 6.2.3 (linear interpolant)**.** Given $f \in W^{h_i}_{\text{grad}}(\Omega_i)$ and a subdomain edge

$\mathcal{E} \in S_{\mathcal{E}_i}$ with endpoints $\boldsymbol{a}$ and $\boldsymbol{b}$, we define the linear function

$$f^{\mathcal{E}\ell}(\boldsymbol{x}) := f(\boldsymbol{a}) + (f(\boldsymbol{b}) - f(\boldsymbol{a}))\, \theta_{\boldsymbol{b}\ell}(\boldsymbol{x}).$$

We note that $f^{\mathcal{E}\ell}(\boldsymbol{a}) = f(\boldsymbol{a})$, $f^{\mathcal{E}\ell}(\boldsymbol{b}) = f(\boldsymbol{b})$, and that

$$\nabla f^{\mathcal{E}\ell}(\boldsymbol{x}) \cdot \boldsymbol{t}_e = \frac{f(\boldsymbol{b}) - f(\boldsymbol{a})}{d_{\mathcal{E}}} \boldsymbol{d}_{\mathcal{E}} \cdot \boldsymbol{t}_e$$

along $\mathcal{E}$.

Lemma 6.2.4. *For any $p \in W^{h_i}_{grad}(\Omega_i)$, there exists a function $p^{\mathcal{E}\Delta} \in W^{h_i}_{grad}(\Omega_i)$ such that $p^{\mathcal{E}\Delta} = p - p^{\mathcal{E}\ell}$ along $\mathcal{E}$. This function vanishes along $\partial\left(\Omega_i \cap \Omega_j'\right) \setminus \mathcal{E}$ and $\partial\Omega_i \setminus \mathcal{E}$, and satisfies*

$$\|\nabla p^{\mathcal{E}\Delta}\|^2_{L^2(\Omega_i)} \leq C\chi_{\mathcal{E}}(\delta_i) \left(1 + \log \frac{\delta_i}{h_i}\right) \left(1 + \frac{d_{\mathcal{E}}}{\delta_i}\right) \left(1 + \log \frac{H_i}{h_i}\right) \|\nabla p\|^2_{L^2(\Omega_i)}$$

for some constant C depending on C_J and the shape regularity of the elements.

Proof. We define $p^{\mathcal{E}\Delta} := I^{h_i}(\theta^{\delta}_{\mathcal{E}}(p - p^{\mathcal{E}\ell}))$. We use the inequality

$$|p(\boldsymbol{b}) - p(\boldsymbol{a})|^2 \leq C \left(1 + \log \frac{H_i}{h_i}\right) \|\nabla p\|^2_{L^2(\Omega_i)},$$

which follows from Lemma 4.2.5, and since $p - p^{\mathcal{E}\ell} = (p - p(\boldsymbol{a})) - (p^{\mathcal{E}\ell} - p(\boldsymbol{a}))$, we have

$$\|p - p^{\mathcal{E}\ell}\|^2_{L^\infty\left(\Omega_i \cap \Omega_j'\right)} \leq C \left(1 + \log \frac{H_i}{h_i}\right) \|\nabla p\|^2_{L^2(\Omega_i)}.$$

Since $\nabla p^{\mathcal{E}\ell}(\boldsymbol{x}) = (p(\boldsymbol{b}) - p(\boldsymbol{a}))\, \nabla \theta_{\boldsymbol{b}\ell}(\boldsymbol{x})$, we have

$$\|\nabla p^{\mathcal{E}\ell}\|^2_{L^2\left(\Omega_i \cap \Omega_j'\right)} \leq C \left(1 + \log \frac{H_i}{h_i}\right) \|\nabla p\|^2_{L^2(\Omega_i)}.$$

From these estimates, Lemma 6.2.1 and

$$\nabla(\theta_{\mathcal{E}}^{\delta}(p-p^{\mathcal{E}\ell})) = \nabla\theta_{\mathcal{E}}^{\delta}(p-p^{\mathcal{E}\ell}) + \nabla(p-p^{\mathcal{E}\ell})\theta_{\mathcal{E}}^{\delta},$$

we find that

$$|\theta_{\mathcal{E}}^{\delta}(p-p^{\mathcal{E}\ell})|^2_{H^1(\Omega_i)} \leq C\chi_{\mathcal{E}}(\delta_i)\left(1+\log\frac{\delta_i}{h_i}\right)\left(1+\frac{d_{\mathcal{E}}}{\delta_i}\right)\left(1+\log\frac{H_i}{h_i}\right)\|\nabla p\|^2_{L^2(\Omega_i)}.$$

The result then follows by using Lemma 2.3.1. □

Lemma 6.2.5. *Given $\mathcal{E} \in S_{\mathcal{E}_i}$, there exists a coarse space function $\boldsymbol{N}_{\mathcal{E}} \in W^{h_i}_{curl}(\Omega_i)$ that vanishes in $\Omega_i \setminus \Omega_j'$, with $\boldsymbol{N}_{\mathcal{E}} \cdot \boldsymbol{t}_e = \boldsymbol{d}_{\mathcal{E}} \cdot \boldsymbol{t}_e$ along $\mathcal{E}$, and $\boldsymbol{N}_{\mathcal{E}} \cdot \boldsymbol{t}_e = 0$ everywhere else on $\partial\Omega_i$, such that*

$$\|\boldsymbol{N}_{\mathcal{E}}\|^2_{L^2(\Omega_i)} \leq C\chi_{\mathcal{E}}(\delta_i) d_{\mathcal{E}}\delta_i,$$

$$\|\nabla \times \boldsymbol{N}_{\mathcal{E}}\|^2_{L^2(\Omega_i)} \leq C\chi_{\mathcal{E}}(\delta_i)\left(1+\log\frac{\delta_i}{h_i}\right)\left(1+\frac{d_{\mathcal{E}}}{\delta_i}\right),$$

for some constant C depending on C_J and the shape regularity of the elements.

Proof. Consider the function

$$\boldsymbol{N}_{\mathcal{E}} := \Pi^{h_i}(\theta_{\mathcal{E}}^{\delta}\boldsymbol{d}_{\mathcal{E}}) + \boldsymbol{b}_{\mathcal{E}}/2,$$

where

$$\boldsymbol{b}_{\mathcal{E}} := (\boldsymbol{d}_{\mathcal{E}} \cdot \boldsymbol{t}_{e_a})\boldsymbol{N}_{e_a} + (\boldsymbol{d}_{\mathcal{E}} \cdot \boldsymbol{t}_{e_b})\boldsymbol{N}_{e_b},$$

and e_a, e_b are the two finite element edges at the ends of $\mathcal{E}$. It is easy to check that $\boldsymbol{N}_{\mathcal{E}}$ matches the specified tangential data and that it vanishes in $\Omega_i \setminus \Omega_j'$.

By using Lemmas 2.5.1 and 2.4.1, we can prove that

$$\|\boldsymbol{b}_{\mathcal{E}}\|^2_{L^2(\Omega_i)} \leq Ch_i^2,\ \|\nabla \times \boldsymbol{b}_{\mathcal{E}}\|^2_{L^2(\Omega_i)} \leq C,$$

$$\|\Pi^{h_i}(\theta^{\delta}_{\mathcal{E}}\boldsymbol{d}_{\mathcal{E}})\|^2_{L^2(\Omega_i)} \leq C\chi_{\mathcal{E}}(\delta_i)d_{\mathcal{E}}\delta_i, \text{ and}$$

$$\|\nabla \times \Pi^{h_i}(\theta^{\delta}_{\mathcal{E}}\boldsymbol{d}_{\mathcal{E}})\|^2_{L^2(\Omega_i)} \leq C\chi_{\mathcal{E}}(\delta_i)\left(1+\log\frac{\delta_i}{h_i}\right)\left(1+\frac{d_{\mathcal{E}}}{\delta_i}\right),$$

where we have also used Lemmas 6.2.1 and 6.2.2. The lemma follows by combining these inequalities. □

Lemma 6.2.6. *Given $\boldsymbol{r} \in W^{h_i}_{curl}(\Omega_i)$ and $\mathcal{E} \in S_{\mathcal{E}_i}$, there exists a function $\boldsymbol{r}^{\mathcal{E}} \in W^{h_i}_{curl}(\Omega_i)$ that vanishes in $\Omega_i \setminus \Omega'_j$, such that $\boldsymbol{r}^{\mathcal{E}} \cdot \boldsymbol{t}_e = \boldsymbol{r} \cdot \boldsymbol{t}_e$ along $\mathcal{E}$, and with vanishing tangential data along $\partial(\Omega_i \cap \Omega'_j) \setminus \mathcal{E}$ and $\partial\Omega_i \setminus \mathcal{E}$. Further,*

$$\|\boldsymbol{r}^{\mathcal{E}}\|^2_{L^2(\Omega_i)} \leq C\chi_{\mathcal{E}}(\delta_i)d_{\mathcal{E}}\delta_i\|\boldsymbol{r}\|^2_{L^\infty(\Omega_i\cap\Omega'_j)},$$

$$\|\nabla \times \boldsymbol{r}^{\mathcal{E}}\|^2_{L^2(\Omega_i)} \leq C\Bigg(\|\nabla \times \boldsymbol{r}\|^2_{L^2(\Omega_i\cap\Omega'_j)} + \\ + \chi_{\mathcal{E}}(\delta_i)\left(1+\log\frac{\delta_i}{h_i}\right)\left(1+\frac{d_{\mathcal{E}}}{\delta_i}\right)\|\boldsymbol{r}\|^2_{L^\infty(\Omega_i\cap\Omega'_j)}\Bigg),$$

for some constant C depending on C_J and the shape regularity of the elements.

Proof. We write the function $\boldsymbol{r}$ in the Nédélec basis as

$$\boldsymbol{r} = \sum_{e\in\mathcal{M}_{\overline{\Omega}_i}} r_e\boldsymbol{N}_e,$$

and define

$$\boldsymbol{r}^{\mathcal{E}} := \sum_{e \in \mathcal{M}_{\overline{\Omega}_i}} \theta_{\mathcal{E}}^{\delta,e} r_e \boldsymbol{N}_e + \left(r_{e_a}\boldsymbol{N}_{e_a} + r_{e_b}\boldsymbol{N}_{e_b}\right)/2,$$

where $\theta_{\mathcal{E}}^{\delta,e}$ is the value of $\theta_{\mathcal{E}}^{\delta}$ at the middle point of e, and e_a, e_b are the edges at the ends of $\mathcal{E}$. We have that

$$\begin{aligned}
\|r_{e_a}\boldsymbol{N}_{e_a} + r_{e_b}\boldsymbol{N}_{e_b}\|^2_{L^2(\Omega_i)} &\leq C h_i^2 \|\boldsymbol{r}\|^2_{L^\infty(\Omega_i \cap \Omega_j')}, \\
\|\nabla \times \left(r_{e_a}\boldsymbol{N}_{e_a} + r_{e_b}\boldsymbol{N}_{e_b}\right)\|^2_{L^2(\Omega_i)} &\leq C \|\boldsymbol{r}\|^2_{L^\infty(\Omega_i \cap \Omega_j')}, \\
\left\| \sum_{e \in \mathcal{M}_{\overline{\Omega}_i}} \theta_{\mathcal{E}}^{\delta,e} r_e \boldsymbol{N}_e \right\|^2_{L^2(\Omega_i)} &\leq C \|\boldsymbol{r}\|^2_{L^2(\Omega_i \cap \Omega_j')}, \text{ and}
\end{aligned}$$

$$\left\| \sum_{e \in \mathcal{M}_{\overline{\Omega}_i}} \nabla \times \theta_{\mathcal{E}}^{\delta,e} r_e \boldsymbol{N}_e \right\|^2_{L^2(\Omega_i)} \leq C \Big(\|\nabla \times \boldsymbol{r}\|^2_{L^2(\Omega_i \cap \Omega_j')} + \\ + \|\boldsymbol{r}\|^2_{L^\infty(\Omega_i \cap \Omega_j')} \|\nabla \theta_{\mathcal{E}}^{\delta}\|^2_{L^2(\Omega_i \cap \Omega_j')} \Big).$$

We conclude our proof by using Lemmas 6.2.1 and 6.2.2. □

Lemma 6.2.7. *Given $\boldsymbol{r} \in W^{h_i}_{curl}(\Omega_i)$, with Ω_i a Jones domain, and a subdomain edge $\mathcal{E} \in S_{\mathcal{E}_i}$, it holds that*

$$|\overline{r}_{\mathcal{E}}|^2 \leq C \left(\|\boldsymbol{r}\|^2_{L^\infty(\Omega_i)} + \|\nabla \times \boldsymbol{r}\|^2_{L^2(\Omega_i)} \right),$$

where

$$\overline{r}_{\mathcal{E}} := \frac{1}{d_{\mathcal{E}}} \int_{\mathcal{E}} \boldsymbol{r} \cdot \boldsymbol{t}_{\mathcal{E}} ds \tag{6.2.3}$$

and the constant C depends only on the Jones parameter $C_U(\Omega_i)$.

Proof. A similar bound is obtained in the proof of [19, Lemma 3.10] over a subset of Ω_i, from which our result follows. □

6.3 Main result

6.3.1 The coarse space component

In this section, we build an explicit function that will provide a bound for the coarse function $\boldsymbol{u}_0$ defined in (6.2.1). We consider the Helmholtz decomposition of Lemma 2.6.3 for each uniform domain Ω_i and write $\boldsymbol{u} = \nabla p_i + \boldsymbol{r}_i$. We have

$$\overline{u}_{\mathcal{E}} = \frac{p_i(\boldsymbol{b}) - p_i(\boldsymbol{a})}{d_{\mathcal{E}}} + \frac{1}{d_{\mathcal{E}}} \int_{\mathcal{E}} \boldsymbol{r}_i \cdot \boldsymbol{t}_{\mathcal{E}} \, ds. \tag{6.3.1}$$

For any edge $\mathcal{E} \in S_{\mathcal{E}_i}$, we define the function

$$\boldsymbol{w}_i^{\mathcal{E}} := \nabla p_i^{\mathcal{E}\Delta} + \boldsymbol{r}_i^{\mathcal{E}} - \overline{r}_{i\mathcal{E}} \boldsymbol{N}_{\mathcal{E}}, \tag{6.3.2}$$

where $\nabla p_i^{\mathcal{E}\Delta}$, $\boldsymbol{r}_i^{\mathcal{E}}$ and $\boldsymbol{N}_{\mathcal{E}}$ are the functions from Lemmas 6.2.4, 6.2.6 and 6.2.5 respectively, and $\overline{r}_{i\mathcal{E}}$ is given by (6.2.3). By construction, $\boldsymbol{w}_i^{\mathcal{E}}$ vanishes in $\Omega_i \setminus \Omega_j'$. We define $\boldsymbol{w}_j^{\mathcal{E}}$ over $\Omega_j \cap \Omega_i'$, similarly. We first find that

$$\begin{aligned} \boldsymbol{w}_i^{\mathcal{E}} \cdot \boldsymbol{t}_e &= \nabla p_i \cdot \boldsymbol{t}_e + \boldsymbol{r}_i \cdot \boldsymbol{t}_e - \nabla p_i^{\mathcal{E}\ell} \cdot \boldsymbol{t}_e - \overline{r}_{i\mathcal{E}} \boldsymbol{N}_{\mathcal{E}} \cdot \boldsymbol{t}_e \\ &= (\boldsymbol{u} - \boldsymbol{u}_0) \cdot \boldsymbol{t}_e \end{aligned}$$

along $\mathcal{E}$, where we have used (6.3.1) in the last step. Similarly $\boldsymbol{w}_j^{\mathcal{E}} \cdot \boldsymbol{t}_e = (\boldsymbol{u} - \boldsymbol{u}_0) \cdot \boldsymbol{t}_e$.

Hence, the function $\boldsymbol{w}^{\mathcal{E}}$ given by

$$\boldsymbol{w}^{\mathcal{E}}(\boldsymbol{x}) := \begin{cases} \boldsymbol{w}_i^{\mathcal{E}}(\boldsymbol{x}) & \text{if } \boldsymbol{x} \in \Omega_i \cap \Omega_j' \\ \boldsymbol{w}_j^{\mathcal{E}}(\boldsymbol{x}) & \text{if } \boldsymbol{x} \in \Omega_j \cap \Omega_i' \end{cases}$$

is well-defined and belongs to $W^{h_i}_{\mathrm{curl}}(\Omega)$, since its tangential data is continuous across $\mathcal{E}$ (in fact, it is equal to the tangential component of $\boldsymbol{u} - \boldsymbol{u}_0$). We note that $\boldsymbol{w}^{\mathcal{E}}$ is supported in $\Omega_i' \cap \Omega_j'$.

Finally, consider the function

$$\boldsymbol{g} := \boldsymbol{u} - \sum_{\mathcal{E} \in S_{\mathcal{E}}} \boldsymbol{w}^{\mathcal{E}}. \tag{6.3.3}$$

We find that $\boldsymbol{g} \cdot \boldsymbol{t}_e = \boldsymbol{u}_0 \cdot \boldsymbol{t}_e$ along the interface. Thus $\boldsymbol{g}$ has the same tangential data as $\boldsymbol{u}_0$ along the interface, and therefore its energy will provide an upper bound for the energy of $\boldsymbol{u}_0$, since $\boldsymbol{u}_0$ minimizes the energy for the specified boundary data.

We next find bounds for the energy of the components of $\boldsymbol{w}^{\mathcal{E}}$. First, from Lemma 6.2.4, (2.6.3a) and (2.5.1), we easily deduce that

$$\begin{aligned} a_i(\nabla p_i^{\mathcal{E}\Delta}, \nabla p_i^{\mathcal{E}\Delta}) &= \beta_i \|\nabla p_i^{\mathcal{E}\Delta}\|^2_{L^2(\Omega_i)} \\ &\leq C \chi_{\mathcal{E}}(\delta_i) \eta_i \left(1 + \log \frac{\delta_i}{h_i}\right) \left(1 + \frac{H_i}{\delta_i}\right) \left(1 + \log \frac{H_i}{h_i}\right) a_i(\boldsymbol{u}, \boldsymbol{u}), \end{aligned} \tag{6.3.4}$$

where $\eta_i := \min\left\{ \dfrac{H_i^2}{h_i^2}, 1 + \dfrac{\beta_i H_i^2}{\alpha_i} \right\}$.

For the second term of (6.3.2), we get from Lemma 6.2.6 and (2.6.3b),

$$\alpha_i \|\nabla \times \boldsymbol{r}_i^{\mathcal{E}}\|^2_{L^2(\Omega_i)} \leq C\chi_{\mathcal{E}}(\delta_i) \left(1 + \log \frac{\delta_i}{h_i}\right) \left(1 + \frac{H_i}{\delta_i}\right) \left(1 + \log \frac{H_i}{h_i}\right) a_i(\boldsymbol{u}, \boldsymbol{u}), \tag{6.3.5}$$

where we have replaced $\nabla \times \boldsymbol{r}_i$ by $\nabla \times \boldsymbol{u}$, since $\nabla \times \nabla p_i = 0$. Also,

$$\begin{aligned} \beta_i \|\boldsymbol{r}_i^{\mathcal{E}}\|^2_{L^2(\Omega_i)} &\leq C\chi_{\mathcal{E}}(\delta_i)\beta_i d_{\mathcal{E}} \delta_i \left(1 + \log \frac{H_i}{h_i}\right) \|\nabla \times \boldsymbol{u}\|^2_{L^2(\Omega_i)} \\ &\leq C\chi_{\mathcal{E}}(\delta_i)\eta_i \left(1 + \log \frac{H_i}{h_i}\right) a_i(\boldsymbol{u}, \boldsymbol{u}). \end{aligned} \tag{6.3.6}$$

From (6.3.5) and (6.3.6), we get

$$a_i(\boldsymbol{r}_i^{\mathcal{E}}, \boldsymbol{r}_i^{\mathcal{E}}) \leq C\chi_{\mathcal{E}}(\delta_i)\eta_i \left(1 + \log \frac{\delta_i}{h_i}\right) \left(1 + \frac{H_i}{\delta_i}\right) \left(1 + \log \frac{H_i}{h_i}\right) a_i(\boldsymbol{u}, \boldsymbol{u}). \tag{6.3.7}$$

Next, from Lemmas 6.2.7 and (2.6.3b),

$$\begin{aligned} |\overline{r}_{i\mathcal{E}}|^2 &\leq C \left(\|\boldsymbol{r}_i\|^2_{L^\infty(\Omega_i)} + \|\nabla \times \boldsymbol{r}_i\|^2_{L^2(\Omega_i)} \right) \\ &\leq C \left(1 + \log \frac{H_i}{h_i}\right) \|\nabla \times \boldsymbol{u}\|^2_{L^2(\Omega_i)}. \end{aligned}$$

Hence, by Lemma 6.2.5,

$$a_i(\overline{r}_{i\mathcal{E}}\boldsymbol{N}_{\mathcal{E}}, \overline{r}_{i\mathcal{E}}\boldsymbol{N}_{\mathcal{E}}) = |\overline{r}_{i\mathcal{E}}|^2 \left(\alpha_i \|\nabla \times \boldsymbol{N}_{\mathcal{E}}\|^2_{L^2(\Omega_i)} + \beta_i \|\boldsymbol{N}_{\mathcal{E}}\|^2_{L^2(\Omega_i)}\right) \\ \leq C\chi_{\mathcal{E}}(\delta_i)\eta_i \left(1 + \log\frac{\delta_i}{h_i}\right)\left(1 + \frac{H_i}{\delta_i}\right)\left(1 + \log\frac{H_i}{h_i}\right) a_i(\boldsymbol{u}, \boldsymbol{u}), \tag{6.3.8}$$

by a similar argument as in (6.3.6). From (6.3.4), (6.3.7) and (6.3.8), we conclude that

$$a_i(\boldsymbol{w}_i^{\mathcal{E}}, \boldsymbol{w}_i^{\mathcal{E}}) \leq C\chi_{\mathcal{E}}(\delta_i)\eta_i \left(1 + \log\frac{\delta_i}{h_i}\right)\left(1 + \frac{H_i}{\delta_i}\right)\left(1 + \log\frac{H_i}{h_i}\right) a_i(\boldsymbol{u}, \boldsymbol{u}). \tag{6.3.9}$$

From (6.3.3) and (6.3.9), we conclude that

$$a(\boldsymbol{u}_0, \boldsymbol{u}_0) \leq a(\boldsymbol{g}, \boldsymbol{g}) \leq C|\Xi|\chi\eta \left(1 + \log\frac{\delta}{h}\right)\left(1 + \frac{H}{\delta}\right)\left(1 + \log\frac{H}{h}\right) a(\boldsymbol{u}, \boldsymbol{u}), \tag{6.3.10}$$

where $\chi := \max_i \max_{\mathcal{E}\in S_{\mathcal{E}_i}} \chi_{\mathcal{E}}(\delta_i)$, $|\Xi|$ is the maximum number of subdomain edges for any subdomain, and $\eta := \max_i \eta_i$. We note that $\eta_i \leq 2$ for the curl-dominated case, where $\beta_i H_i^2 \leq \alpha_i$. For the mass-dominated case, where $\beta_i H_i^2 > \alpha_i$, we cannot always remove the factor η, but see Theorem 6.3.2 and Remark 6.3.3 for some comments and bounds independent on η.

6.3.2 Local subspaces

For the decomposition in local components, we write

$$\boldsymbol{u} - \boldsymbol{u}_0 = (\boldsymbol{u} - \boldsymbol{g}) + (\boldsymbol{g} - \boldsymbol{u}_0) = \sum_{\mathcal{E}\in S_{\mathcal{E}}} \boldsymbol{w}^{\mathcal{E}} + \boldsymbol{w}_r,$$

with $\boldsymbol{w}_r := \boldsymbol{g} - \boldsymbol{u}_0$. We have that $\boldsymbol{w}_r \cdot \boldsymbol{t}_e = 0$ along the interface. Thus, we can write $\boldsymbol{w}_r = \sum_{i=1}^{N} \boldsymbol{w}_{ir}$, with $\boldsymbol{w}_{ir}$ the restriction of $\boldsymbol{w}_r$ to Ω_i. We can naturally consider a zero extension for $\boldsymbol{w}_{ir}$ to Ω_i', denoted still by $\boldsymbol{w}_{ir}$, that satisfies

$$a_i'(\boldsymbol{w}_{ir}, \boldsymbol{w}_{ir}) \leq C|\Xi|\chi\eta \left(1 + \log \frac{\delta}{h}\right) \left(1 + \frac{H}{\delta}\right) \left(1 + \log \frac{H}{h}\right) a_i(\boldsymbol{u}, \boldsymbol{u}). \quad (6.3.11)$$

We write also

$$\sum_{\mathcal{E} \in S_{\mathcal{E}}} \boldsymbol{w}^{\mathcal{E}} = \sum_{i=1}^{N} \boldsymbol{w}_i^{\mathcal{E}},$$

with

$$\boldsymbol{w}_i^{\mathcal{E}} := \frac{1}{2} \sum_{\mathcal{E} \in S_{\mathcal{E}_i}} \boldsymbol{w}^{\mathcal{E}}.$$

Note that $\boldsymbol{w}_i^{\mathcal{E}}$ is supported in Ω_i' and satisfies

$$a_i'(\boldsymbol{w}_i^{\mathcal{E}}, \boldsymbol{w}_i^{\mathcal{E}}) \leq C|\Xi|\chi\eta \left(1 + \log \frac{\delta}{h}\right) \left(1 + \frac{H}{\delta}\right) \left(1 + \log \frac{H}{h}\right) (a_i(\boldsymbol{u}, \boldsymbol{u}) + a_j(\boldsymbol{u}, \boldsymbol{u})). \quad (6.3.12)$$

Therefore, we have the decomposition

$$\boldsymbol{u} = \boldsymbol{u}_0 + \sum_{i=1}^{N} \left(\boldsymbol{w}_{ir} + \boldsymbol{w}_i^{\mathcal{E}}\right),$$

and by (6.3.10), (6.3.11) and (6.3.12), we conclude that

$$C_0^2 \leq C|\Xi|\chi\eta \left(1 + \log \frac{\delta}{h}\right) \left(1 + \frac{H}{\delta}\right) \left(1 + \log \frac{H}{h}\right). \quad (6.3.13)$$

From (5.2.1) and (6.3.13), we obtain our main result:

Theorem 6.3.1. *The condition number $\kappa(P_{ad})$ of our overlapping additive two-*

level Schwarz method is bounded by

$$\kappa(P_{ad}) \leq C|\Xi|\chi\eta\left(1+\log\frac{\delta}{h}\right)\left(1+\frac{H}{\delta}\right)\left(1+\log\frac{H}{h}\right),$$

with $\chi = \max_i \max_{\mathcal{E}\in S_{\mathcal{E}_i}} \chi_{\mathcal{E}}(\delta_i)$, $\eta = \max_i\{\min\{(H_i/h_i)^2, 1+\beta_i H_i^2/\alpha_i\}\}$, *and* $|\Xi|$ *is the maximum number of subdomain edges for any subdomain. The constant* C *is independent of* h_i, H_i, δ_i *and the coefficients* α_i, β_i.

We can obtain a bound independent of the jumps in the coefficients across the interface with an additional condition:

Theorem 6.3.2. *If the mass-dominated subdomains are convex, then the condition number of our overlapping additive two-level Schwarz method is bounded by*

$$\kappa(P_{ad}) \leq C|\Xi|\chi\left(1+\log\frac{\delta}{h}\right)\left(1+\frac{H}{\delta}\right)\left(1+\log\frac{H}{h}\right), \tag{6.3.14}$$

where C *is independent of* h_i, H_i, δ_i *and the coefficients* α_i, β_i.

Proof. We can improve our result by using a stronger estimate than (2.6.3a): $\|\nabla p\|^2_{L^2(\Omega_i)} \leq C\|\boldsymbol{u}\|^2_{L^2(\Omega_i)}$; see Lemma 2.6.2. Therefore, we can simplify our estimate in (6.3.4) and can deduce (6.3.14). □

Remark 6.3.3. Numerical experiments confirm the estimates of Theorems 6.3.1 and 6.3.2. The factor η affects the condition number only when we consider some non-convex decompositions with mass-dominated subdomains ($\alpha_i \leq H_i^2\beta_i$); see Example 6.4.3. We also note that the factor $1+\log\frac{\delta}{h}$ is not relevant. Numerical results show that a small overlap gives small condition numbers for most of the decompositions considered, with the advantage that we obtain local problems in

Ω_i' without a significant increase in the size, compared with the local solvers over Ω_i.

6.4 Numerical results

Numerical examples are presented in this section to confirm the bound of Theorems 6.3.1 and 6.3.2 for four different types of subdomains shown in Figure 6.1, which have been subdivided into triangular linear edge elements. Type 1 subdomains have a square geometry, Type 2 subdomains include boundaries with a "sawtooth" shape, and for Type 3 we use equilateral triangles with edges that are part straight, part fractal. The fourth type of subdomains are obtained by the graph partitioning software METIS [38]. Our choices of subdomain geometries are similar to those of [18, Section 5]. See also [19, Section 6.1] for some implementation details.

Some numerical results for an overlapping Schwarz method with square edge elements are presented in [19, Section 6] without a theoretical bound. Here we include similar experiments and have provided an analysis. We notice that our condition numbers, in general, are smaller than those obtained in [19]. For purposes of comparison, we also present results for multiplicative and hybrid Schwarz algorithms, see Section 5.2.

For Type 1 and 2 subdomains, the ratio H/h is increased by a a factor of 2 with each additional level of mesh refinement. At the $i-$th ($i \geq 0$) level of refinement for Type 3 subdomains, $H/h = (H/H_f)3^{i+1}$, where $H/H_f = 5$ is fixed. We note that the fractal segment lengths grow by a factor of 4/3 with each mesh refinement whereas the straight line segments remain constant. For each refinement of Type

3 subdomains, every element edge on the fractal part of the boundary is first divided into three shorter edges of 1/3 the length. The middle of these edges is then replaced by two other edges with which it forms an equilateral triangle.

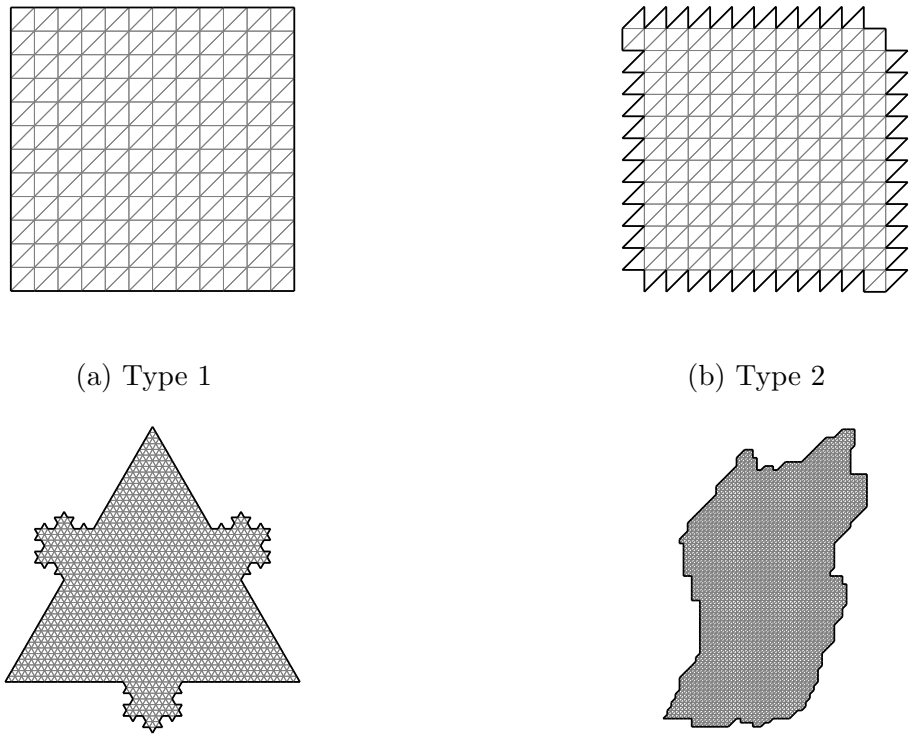

(a) Type 1

(b) Type 2

(c) Type 3

(d) Type METIS

Figure 6.1: Four types of subdomains used in the numerical examples.

We solve the resulting linear systems by using a preconditioned conjugate gradient method and random right-hand sides, to a relative residual tolerance of 10^{-8}. The number of iterations and condition number estimates (in parenthesis) are reported for each of the experiments. These estimates are obtained as mentioned in Section 1.2.

We notice that the numerical experiments for our algorithm show an improvement in the iteration count and the condition number estimates, compared to an

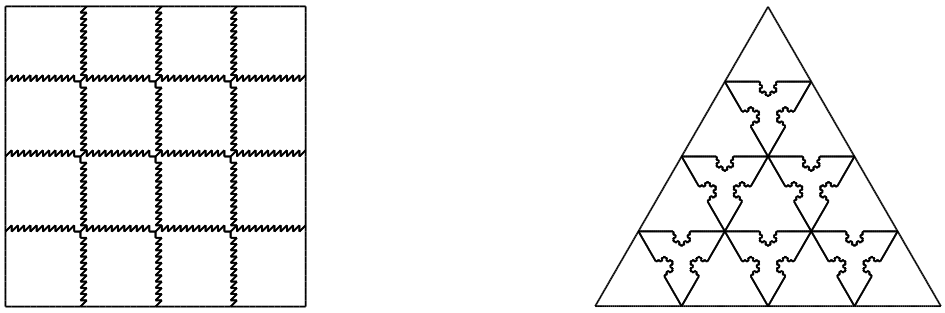

(a) Type 2 (b) Type 3

Figure 6.2: Two domain decompositions used in numerical examples for $N = 16$.

iterative substructuring method presented in [19]. Nevertheless, the BDDC algorithm with deluxe scaling considered in the next chapter gives a further significant improvement in the iteration counts and estimates. We note that the overlapping Schwarz method can be used for problems for which only the fully assembled matrix is available, while the BDDC and FETI methods require subdomain matrices corresponding to subdomains problems with natural boundary conditions.

Example 6.4.1. We verify the scalability of the algorithm for Type 1 and 2 subdomains over the unit square. As shown in Table 6.1, it is clear that the condition number is independent of the number of subdomains.

Example 6.4.2. This example is used to study the behavior of our algorithm for increasing values of H/h. We present two experiments. First, we use Type 1, 2 and 3 subdomains with constant coefficients. Second, we consider non-constant coefficients, arranged in a "checkerboard" pattern, using alternating values of 10^{-3} and 10^3 for β_i; results are shown in Table 6.2. We note that the condition number is not sensitive to the mesh parameter H/h.

Table 6.1: Results for Type 1 and 2 subdomains, where the unit square is decomposed into N subdomains, with $H/h = 4$, $H/\delta = 4$, $\alpha_i = 1$ and $\beta_i = \beta$.

Type	N	$\beta = 10^{-3}$	$\beta = 1$	$\beta = 10^3$
1	256	26(5.7)	23(5.8)	20(5.2)
	576	27(5.8)	24(5.8)	21(5.5)
	784	27(5.8)	24(5.9)	21(5.5)
	1024	27(5.8)	24(5.9)	21(5.5)
2	256	30(7.2)	26(7.3)	20(5.3)
	576	31(7.5)	28(7.6)	21(5.5)
	784	31(7.6)	28(7.7)	21(6.0)
	1024	31(7.7)	28(7.8)	22(6.4)

Table 6.2: Results for the unit square decomposed into 16 subdomains, with $\alpha_i = 1$, $\beta_i = \beta$, $H/\delta = 4$ for Type 1 and 2, and $H/\delta = 5$ for Type 3 subdomains . For the last column, β_i alternates for adjacent subdomains, taking the values 10^{-3} and 10^3 in a checkerboard configuration.

Type	H/h	$\beta = 10^{-3}$	$\beta = 1$	$\beta = 10^3$	Disc.
1	16	23(5.5)	21(5.6)	17(5.0)	20(4.8)
	32	23(5.5)	21(5.5)	17(4.8)	20(4.6)
	64	23(5.3)	22(5.4)	17(4.6)	20(4.6)
	128	23(5.4)	22(5.2)	18(4.7)	21(4.6)
2	16	24(6.3)	23(5.7)	17(5.1)	21(5.0)
	32	25(6.8)	23(5.9)	18(5.1)	22(5.1)
	64	25(6.5)	22(5.6)	18(5.1)	22(5.1)
	128	25(6.7)	23(6.1)	18(5.1)	22(5.1)
3	15	28(8.2)	26(8.0)	20(7.1)	23(7.8)
	45	28(8.0)	26(8.0)	21(7.1)	24(7.0)
	135	28(8.0)	26(8.0)	22(7.2)	24(7.1)

Example 6.4.3. This example is used to confirm the factor $(1 + H/\delta)$ in the condition number estimate. For Type 1 and 2 subdomains we use $H/h = 100$ and for Type 3 subdomains, $H/h = 135$, with $N = 16$ in all the cases. Results are shown in Table 6.3. We notice that in these examples the growth is linear, as expected. We also consider the decomposition shown in Figure 6.3. Results are presented in Table 6.4. In this case, for large values of β we observe a quadratic dependence on H/δ, but the condition numbers are in fact quite small; see Figure 6.4.

Table 6.3: Results for Type 1, 2 and 3 subdomains with 16 subdomains, $\alpha_i = 1$ and $\beta_i = \beta$. For Type 1 and 2 subdomains, $H/h = 100$; for Type 3, $H/h = 135$. See also Figure 6.4.

Type	H/δ	$\beta = 10^{-3}$	$\beta = 1$	$\beta = 10^3$
1	10	30(9.8)	26(9.9)	19(5.5)
	20	37(17.8)	35(17.6)	22(7.9)
	25	40(22.6)	38(21.1)	24(8.8)
	50	54(40.8)	52(40.7)	30(14.6)
2	10	30(10.2)	27(10.4)	21(6.7)
	20	38(17.0)	34(17.1)	23(7.6)
	25	40(19.7)	38(19.6)	24(9.1)
	50	54(34.5)	49(34.1)	29(13.4)
3	15	45(33.3)	40(31.9)	26(12.1)
	27	56(64.7)	52(57.6)	31(20.1)
	45	73(121)	67(111)	37(31.0)
	67.5	92(185)	81(203)	42(56.0)

Table 6.4: Results for domain decomposition shown in Figure 6.3, with 12 subdomains, $H/h = 96$, $\alpha_i = 1$ and $\beta_i = \beta$. See also Figure 6.4.

H/δ	$\beta = 10^{-3}$	$\beta = 10^3$
24	43(23.1)	23(7.1)
32	47(28.8)	24(9.0)
48	58(47.0)	28(14.1)
96	79(99.5)	36(39.4)

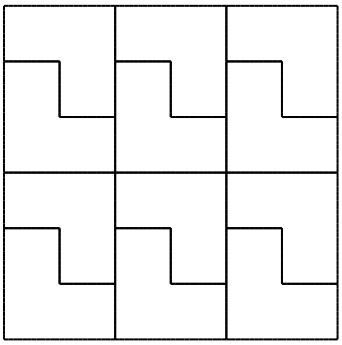

Figure 6.3: L-shaped domain decomposition used in Example 6.4.3. See also Figure 6.4 and Table 6.4.

Example 6.4.4. This example is used to confirm that the condition number estimate does not require all subdomain edges to be of comparable length. Here, the smaller subdomains shown in Figure 6.5 have only 6 elements, while the mesh parameter H/h is increased for the larger surrounding subdomains. We use $N = 16$ and $H/\delta = 4$. The results are shown in Table 6.5.

Table 6.5: Results for the unit square decomposed into 16 large and 9 small subdomains, with $H/\delta = 4$, $\alpha_i = 1$, $\beta_i = \beta$. See also Figure 6.5.

H/h	$\beta = 10^{-3}$	$\beta = 1$	$\beta = 10^{3}$
8	26(6.8)	24(7.0)	19(6.1)
16	27(7.6)	25(7.0)	20(6.1)
32	28(8.3)	25(7.1)	20(6.8)
64	27(8.3)	25(7.0)	20(6.5)
128	27(8.1)	25(7.2)	21(6.2)

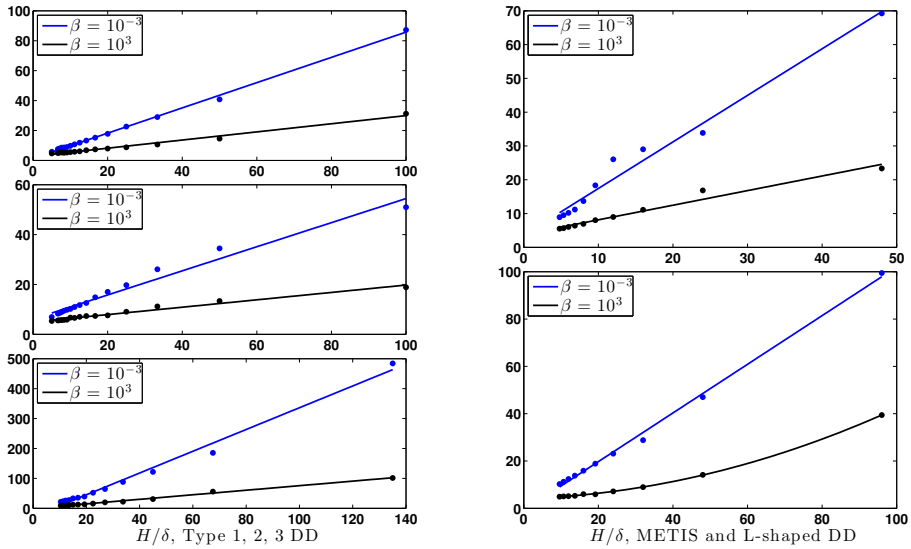

Figure 6.4: Condition number as a function of H/δ. (Left) Least-squares fit to a linear polynomial in H/δ for data in Table 6.3 for $\beta = 10^{-3}$ and $\beta = 10^{3}$. (Right) Least-squares fit to a polynomial in H/δ for a METIS and a L-shaped domain decomposition; see data in Table 6.4.

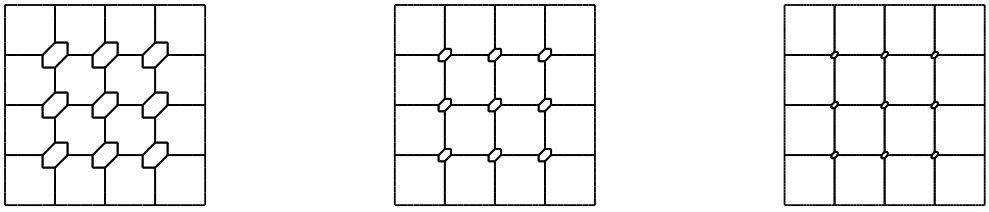

(a) $H/h = 4$ (b) $H/h = 8$ (c) $H/h = 16$

Figure 6.5: Domain decomposition used in Example 6.4.4. See also Table 6.5

Example 6.4.5. This example is used to confirm that the estimate is independent of the material property values in the subdomains. Insensitivity to jumps in material properties is evident in Table 6.6. We also include results with random coefficients, where we generate random numbers $r_{i1}, r_{i2} \in [-3, 3]$ with a uniform distribution, and assign $\alpha_i = 10^{r_{i1}}$, $\beta_i = 10^{r_{i2}}$.

Table 6.6: Results for the unit square decomposed into 256 subdomains, with $H/\delta = 8$, $H/h = 16$. For the first set of experiments, the subdomains along the diagonal have $\alpha_i = \alpha$ and $\beta_i = \beta$, while the remaining subdomains have $\alpha_i = 1$ and $\beta_i = 1$. For the second set of experiments, all the coefficients are random numbers, from 10^{-3} to 10^3.

α	β	Type 1	Type 2
10^{-3}	10^{-3}	31(11.2)	31(10.7)
10^{-3}	1	28(8.1)	27(7.7)
10^{-3}	10^3	29(8.8)	28(8.0)
1	10^{-3}	27(9.7)	27(9.9)
1	1	27(8.4)	25(7.8)
1	10^3	31(10.8)	27(8.3)
10^3	10^{-3}	27(9.6)	27(9.9)
10^3	1	27(8.4)	26(7.8)
10^3	10^3	34(11.1)	26(8.3)
α_{r_1}	β_{r_1}	30(9.1)	27(8.3)
α_{r_2}	β_{r_2}	29(8.2)	28(8.4)
α_{r_3}	β_{r_3}	29(8.1)	27(8.3)
α_{r_4}	β_{r_4}	30(9.1)	27(7.9)
α_{r_5}	β_{r_5}	29(9.1)	27(7.9)

Example 6.4.6. This example is used to demonstrate that the performance of the algorithm need not diminish significantly when a mesh partitioner is used to decompose the mesh. Example mesh decompositions for $N = 16$, $N = 64$ and $N = 144$, shown in Figure 6.6, were obtained using the graph partitioning software METIS [38]. Results are shown in Table 6.7.

Table 6.7: Comparison of results for Type 1 subdomains and subdomains generated by METIS. Material properties are homogeneous with $\alpha_i = 1$, $\beta_i = \beta$. For Type 1 subdomains, $H/h = 8$. For subdomains generated by METIS, see Figure 6.6.

Type	N	$\beta = 10^{-3}$	$\beta = 1$	$\beta = 10^{3}$
1	16	23(5.4)	21(5.5)	16(5.0)
	64	24(5.6)	22(5.4)	19(4.7)
	144	24(5.6)	22(5.5)	19(4.9)
	256	24(5.5)	23(5.5)	20(5.1)
	400	24(5.5)	23(5.5)	21(5.2)
METIS	16	27(7.1)	23(6.8)	19(5.3)
	64	33(8.8)	29(8.8)	23(5.8)
	144	35(11.4)	31(10.9)	25(7.3)
	256	36(12.2)	31(12.0)	26(7.8)
	400	38(11.2)	33(11.1)	27(8.7)

(a) $N = 64$ (b) $N = 144$

Figure 6.6: Decomposition used in Example 6.4.6, obtained with the software METIS.

Example 6.4.7. We present some results for Type 1 subdomains with the multiplicative and hybrid operators. We use GMRES [59] to solve the associated linear system in the case of the non-symmetric operator P_{mu}. Experimental results show that the symmetrized multiplicative Schwarz method ($P_{mu}^{sym} = I - E_{mu}^{*}E_{mu}$) does not offer a significant advantage. See results in Table 6.8. The multiplicative method improves considerably the number of iterations and the hybrid method behaves slightly better than the additive operator.

Table 6.8: Results for Type 1 subdomains, where the unit square is decomposed into N subdomains, with $H/h = 4$, $H/\delta = 4$, $\alpha_i = 1$ and $\beta_i = \beta$.

β	N	P_{ad}	P_{hy}	P_{mu}
10^3	144	20(5.0)	18(4.5)	4
	400	21(5.4)	19(5.1)	5
	784	21(5.5)	19(5.5)	5
	1024	21(5.5)	19(5.6)	5
1	144	23(5.8)	22(5.3)	8
	400	23(5.8)	22(5.2)	9
	784	24(5.9)	22(5.2)	9
	1024	24(5.9)	22(5.3)	9
10^{-3}	144	26(5.7)	25(4.9)	12
	400	26(5.8)	25(4.9)	12
	784	27(5.8)	25(5.0)	12
	1024	27(5.8)	25(5.0)	12

Example 6.4.8. This example is used to compare the behavior of our algorithm when the matrix

$$B = \begin{pmatrix} b_{11} & b_{12} \\ b_{12} & b_{22} \end{pmatrix}$$

in (3.1.2) is not a constant multiple of the identity. We note that our theory does not cover these cases, but that bounds depending on the eigenvalues of B can be found. First we study the variation in the condition number as a function of

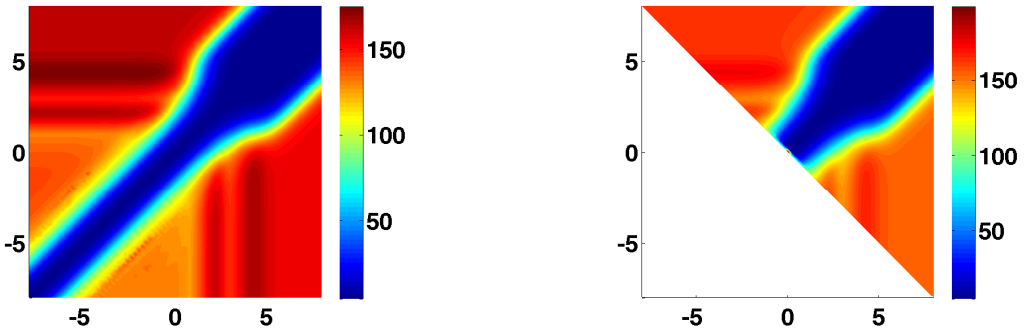

(a) $b_{12} = 0$

(b) $b_{12} = 1$

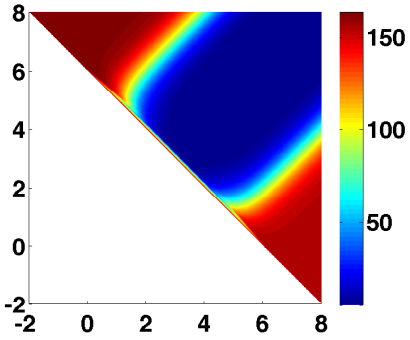

(c) $b_{12} = 10^{-3}$

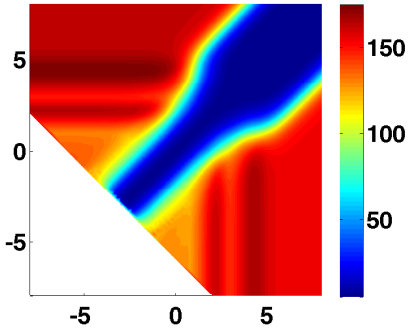

(d) $b_{12} = 10^{3}$

Figure 6.7: Condition number for different values of $\log b_{11}$ (x-axis) and $\log b_{22}$ (y-axis).

the entries of B. For this purpose, we consider Type 1 subdomains, with $N = 64$, $H/h = 8$, $H/\delta = 4$, $\alpha = 1$; see Figure 6.7. In general, the condition number slightly increases when there is a big difference between b_{11} and b_{22}, but does not vary in the extreme cases. We also notice a growth in the condition number as the number of subdomains increases. Hence, in this case our coarse space is not satisfactory and the algorithm is not scalable. Nevertheless, it only increases logarithmically, and numerical experiments show that the condition number does not deteriorates significantly, see Figure 6.8.

Example 6.4.9. This example is used to compare the behavior of our algorithm

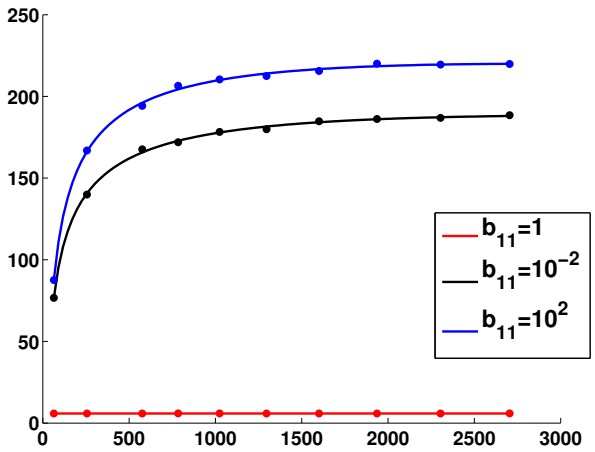

Figure 6.8: Condition number as a function of the number of subdomains, for Type 1 subdomains with $H/h = 4$, $H/\delta = 4$, $\alpha = 1$, $b_{22} = 1$, $b_{12} = b_{21} = 0$.

when there are discontinuous coefficients inside each substructure. Each subdomain is divided in two subregions: in the interior we impose $\alpha = \beta = 1$, and in the second region the coefficients are assigned randomly as in Example 6.4.5, and then these values are used for all the experiments; see Figure 6.9, Table 6.9 and Table 6.10. For this particular discontinuity pattern, results are similar for any set of random numbers. We note that our theory does not cover these cases. However, our algorithm works well even though there are discontinuities inside each subdomain. A second set of experiments is presented in Table 6.11. Here, each coefficient has four different values for each quarter of the subdomain, assigned randomly for each test; see Figure 6.10. Experimental results show that the condition number deteriorates when we have discontinuities only for β_i, as shown in Table 6.11.

Table 6.9: Results for the unit square decomposed into 64 subdomains, with $H/\delta = 8$ for Type 1 and 2, $H/\delta = 15$ for Type 3, α_i and β_i discontinuous inside each subdomain, as shown in Figure 6.9, where the width of the band is 1/4 of the subdomain diameter.

Type	H/h	$\alpha = 1$, β_i disc.	$\beta = 1$, α_i disc.	α_i, β_i disc.
1	16	29(9.3)	29(7.3)	30(8.4)
	24	30(9.4)	29(7.4)	31(8.8)
	32	30(9.5)	29(7.5)	31(9.1)
2	16	29(9.2)	28(7.2)	29(9.1)
	24	30(9.5)	28(7.5)	30(10.1)
	32	30(9.7)	29(7.7)	31(10.9)
3	15	32(21.0)	45(26.0)	30(13.2)
	45	33(23.0)	44(27.8)	30(14.7)
	135	33(24.4)	45(28.7)	32(15.1)

Table 6.10: Results for the unit square decomposed into 16 subdomains, with $H/h = 48$ for Type 1 and 2, $H/\delta = 45$ for Type 3, α_i and β_i discontinuous inside each subdomain, as shown in Figure 6.9, where the width of the band is 1/4 of the subdomain diameter.

Type	H/δ	$\alpha = 1$, β_i disc.	$\beta = 1$, α_i disc.	α_i, β_i disc.
1	3	22(5.2)	24(5.1)	23(5.4)
	6	25(6.2)	26(6.3)	27(6.9)
	24	37(17.7)	42(18.1)	38(16.7)
2	3	23(5.4)	24(5.4)	24(5.4)
	6	26(6.9)	27(6.8)	27(7.0)
	24	36(18.7)	40(16.1)	39(16.4)
3	5	27(8.7)	28(8.4)	25(6.4)
	15	32(22.7)	42(28.0)	30(14.2)
	22.5	35(25.9)	52(42.2)	33(18.0)

Table 6.11: Results for the unit square decomposed into 16 Type 1 subdomains, with $H/h = 16$, $H/\delta = 8$, α_i and β_i discontinuous inside each Ω_i and on its interface Γ_i, as shown in Figure 6.10.

Test	$\alpha = 1$, β_i disc.	$\beta = 1$, α_i disc.	α_i, β_i disc.
1	45(63)	35(14)	56(167)
2	47(34)	34(14)	45(47)
3	54(61)	35(14)	45(50)
4	42(39)	36(15)	54(217)
5	46(107)	34(14)	46(42)

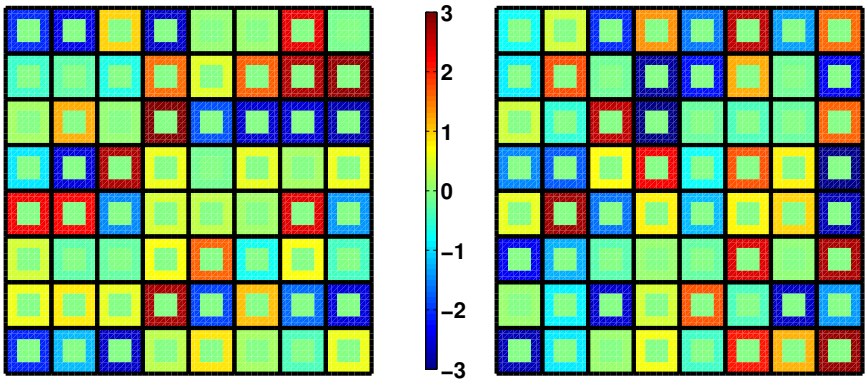

Figure 6.9: Coefficient distribution for α (left) and β (right) with Type 1 subdomains used in Example 6.4.9 for $N = 64$. The coefficients were obtained randomly, and then fixed for all the experiments. They vary from 10^{-3} (blue) to 10^{3} (red). See Tables 6.9 and 6.10.

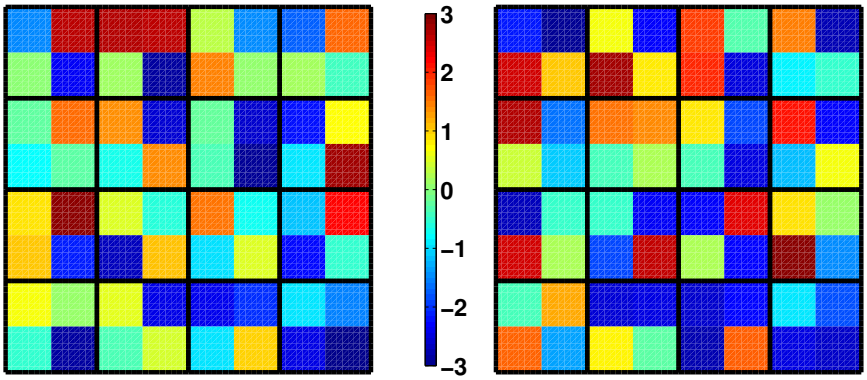

Figure 6.10: Coefficient distribution for α (left) and β (right) with Type 1 subdomains used in Example 6.4.9 for $N = 16$. The coefficients vary randomly over the 16 subdomains, from 10^{-3} (blue) to 10^{3} (red). See Table 6.11.

Chapter 7

A BDDC deluxe algorithm for Nédélec vector fields in 2D

7.1 Introduction

The BDDC method was first proposed in [15] and convergence bounds for these algorithms were provided in [47]. The BDDC methods are closely related to the dual-primal finite element tearing and interconnecting methods (FETI-DP): the spectra of the relevant operators of these two algorithms with the same set of primal constraints are the same, except possibly for eigenvalues of 0 and 1; see, e.g., [48, 45, 7].

In the construction of a BDDC preconditioner, a set of primal constraints and a weighted average need to be chosen and these choices affect the rate of convergence. For the primal variable space, we impose a continuity constraint for the tangential average over each subdomain edge; see Section 7.2 for more details.

Classical choices for the weighted average include the inverse of the cardinality

of a subdomain edge (the number of subdomains sharing the edge) and weights proportional to entries on the diagonals of subdomain matrices. A scaling that depends on the coefficients α and β is considered in [63], but with the limitation that only one coefficient is allowed to present discontinuities. We will use a deluxe average, introduced in [20] for three dimensional problems. This technique is used in [11], where a BDDC preconditioner is extended to Isogeometric Analysis for scalar elliptic problems. The bound is independent of discontinuities in the coefficients across the interface. This deluxe average is also used in [42, 54, 21].

Our study applies to a broad range of material properties and subdomain geometries. We obtain the optimal bound

$$\kappa \leq C\chi^2|\Xi| \left(1 + \log \frac{H}{h}\right)^2$$

for our deluxe BDDC method with Jones subdomains, a bound independent of the jumps of the coefficients between the subdomains. We recall that condition number estimates obtained in previous studies for equivalent FETI-DP methods depend on the coefficients of the problem, and other papers include certain restrictions on the coefficients. The constant χ is related to the geometry of the subdomains and it is quite small even for fractal edges and large values of H/h, and $|\Xi|$ represents the maximum number of neighbors for any subdomain.

7.2 Primal constraints

For $\mathcal{E} \in S_{\mathcal{E}}$, we define the coarse function $\boldsymbol{c}_{\mathcal{E}}$ similarly as in Section 6.2.1. The primal space will be spanned by these coarse basis functions, and therefore its dimension is the same as the number of interior subdomain edges.

Given $\boldsymbol{u}^{(i)} \in W^{(i)}$ and $\boldsymbol{u}^{(j)} \in W^{(j)}$, we impose the constraint

$$\int_{\mathcal{E}^{ij}} \boldsymbol{u}^{(i)} \cdot \boldsymbol{t}_{\mathcal{E}} ds = \int_{\mathcal{E}^{ij}} \boldsymbol{u}^{(j)} \cdot \boldsymbol{t}_{\mathcal{E}} ds.$$

We recall that we make a change of variables in order to work explicitly with these primal variables; see Section 5.3. The complementary dual space will then be represented by elements with zero values at the primal degrees of freedom, i.e., they will satisfy

$$\int_{\mathcal{E}} \boldsymbol{u}_{\Delta}^{(i)} \cdot \boldsymbol{t}_{\mathcal{E}} ds = 0$$

for all the subdomain edges $\mathcal{E} \in S_{\mathcal{E}_i}$.

7.3 Deluxe averaging

In this section we define the weighted operators $D^{(i)}$. For our deluxe scaling, we consider the Schur complements related to a coarse edge $\mathcal{E}^{ij}$. Let

$$A_{\mathcal{E}^{ij}}^{(k)} := \begin{pmatrix} A_{II}^{(k)} & A_{I\mathcal{E}^{ij}}^{(k)} \\ A_{\mathcal{E}^{ij}I}^{(k)} & A_{\mathcal{E}^{ij}\mathcal{E}^{ij}}^{(k)} \end{pmatrix},$$

for $k \in \{i, j\}$. The two Schur complements associated with $\mathcal{E}^{ij}$ are given by

$$S_{\mathcal{E}^{ij}}^{(k)} := A_{\mathcal{E}^{ij}\mathcal{E}^{ij}}^{(k)} - A_{\mathcal{E}^{ij}I}^{(k)} A_{II}^{(k)^{-1}} A_{I\mathcal{E}^{ij}}^{(k)}$$

for $k \in \{i, j\}$. We define the scaling matrices $D_j^{(i)} := \left(S_{\mathcal{E}^{ij}}^{(i)} + S_{\mathcal{E}^{ij}}^{(j)}\right)^{-1} S_{\mathcal{E}^{ij}}^{(i)}$. The deluxe scaling operator $D^{(i)}$ is given by

$$D^{(i)} := \begin{pmatrix} D_{j_1}^{(i)} & & & \\ & D_{j_2}^{(i)} & & \\ & & \ddots & \\ & & & D_{j_k}^{(i)} \end{pmatrix}$$

where $j_1, \ldots, j_k \in \Xi_i$, with Ξ_i the set of indices of the subdomains Ω_j, $j \neq i$, which share a subdomain edge with Ω_i. Denote by $\boldsymbol{u}_{\mathcal{E}^{ij}}^{(i)} := R_{\mathcal{E}^{ij}} \boldsymbol{u}^{(i)}$ the restriction of $\boldsymbol{u}^{(i)}$ to the edge $\mathcal{E}^{ij}$. We can rewrite the average over $\mathcal{E}^{ij}$ as

$$\overline{\boldsymbol{u}}_{\mathcal{E}^{ij}} = \left(S_{\mathcal{E}^{ij}}^{(i)} + S_{\mathcal{E}^{ij}}^{(j)}\right)^{-1} \left(S_{\mathcal{E}^{ij}}^{(i)} \boldsymbol{u}_{\mathcal{E}^{ij}}^{(i)} + S_{\mathcal{E}^{ij}}^{(j)} \boldsymbol{u}_{\mathcal{E}^{ij}}^{(j)}\right).$$

7.4 Technical tools

In this section, we collect some technical tools and define functions that will be used in the proof of our main theorem.

7.4.1 Convergence analysis

Following [11, Theorem 4.4], in order to get an estimate for $\|E_D\|_{\widetilde{S}_\Gamma}^2$, we will reduce the problem to obtaining a bound for $\|D_i^{(j)}(\boldsymbol{u}_{\mathcal{E}}^{(i)} - \boldsymbol{u}_{\Pi\mathcal{E}}^{(i)})\|_{S_{\mathcal{E}}^{(i)}}^2$, where $\boldsymbol{u}_{\Pi\mathcal{E}}^{(i)}$ is the primal component of $\boldsymbol{u}_{\Pi}^{(i)}$ restricted to the edge $\mathcal{E}$. By using the fact that $S_{\mathcal{E}}^{(i)} \left(S_{\mathcal{E}}^{(i)} + S_{\mathcal{E}}^{(j)}\right)^{-1} S_{\mathcal{E}}^{(j)}$ is symmetric and that

$$S_{\mathcal{E}}^{(i)} \left(S_{\mathcal{E}}^{(i)} + S_{\mathcal{E}}^{(j)}\right)^{-1} S_{\mathcal{E}}^{(j)} = \left(S_{\mathcal{E}}^{(i)^{-1}} + S_{\mathcal{E}}^{(j)^{-1}}\right)^{-1} < S_{\mathcal{E}}^{(i)},$$

by simple algebra we can deduce that

$$\begin{aligned}
&\|D_i^{(j)}(\boldsymbol{u}_{\mathcal{E}}^{(i)} - \boldsymbol{u}_{\Pi\mathcal{E}}^{(i)})\|^2_{S_{\mathcal{E}}^{(i)}} + \|D_j^{(i)}(\boldsymbol{u}_{\mathcal{E}}^{(i)} - \boldsymbol{u}_{\Pi\mathcal{E}}^{(i)})\|^2_{S_{\mathcal{E}}^{(j)}} \\
&\qquad = (\boldsymbol{u}_{\mathcal{E}}^{(i)} - \boldsymbol{u}_{\Pi\mathcal{E}}^{(i)})^T \Big(S_{\mathcal{E}}^{(j)} \left(S_{\mathcal{E}}^{(i)} + S_{\mathcal{E}}^{(j)} \right)^{-1} S_{\mathcal{E}}^{(i)} \left(S_{\mathcal{E}}^{(i)} + S_{\mathcal{E}}^{(j)} \right)^{-1} S_{\mathcal{E}}^{(j)} + \\
&\qquad + S_{\mathcal{E}}^{(i)} \left(S_{\mathcal{E}}^{(i)} + S_{\mathcal{E}}^{(j)} \right)^{-1} S_{\mathcal{E}}^{(j)} \left(S_{\mathcal{E}}^{(i)} + S_{\mathcal{E}}^{(j)} \right)^{-1} S_{\mathcal{E}}^{(i)} \Big) (\boldsymbol{u}_{\mathcal{E}}^{(i)} - \boldsymbol{u}_{\Pi\mathcal{E}}^{(i)}) \\
&\qquad = (\boldsymbol{u}_{\mathcal{E}}^{(i)} - \boldsymbol{u}_{\Pi\mathcal{E}}^{(i)})^T \left(S_{\mathcal{E}}^{(i)^{-1}} + S_{\mathcal{E}}^{(j)^{-1}} \right)^{-1} (\boldsymbol{u}_{\mathcal{E}}^{(i)} - \boldsymbol{u}_{\Pi\mathcal{E}}^{(i)}) \\
&\qquad \leq \|\boldsymbol{u}_{\mathcal{E}}^{(i)} - \boldsymbol{u}_{\Pi\mathcal{E}}^{(i)}\|^2_{S_{\mathcal{E}}^{(i)}}. \qquad (7.4.1)
\end{aligned}$$

Thus, we only need to obtain local bounds for the individual terms in the right-hand side. For this purpose, we will construct explicit functions with the required tangential data on $\mathcal{E}$ and a proper bound. This construction is presented in Section 7.4.4, where we closely follow [19, Section 4].

7.4.2 Discrete curl extensions

The space of discrete harmonic functions is directly related to the Schur complements. Given $\boldsymbol{u}_{\Gamma}^{(i)} \in W_{\Gamma}^{(i)}$, we define the discrete curl extension of $\boldsymbol{u}_{\Gamma}^{(i)}$ into Ω_i as $\mathcal{H}_i(\boldsymbol{u}_{\Gamma}^{(i)}) := \boldsymbol{u}^{(i)}$ where $\boldsymbol{u}^{(i)}$ satisfies

$$A_{II}^{(i)} \boldsymbol{u}_I^{(i)} + A_{I\Gamma}^{(i)} \boldsymbol{u}_{\Gamma}^{(i)} = 0.$$

Clearly $\mathcal{H}_i(\boldsymbol{u}_{\Gamma}^{(i)})$ is completely defined by the tangential data on Γ_i. We have the following lemma:

Lemma 7.4.1. *The discrete curl extension* $\boldsymbol{u}^{(i)} = \mathcal{H}_i(\boldsymbol{u}_\Gamma^{(i)})$ *into* Ω_i *satisfies*

$$a_i(\boldsymbol{u}^{(i)}, \boldsymbol{u}^{(i)}) = \min_{\boldsymbol{v}^{(i)} \times \boldsymbol{n}^{(i)} = \boldsymbol{u}_\Gamma^{(i)}} a_i(\boldsymbol{v}^{(i)}, \boldsymbol{v}^{(i)})$$

and

$$\|\boldsymbol{u}_\Gamma^{(i)}\|^2_{S_\Gamma^{(i)}} = a_i(\boldsymbol{u}^{(i)}, \boldsymbol{u}^{(i)}).$$

Proof. The proof in [66, Lemma 4.9] for $W^{h_i}_{\text{grad}}(\Omega_i)$ can be easily modified for functions in $W^{h_i}_{\text{curl}}(\Omega_i)$. □

7.4.3 Estimates for auxiliary functions

We borrow some results from [19], which are modifications from the technical tools from Chapter 6, for functions now with support $\widehat{\mathcal{R}}_\mathcal{E}$, instead of an overlapping region. We start by introducing a coarse linear interpolant for functions in $W^{h_i}_{\text{grad}}(\Omega_i)$, similar to the one in Definition 6.2.3.

Definition 7.4.2 (linear interpolant)**.** Given $f \in W^{h_i}_{\text{grad}}(\Omega_i)$ and a subdomain edge $\mathcal{E} \in S_{\mathcal{E}_i}$, we define the linear function

$$f^{\mathcal{E}\ell}(\boldsymbol{x}) := f(\boldsymbol{a}) + \frac{f(\boldsymbol{b}) - f(\boldsymbol{a})}{d_\mathcal{E}} (\boldsymbol{x} - \boldsymbol{a}) \cdot \boldsymbol{d}_\mathcal{E}.$$

We note that $f^{\mathcal{E}\ell}(\boldsymbol{a}) = f(\boldsymbol{a})$, $f^{\mathcal{E}\ell}(\boldsymbol{b}) = f(\boldsymbol{b})$ and that $f^{\mathcal{E}\ell}$ varies linearly in the direction $\boldsymbol{d}_\mathcal{E}$. We will use the following lemmas:

Lemma 7.4.3. *Let* $\widehat{\mathcal{R}}_\mathcal{E}$ *be the uniform domain of Lemma 4.2.10. For any* $p \in W^{h_i}_{grad}(\Omega_i)$*, there exists a function* $p^{\mathcal{E}\Delta} \in W^{h_i}_{grad}(\Omega_i)$ *such that* $p^{\mathcal{E}\Delta} = p - p^{\mathcal{E}\ell}$ *along*

$\mathcal{E}$. *This function vanishes along* $\partial\widehat{\mathcal{R}}_{\mathcal{E}} \setminus \mathcal{E}$ *and* $\partial\Omega_i \setminus \mathcal{E}$, *and satisfies*

$$\|\nabla p^{\mathcal{E}\Delta}\|^2_{L^2(\Omega_i)} \leq C\left(1 + \log\frac{d_{\mathcal{E}}}{h_i}\right)^2 \|\nabla p\|^2_{L^2(\widehat{\mathcal{R}}_{\mathcal{E}})},$$

for some constant C *depending on* C_U *and the shape regularity of the elements.*

Proof. The proof is similar to Lemma 6.2.4, where we also need to use Lemma 4.2.10. □

Lemma 7.4.4. *Given* $\boldsymbol{r} \in W^{h_i}_{curl}(\Omega_i)$ *and a subdomain edge* $\mathcal{E} \in S_{\mathcal{E}_i}$, *it holds that*

$$|\bar{r}_{\mathcal{E}}|^2 \leq C\left(\|\boldsymbol{r}\|^2_{L^\infty(\widehat{\mathcal{R}}_{\mathcal{E}})} + \|\nabla \times \boldsymbol{r}\|^2_{L^2(\widehat{\mathcal{R}}_{\mathcal{E}})}\right),$$

where

$$\bar{r}_{\mathcal{E}} := \frac{1}{d_{\mathcal{E}}}\int_{\mathcal{E}} \boldsymbol{r}\cdot\boldsymbol{t}_{\mathcal{E}} ds, \tag{7.4.2}$$

and the constant C *depends only on the uniform parameter* $C_U(\Omega_i)$.

Proof. This result follows from [19, Lemma 3.10] and the fact that $\mathcal{R}_{\mathcal{E}} \subset \widehat{\mathcal{R}}_{\mathcal{E}}$. □

Lemma 7.4.5. *Given* $\mathcal{E} \in S_{\mathcal{E}_i}$, *there exists a coarse space function* $\boldsymbol{N}_{\mathcal{E}} \in W^{h_i}_{curl}(\Omega_i)$ *with* $\lambda_e(\boldsymbol{N}_{\mathcal{E}}) = \lambda_e(\boldsymbol{d}_{\mathcal{E}})$ *along* $\mathcal{E}$ *and with* $\lambda_e(\boldsymbol{N}_{\mathcal{E}}) = 0$ *everywhere else on* $\partial\Omega_i$ *such that*

$$\|\boldsymbol{N}_{\mathcal{E}}\|^2_{L^2(\Omega_i)} \leq C d^2_{\mathcal{E}},$$

$$\|\nabla \times \boldsymbol{N}_{\mathcal{E}}\|^2_{L^2(\Omega_i)} \leq C\left(1 + \log\frac{d_{\mathcal{E}}}{h_i}\right),$$

for some constant C *depending on* C_U *and the shape regularity of the elements.*

Proof. The proof is similar to Lemma 6.2.5. □

Lemma 7.4.6. *Given $\boldsymbol{r} \in W^{h_i}_{curl}(\Omega_i)$ and $\mathcal{E} \in S_{\mathcal{E}_i}$, there exists a function $\boldsymbol{r}^{\mathcal{E}} \in W^{h_i}_{curl}(\Omega_i)$ such that $\lambda_e(\boldsymbol{r}^{\mathcal{E}}) = \lambda_e(\boldsymbol{r})$ along $\mathcal{E}$ and with vanishing tangential data along $\partial\widehat{\mathcal{R}}_{\mathcal{E}} \setminus \mathcal{E}$ and $\partial\Omega_i \setminus \mathcal{E}$. Further,*

$$\|\boldsymbol{r}^{\mathcal{E}}\|^2_{L^2(\Omega_i)} \leq C d^2_{\mathcal{E}} \|\boldsymbol{r}\|^2_{L^\infty(\widehat{\mathcal{R}}_{\mathcal{E}})},$$

$$\|\nabla \times \boldsymbol{r}^{\mathcal{E}}\|^2_{L^2(\Omega_i)} \leq C \left(\|\nabla \times \boldsymbol{r}\|^2_{L^2(\widehat{\mathcal{R}}_{\mathcal{E}})} + \left(1 + \log \frac{d_{\mathcal{E}}}{h_i}\right) \|\boldsymbol{r}\|^2_{L^\infty(\widehat{\mathcal{R}}_{\mathcal{E}})} \right),$$

for some constant C depending on C_U and the shape regularity of the elements.

Proof. The proof is similar to Lemma 6.2.6. □

7.4.4 A stability estimate

In this section, we will derive an edge lemma that will provide a bound for the terms in the right-hand side of (7.4.1). For that, we split the set of edges $S_{\mathcal{E}_i}$ into two subsets. We define

$$\hat{d}_i := \max\left(h_i, \sqrt{\alpha_i/\beta_i}\right)$$

and consider the two cases $d_{\mathcal{E}} < \hat{d}_i$ (curl-dominated) and $d_{\mathcal{E}} \geq \hat{d}_i$ (mass-dominated) separately. Accordingly, we partition the set of subdomain edges of Ω_i as

$$S_{\mathcal{E}_i} = S^c_{\mathcal{E}_i} \cup S^m_{\mathcal{E}_i},$$

where $d_{\mathcal{E}} < \hat{d}_i$ for all the edges in $S^c_{\mathcal{E}_i}$, and $d_{\mathcal{E}} \geq \hat{d}_i$ for those in $S^m_{\mathcal{E}_i}$. We will prove the next lemma, using a similar construction as in [19].

Lemma 7.4.7. *For $\boldsymbol{u}^{(i)} \in W^{(i)}$ and $\mathcal{E} \in S_{\mathcal{E}_i}$, there exist $\boldsymbol{v}_{\mathcal{E}}^{(i)}, \boldsymbol{v}_{\Pi\mathcal{E}}^{(i)} \in W^{(i)}$ such that*

$$\begin{cases} \lambda_e(\boldsymbol{v}_{\mathcal{E}}^{(i)}) = \lambda_e(\boldsymbol{u}^{(i)}) & \text{if } e \subset \mathcal{E} \\ \lambda_e(\boldsymbol{v}_{\mathcal{E}}^{(i)}) = 0 & \text{if } e \subset \partial\Omega_i \setminus \mathcal{E}, \end{cases} \tag{7.4.3}$$

and

$$\begin{cases} \lambda_e(\boldsymbol{v}_{\Pi\mathcal{E}}^{(i)}) = \bar{u}_{\mathcal{E}} \lambda_e(\boldsymbol{d}_{\mathcal{E}}) & \text{if } e \subset \mathcal{E} \\ \lambda_e(\boldsymbol{v}_{\Pi\mathcal{E}}^{(i)}) = 0 & \text{if } e \subset \partial\Omega_i \setminus \mathcal{E}. \end{cases} \tag{7.4.4}$$

Furthermore,

$$a_i(\boldsymbol{v}_{\mathcal{E}}^{(i)} - \boldsymbol{v}_{\Pi\mathcal{E}}^{(i)}, \boldsymbol{v}_{\mathcal{E}}^{(i)} - \boldsymbol{v}_{\Pi\mathcal{E}}^{(i)}) \leq C\chi^2 \left(1 + \log \frac{H}{h}\right)^2 a_i(\boldsymbol{u}^{(i)}, \boldsymbol{u}^{(i)}),$$

where $\chi = \max_i \max_{\mathcal{E} \in S_{\mathcal{E}_i}^m} \chi_{\mathcal{E}}(\hat{d}_i)$ and C depends only on $C_U(\Omega_i)$ and the shape regularity of the elements.

Proof. Let us first consider an edge $\mathcal{E} \in S_{\mathcal{E}_i}^c$ and its corresponding region $\widehat{\mathcal{R}}_{\mathcal{E}}$ from Lemma 4.2.10. We use the Helmholtz decomposition from Lemma 2.6.3 in this region and write $\boldsymbol{u}^{(i)} = \nabla p + \boldsymbol{r}$. Define the functions $\boldsymbol{w}^{\mathcal{E},c}, \boldsymbol{w}_{\Pi}^{\mathcal{E},c} \in W^{(i)}$ by

$$\boldsymbol{w}^{\mathcal{E},c} := \nabla p^{\mathcal{E}\Delta} + \boldsymbol{r}^{\mathcal{E}} + \frac{p(\boldsymbol{b}) - p(\boldsymbol{a})}{d_{\mathcal{E}}} \boldsymbol{N}_{\mathcal{E}} \text{ and} \tag{7.4.5}$$

$$\boldsymbol{w}_{\Pi}^{\mathcal{E},c} := \left(\frac{p(\boldsymbol{b}) - p(\boldsymbol{a})}{d_{\mathcal{E}}} + \bar{r}_{\mathcal{E}}\right) \boldsymbol{N}_{\mathcal{E}},$$

where $\nabla p^{\mathcal{E}\Delta}$, $\boldsymbol{r}^{\mathcal{E}}$ and $\boldsymbol{N}_{\mathcal{E}}$ are the functions from Lemmas 7.4.3, 7.4.6 and 7.4.5, and $\bar{r}_{\mathcal{E}}$ is given by (7.4.2). We find that $\lambda_e(\boldsymbol{w}^{\mathcal{E},c}) = \lambda_e(\boldsymbol{u}^{(i)})$ and $\lambda_e(\boldsymbol{w}_{\Pi}^{\mathcal{E},c}) = \bar{u}_{\mathcal{E}} \lambda_e(\boldsymbol{d}_{\mathcal{E}})$ along $\mathcal{E}$, and that they vanish on $\partial\Omega_i \setminus \mathcal{E}$. Hence, $\boldsymbol{w}^{\mathcal{E},c}$ and $\boldsymbol{w}_{\Pi}^{\mathcal{E},c}$ satisfy (7.4.3) and (7.4.4).

We next find bounds for the energy of the components of $\boldsymbol{w}^{\mathcal{E},c}$ and $\boldsymbol{w}_{\Pi}^{\mathcal{E},c}$. First,

from Lemma 7.4.3, (2.6.3a) and the fact that $\beta_i d_{\mathcal{E}}^2 \leq \alpha_i$ for $\mathcal{E} \in S_{\mathcal{E}_i}^c$, we obtain

$$E_i(\nabla p^{\mathcal{E}\Delta}) = \beta_i \|\nabla p^{\mathcal{E}\Delta}\|^2_{L^2(\Omega_i)} \leq C \left(1 + \log \frac{d_{\mathcal{E}}}{h_i}\right)^2 E_{\widehat{\mathcal{R}}_{\mathcal{E}}}(\boldsymbol{u}^{(i)}). \tag{7.4.6}$$

For the second term of (7.4.5), from Lemma 7.4.6 and (2.6.3b), we get

$$\begin{aligned} E_i(\boldsymbol{r}^{\mathcal{E}}) &= \alpha_i \|\nabla \times \boldsymbol{r}^{\mathcal{E}}\|^2_{L^2(\Omega_i)} + \beta_i \|\boldsymbol{r}^{\mathcal{E}}\|^2_{L^2(\Omega_i)} \\ &\leq C \left(1 + \log \frac{d_{\mathcal{E}}}{h_i}\right)^2 E_{\widehat{\mathcal{R}}_{\mathcal{E}}}(\boldsymbol{u}^{(i)}), \end{aligned} \tag{7.4.7}$$

where we have replaced $\nabla \times \boldsymbol{r}$ by $\nabla \times \boldsymbol{u}^{(i)}$, since $\nabla \times \nabla p = 0$. Next, from Lemmas 7.4.4 and (2.6.3b),

$$|\bar{r}_{\mathcal{E}}|^2 \leq C \left(1 + \log \frac{d_{\mathcal{E}}}{h_i}\right) \|\nabla \times \boldsymbol{u}^{(i)}\|^2_{L^2(\widehat{\mathcal{R}}_{\mathcal{E}})}. \tag{7.4.8}$$

Hence, by Lemma 7.4.5,

$$\begin{aligned} E_i(\bar{r}_{\mathcal{E}} \boldsymbol{N}_{\mathcal{E}}) &= |\bar{r}_{\mathcal{E}}|^2 \left(\alpha_i \|\nabla \times \boldsymbol{N}_{\mathcal{E}}\|^2_{L^2(\Omega_i)} + \beta_i \|\boldsymbol{N}_{\mathcal{E}}\|^2_{L^2(\Omega_i)}\right) \\ &\leq C \left(1 + \log \frac{d_{\mathcal{E}}}{h_i}\right)^2 E_{\widehat{\mathcal{R}}_{\mathcal{E}}}(\boldsymbol{u}^{(i)}). \end{aligned} \tag{7.4.9}$$

From (7.4.6), (7.4.7) and (7.4.9), we conclude that

$$a_i(\boldsymbol{w}^{\mathcal{E},c} - \boldsymbol{w}_{\Pi}^{\mathcal{E},c}, \boldsymbol{w}^{\mathcal{E},c} - \boldsymbol{w}_{\Pi}^{\mathcal{E},c}) \leq C \left(1 + \log \frac{d_{\mathcal{E}}}{h_i}\right)^2 E_{\widehat{\mathcal{R}}_{\mathcal{E}}}(\boldsymbol{u}^{(i)}). \tag{7.4.10}$$

We next consider an edge $\mathcal{E} \in S_{\mathcal{E}_i}^m$. We divide $\mathcal{E}$ in the following way: starting at $\boldsymbol{a}$ and moving towards $\boldsymbol{b}$, we pick $\boldsymbol{p}_1 := \boldsymbol{a}$ and then $\boldsymbol{p}_2 \in \mathcal{E}$ as the edge node closest to the last point of exit of $\mathcal{E}$ from the circular disk of radius $\hat{d}_i$ centered at

$\boldsymbol{p}_1$. Similarly, $\boldsymbol{p}_3 \in \mathcal{E}$ is chosen as the edge node closest to the last point of exit of $\mathcal{E}$ from the circular disk of radius $\hat{d}_i$ centered at $\boldsymbol{p}_2$. This process is repeated until $|\boldsymbol{p}_M - \boldsymbol{b}| < \hat{d}_i$, and we then set $\boldsymbol{p}_{M+1} = \boldsymbol{b}$. We denote the segment of $\mathcal{E}$ between $\boldsymbol{p}_k$ and $\boldsymbol{p}_{k+1}$ by $\mathcal{E}_k$. We have an M on the order of $\chi_{\mathcal{E}}(\hat{d}_i)(d_{\mathcal{E}}/\hat{d}_i)$. By construction, we have that $\hat{d}_i \leq d_{\mathcal{E}_k} \leq 2\hat{d}_i$.

For each subedge $\mathcal{E}_k$, $k = 1, \ldots, M(\mathcal{E}, \hat{d}_i)$, we consider the region $\widehat{\mathcal{R}}_{\mathcal{E}_k}$ from Lemma 4.2.10 and the corresponding Helmholtz decomposition $\boldsymbol{u}^{(i)} = \nabla p_k + \boldsymbol{r}_k$. For each term, we define $p^{\mathcal{E}_k\Delta}$, $\boldsymbol{r}^{\mathcal{E}_k}$ and $\boldsymbol{N}_{\mathcal{E}_k}$ similarly as in (7.4.5), and consider

$$\boldsymbol{w}^{\mathcal{E},m} := \sum_{k=1}^{M(\mathcal{E},\hat{d}_i)} \nabla p^{\mathcal{E}_k\Delta} + \boldsymbol{r}^{\mathcal{E}_k} + \bar{p}_{\mathcal{E}_k}\boldsymbol{N}_{\mathcal{E}_k}, \tag{7.4.11}$$

$$\boldsymbol{w}_{\Pi}^{\mathcal{E},m} := \bar{u}_{\mathcal{E}} \sum_{k=1}^{M(\mathcal{E},\hat{d}_i)} \boldsymbol{N}_{\mathcal{E}_k}, \text{ where } \bar{p}_{\mathcal{E}_k} := \frac{p(\boldsymbol{b}_k) - p(\boldsymbol{a}_k)}{d_{\mathcal{E}_k}}$$

and $\boldsymbol{a}_k$, $\boldsymbol{b}_k$ are the endpoints of $\mathcal{E}_k$. Now, $(\nabla p^{\mathcal{E}_k\Delta} + \boldsymbol{r}^{\mathcal{E}_k} + \bar{p}_{\mathcal{E}_k}\boldsymbol{N}_{\mathcal{E}_k}) \cdot \boldsymbol{t}_e = \boldsymbol{u}^{(i)} \cdot \boldsymbol{t}_e$ along $\mathcal{E}_k$. It vanishes everywhere else on $\mathcal{E}$ and therefore $\lambda_e(\boldsymbol{w}^{\mathcal{E},m}) = \lambda_e(\boldsymbol{u}^{(i)})$ along $\mathcal{E}$ and $\lambda_e(\boldsymbol{w}^{\mathcal{E},m}) = 0$ along $\partial\Omega_i \setminus \mathcal{E}$. We also obtain that $\lambda_e(\boldsymbol{w}_{\Pi}^{\mathcal{E},m}) = \bar{u}_{\mathcal{E}}\lambda_e(\boldsymbol{d}_{\mathcal{E}})$ along $\mathcal{E}$ and that $\lambda_e(\boldsymbol{w}_{\Pi}^{\mathcal{E},m}) = 0$ along $\partial\Omega_i \setminus \mathcal{E}$. Hence, the two functions satisfy (7.4.3) and (7.4.4).

By a similar argument as the one that led to (7.4.6), and using the fact that $d_{\mathcal{E}_k} \leq 2\hat{d}_i$, we obtain

$$E_i(\nabla p^{\mathcal{E}_k\Delta}) \leq C\left(1 + \log\frac{\hat{d}_i}{h_i}\right)^2 \beta_i \left(\|\boldsymbol{u}^{(i)}\|^2_{L^2(\widehat{\mathcal{R}}_{\mathcal{E}_k})} + \hat{d}_i^2\|\nabla \times \boldsymbol{u}^{(i)}\|^2_{L^2(\widehat{\mathcal{R}}_{\mathcal{E}_k})}\right).$$

From the definition of $\hat{d}_i$, we observe that if $\hat{d}_i = h_i$, we can use the inverse estimate (2.5.1) to bound the term $h_i^2\|\nabla \times \boldsymbol{u}^{(i)}\|^2_{L^2(\widehat{\mathcal{R}}_{\mathcal{E}_k})}$ by $\|\boldsymbol{u}^{(i)}\|^2_{L^2(\widehat{\mathcal{R}}_{\mathcal{E}_k})}$ and if

$\hat{d}_i = \sqrt{\alpha_i/\beta_i}$ it follows that $\beta_i \hat{d}_i^2 = \alpha_i$. In both cases, we can conclude that

$$E_i(\nabla p^{\mathcal{E}_k \Delta}) \leq C \left(1 + \log \frac{\hat{d}_i}{h_i}\right)^2 E_{\widehat{\mathcal{R}}_{\mathcal{E}_k}}(\boldsymbol{u}^{(i)}). \tag{7.4.12}$$

The bound

$$E_i(\boldsymbol{r}^{\mathcal{E}_k}) \leq C \left(1 + \log \frac{\hat{d}_i}{h_i}\right)^2 E_{\widehat{\mathcal{R}}_{\mathcal{E}_k}}(\boldsymbol{u}^{(i)}) \tag{7.4.13}$$

follows similarly as (7.4.7) by considering both cases for $\hat{d}_i$ as in (7.4.12). For the third term of (7.4.11), we have that

$$|\bar{p}_{\mathcal{E}_k}|^2 \leq \frac{C}{\hat{d}_i^2} \left(1 + \log \frac{\hat{d}_i}{h_i}\right) \left(\|\boldsymbol{u}^{(i)}\|^2_{L^2(\widehat{\mathcal{R}}_{\mathcal{E}_k})} + \hat{d}_i^2 \|\nabla \times \boldsymbol{u}^{(i)}\|^2_{L^2(\widehat{\mathcal{R}}_{\mathcal{E}_k})} \right), \tag{7.4.14}$$

where we have used Lemma 4.2.5 and (2.6.3a). By Lemma 7.4.5,

$$E_i(\boldsymbol{N}_{\mathcal{E}_k}) \leq C \beta_i \hat{d}_i^2 \left(1 + \log \frac{\hat{d}_i}{h_i}\right), \tag{7.4.15}$$

since $\alpha_i \leq \beta_i \hat{d}_i^2$. From (7.4.14) and (7.4.15), we deduce that

$$E_i(\bar{p}_{\mathcal{E}_k} \boldsymbol{N}_{\mathcal{E}_k}) \leq C \left(1 + \log \frac{\hat{d}_i}{h_i}\right)^2 \beta_i \left(\|\boldsymbol{u}^{(i)}\|^2_{L^2(\widehat{\mathcal{R}}_{\mathcal{E}_k})} + \hat{d}_i^2 \|\nabla \times \boldsymbol{u}^{(i)}\|^2_{L^2(\widehat{\mathcal{R}}_{\mathcal{E}_k})} \right).$$

By considering both cases for $\hat{d}_i$ as in (7.4.12), we obtain

$$E_i(\bar{p}_{\mathcal{E}_k} \boldsymbol{N}_{\mathcal{E}_k}) \leq C \left(1 + \log \frac{\hat{d}_i}{h_i}\right)^2 E_{\widehat{\mathcal{R}}_{\mathcal{E}_k}}(\boldsymbol{u}^{(i)}). \tag{7.4.16}$$

Now, since $\bar{u}_{\mathcal{E}} = \dfrac{1}{d_{\mathcal{E}}} \displaystyle\sum_{k=1}^{M(\mathcal{E}, \hat{d}_i)} \int_{\mathcal{E}_k} (\nabla p_k + \boldsymbol{r}_k) \cdot \boldsymbol{t}_{\mathcal{E}} \, ds$, by Cauchy-Schwarz and the

fact that $M(\mathcal{E}, \hat{d}_i)$ is of order $\chi_{\mathcal{E}}(\hat{d}_i) d_{\mathcal{E}}/\hat{d}_i$, we have

$$
\begin{aligned}
|\bar{u}_{\mathcal{E}}|^2 &\leq \frac{C}{d_{\mathcal{E}}^2} \chi_{\mathcal{E}}(\hat{d}_i) \frac{d_{\mathcal{E}}}{\hat{d}_i} \sum_{k=1}^{M(\mathcal{E},\hat{d}_i)} d_{\mathcal{E}_k}^2 \left(|\bar{p}_{\mathcal{E}_k}|^2 + |\bar{r}_{\mathcal{E}_k}|^2 \right) \\
&\leq \frac{C\chi_{\mathcal{E}}(\hat{d}_i)}{d_{\mathcal{E}} \hat{d}_i} \left(1 + \log \frac{\hat{d}_i}{h_i} \right) \sum_{k=1}^{M(\mathcal{E},\hat{d}_i)} \left(\|\boldsymbol{u}^{(i)}\|_{L^2(\widehat{\mathcal{R}}_{\mathcal{E}_k})}^2 + \hat{d}_i^2 \|\nabla \times \boldsymbol{u}^{(i)}\|_{L^2(\widehat{\mathcal{R}}_{\mathcal{E}_k})}^2 \right) \\
&\leq \frac{C\chi_{\mathcal{E}}(\hat{d}_i)}{\beta_i d_{\mathcal{E}} \hat{d}_i} \left(1 + \log \frac{\hat{d}_i}{h_i} \right) \sum_{k=1}^{M(\mathcal{E},\hat{d}_i)} E_{\widehat{\mathcal{R}}_{\mathcal{E}_k}}(\boldsymbol{u}^{(i)}) \\
&\leq \frac{C\chi_{\mathcal{E}}(\hat{d}_i)}{\beta_i d_{\mathcal{E}} \hat{d}_i} \left(1 + \log \frac{\hat{d}_i}{h_i} \right) E_{\widetilde{\mathcal{R}}_{\mathcal{E}}}(\boldsymbol{u}^{(i)}),
\end{aligned} \tag{7.4.17}
$$

with $\widetilde{\mathcal{R}}_{\mathcal{E}} = \bigcup_k \widehat{\mathcal{R}}_{\mathcal{E}_k}$. Here we have used (7.4.14) and (7.4.8) in the second step, and the fact that each $\widehat{\mathcal{R}}_{\mathcal{E}_k}$ intersects only a bounded number of other such regions in the last inequality.

From (7.4.15) and (7.4.17), we obtain

$$
E_i(\boldsymbol{w}_{\Pi}^{\mathcal{E},m}) \leq C\chi_{\mathcal{E}}^2(\hat{d}_i) \left(1 + \log \frac{\hat{d}_i}{h_i} \right)^2 E_{\widetilde{\mathcal{R}}_{\mathcal{E}}}(\boldsymbol{u}^{(i)}). \tag{7.4.18}
$$

Hence, from (7.4.12), (7.4.13), (7.4.16) and (7.4.18), we obtain

$$
a_i(\boldsymbol{w}^{\mathcal{E},m} - \boldsymbol{w}_{\Pi}^{\mathcal{E},m}, \boldsymbol{w}^{\mathcal{E},m} - \boldsymbol{w}_{\Pi}^{\mathcal{E},m}) \leq C\chi_{\mathcal{E}}^2(\hat{d}_i) \left(1 + \log \frac{\hat{d}_i}{h_i} \right)^2 E_{\widetilde{\mathcal{R}}_{\mathcal{E}}}(\boldsymbol{u}^{(i)}). \tag{7.4.19}
$$

Finally, for $\mathcal{E} \in S_{\mathcal{E}_i}$ consider the functions $\boldsymbol{v}_{\mathcal{E}}^{(i)}, \boldsymbol{v}_{\Pi\mathcal{E}}^{(i)}$ defined by

$$
\boldsymbol{v}_{\mathcal{E}}^{(i)} := \begin{cases} \boldsymbol{w}^{\mathcal{E},c} & \text{if } \mathcal{E} \in S_{\mathcal{E}_i}^c \\ \boldsymbol{w}^{\mathcal{E},m} & \text{if } \mathcal{E} \in S_{\mathcal{E}_i}^m \end{cases}, \quad \boldsymbol{v}_{\Pi\mathcal{E}}^{(i)} := \begin{cases} \boldsymbol{w}_{\Pi}^{\mathcal{E},c} & \text{if } \mathcal{E} \in S_{\mathcal{E}_i}^c \\ \boldsymbol{w}_{\Pi}^{\mathcal{E},m} & \text{if } \mathcal{E} \in S_{\mathcal{E}_i}^m \end{cases}.
$$

By (7.4.10) and (7.4.19),

$$a_i(\boldsymbol{v}_{\mathcal{E}}^{(i)} - \boldsymbol{v}_{\Pi\mathcal{E}}^{(i)}, \boldsymbol{v}_{\mathcal{E}}^{(i)} - \boldsymbol{v}_{\Pi\mathcal{E}}^{(i)}) \leq C\chi^2 \left(1 + \log \frac{H}{h}\right)^2 a_i(\boldsymbol{u}^{(i)}, \boldsymbol{u}^{(i)}).$$

These functions also satisfy conditions (7.4.3) and (7.4.4) and the lemma holds. □

Remark 7.4.8. We note that the constant C used in (2.6.3a) and (2.6.3b) is different for each region $\widehat{\mathcal{R}}_{\mathcal{E}}$ and $\widehat{\mathcal{R}}_{\mathcal{E}_k}$. This constant deteriorates for large aspect ratios, but this is not our case, due to Lemma 4.2.10.

We are now ready to prove the following edge extension lemma:

Lemma 7.4.9. *Given $\boldsymbol{u}_{\Gamma}^{(i)} = \boldsymbol{u}_{\Pi}^{(i)} + \boldsymbol{u}_{\Delta}^{(i)} \in W_{\Gamma}^{(i)}$, denote by $\boldsymbol{u}_{\mathcal{E}}^{(i)}$ and $\boldsymbol{u}_{\Pi\mathcal{E}}^{(i)}$ the restrictions of $\boldsymbol{u}_{\Gamma}^{(i)}$ and $\boldsymbol{u}_{\Pi}^{(i)}$ to the subdomain edge $\mathcal{E}$. There exists a constant C, independent of α_i, β_i, h_i and H_i, such that*

$$\|\boldsymbol{u}_{\mathcal{E}}^{(i)} - \boldsymbol{u}_{\Pi\mathcal{E}}^{(i)}\|^2_{S_{\mathcal{E}}^{(i)}} \leq C\chi^2 \left(1 + \log \frac{H}{h}\right)^2 \|\boldsymbol{u}_{\Gamma}^{(i)}\|^2_{S_{\Gamma}^{(i)}}.$$

Proof. Let $\boldsymbol{u}^{(i)} := \mathcal{H}_i(\boldsymbol{u}_{\Gamma}^{(i)})$ be the discrete curl extension of $\boldsymbol{u}_{\Gamma}^{(i)}$ over Ω_i. By Lemma 7.4.7 applied to $\boldsymbol{u}^{(i)}$, there exist $\boldsymbol{v}_{\mathcal{E}}^{(i)}$ and $\boldsymbol{v}_{\Pi\mathcal{E}}^{(i)}$ such that

$$\begin{aligned}
\|\boldsymbol{u}_{\mathcal{E}}^{(i)} - \boldsymbol{u}_{\Pi\mathcal{E}}^{(i)}\|^2_{S_{\mathcal{E}}^{(i)}} &\leq a_i(\boldsymbol{v}_{\mathcal{E}}^{(i)} - \boldsymbol{v}_{\Pi\mathcal{E}}^{(i)}, \boldsymbol{v}_{\mathcal{E}}^{(i)} - \boldsymbol{v}_{\Pi\mathcal{E}}^{(i)}) \\
&\leq C\chi^2 \left(1 + \log \frac{H}{h}\right)^2 a_i(\boldsymbol{u}^{(i)}, \boldsymbol{u}^{(i)}) \\
&= C\chi^2 \left(1 + \log \frac{H}{h}\right)^2 \|\boldsymbol{u}_{\Gamma}^{(i)}\|^2_{S_{\Gamma}^{(i)}},
\end{aligned}$$

where we have used Lemma 7.4.1 and the fact that the degrees of freedom satisfy $\lambda_e(\boldsymbol{u}_{\mathcal{E}}^{(i)}) = \lambda_e(\boldsymbol{v}_{\mathcal{E}}^{(i)})$ and $\lambda_e(\boldsymbol{u}_{\Pi\mathcal{E}}^{(i)}) = \lambda_e(\boldsymbol{v}_{\Pi\mathcal{E}}^{(i)})$ for $e \subset \partial\Omega_i$. □

7.5 Condition number for the BDDC deluxe algorithm

In this section, we present the proof of our main result, Theorem 7.5.3. The analysis is done in a similar way as in [11, Section 4].

Lemma 7.5.1. *For $\boldsymbol{u} \in \widehat{W}_\Gamma$, we have that $\boldsymbol{u}^T M_{BDDC}\boldsymbol{u} \leq \boldsymbol{u}^T \widehat{S}_\Gamma \boldsymbol{u}$. In particular, the eigenvalues of the BDDC deluxe operator are bounded from below by 1.*

Proof. Let $\boldsymbol{w} = M_{BDDC}\boldsymbol{u}$, with $\boldsymbol{u} \in \widehat{W}_\Gamma$. Using (5.3.4), we have

$$\begin{aligned}
\boldsymbol{u}^T M_{BDDC}\boldsymbol{u} = \boldsymbol{u}^T\boldsymbol{w} &= \boldsymbol{u}^T \widetilde{R}_\Gamma^T \widetilde{R}_{D,\Gamma}\boldsymbol{w} = \boldsymbol{u}^T \widetilde{R}_\Gamma^T \widetilde{S}_\Gamma \widetilde{S}_\Gamma^{-1} \widetilde{R}_{D,\Gamma}\boldsymbol{w} \\
&\leq \left(\boldsymbol{u}^T \widetilde{R}_\Gamma^T \widetilde{S}_\Gamma \widetilde{R}_\Gamma \boldsymbol{u}\right)^{1/2} \left(\boldsymbol{w}^T \widetilde{R}_{D,\Gamma}^T \widetilde{S}_\Gamma^{-1} \widetilde{S}_\Gamma \widetilde{S}_\Gamma^{-1} \widetilde{R}_{D,\Gamma}\boldsymbol{w}\right)^{1/2} \\
&= (\boldsymbol{u}^T \widehat{S}_\Gamma \boldsymbol{u})^{1/2} (\boldsymbol{u}^T M_{BDDC}\boldsymbol{u})^{1/2}.
\end{aligned}$$

Therefore $\boldsymbol{u}^T M_{BDDC}\boldsymbol{u} \leq \boldsymbol{u}^T \widehat{S}_\Gamma \boldsymbol{u}$ for all $\boldsymbol{u} \in \widehat{W}_\Gamma$ and the result follows. □

Lemma 7.5.2. *If $\|E_D\boldsymbol{u}\|^2_{\widetilde{S}_\Gamma} \leq C_E \|\boldsymbol{u}\|^2_{\widetilde{S}_\Gamma}$ for all $\boldsymbol{u} \in \widetilde{W}_\Gamma$, then the eigenvalues of the BDDC deluxe operator are bounded from above by C_E.*

Proof. Let $\boldsymbol{w} = M_{BDDC}\boldsymbol{u}$, with $\boldsymbol{u} \in \widehat{W}_\Gamma$. We have that

$$\begin{aligned}
\boldsymbol{u}^T \widehat{S}\boldsymbol{u} &= \boldsymbol{u}^T \widetilde{R}_\Gamma^T \widetilde{S}_\Gamma \widetilde{R}_\Gamma \widetilde{R}_{D,\Gamma}^T \widetilde{S}_\Gamma^{-1} \widetilde{R}_{D,\Gamma}\boldsymbol{w} \\
&\leq (\widetilde{R}_\Gamma \boldsymbol{u}, \widetilde{R}_\Gamma \boldsymbol{u})^{1/2}_{\widetilde{S}_\Gamma} \left(E_D \widetilde{S}_\Gamma^{-1} \widetilde{R}_{D,\Gamma}\boldsymbol{w}, E_D \widetilde{S}_\Gamma^{-1} \widetilde{R}_{D,\Gamma}\boldsymbol{w}\right)^{1/2}_{\widetilde{S}_\Gamma} \\
&\leq \left(\boldsymbol{u}^T \widetilde{R}_\Gamma^T \widetilde{S}_\Gamma \widetilde{R}_\Gamma \boldsymbol{u}\right)^{1/2} C_E^{1/2} \left(\widetilde{S}_\Gamma^{-1} \widetilde{R}_{D,\Gamma}\boldsymbol{w}, \widetilde{S}_\Gamma^{-1} \widetilde{R}_{D,\Gamma}\boldsymbol{w}\right)^{1/2}_{\widetilde{S}_\Gamma} \\
&= C_E^{1/2} \left(\boldsymbol{u}^T \widehat{S}_\Gamma \boldsymbol{u}\right)^{1/2} (\boldsymbol{u}^T M_{BDDC}\boldsymbol{u})^{1/2},
\end{aligned}$$

and therefore $\boldsymbol{u}^T \widehat{S}_\Gamma \boldsymbol{u} \leq C_E \boldsymbol{u}^T M_{BDDC}\boldsymbol{u}$ for all $\boldsymbol{u} \in \widehat{W}_\Gamma$. □

Theorem 7.5.3. *The condition number of the BDDC deluxe operator satisfies*

$$\kappa(M_{BDDC}^{-1}\widehat{S}) \leq C\chi^2|\Xi|\left(1+\log\frac{H}{h}\right)^2,$$

for some constant C that is independent of H, h, β and α. Here

$$\chi = \max_i \max_{\mathcal{E}\in S_{\mathcal{E}_i}^m} \chi_{\mathcal{E}}(\hat{d}_i)$$

and $|\Xi| = \max_i |\Xi_i|$ is the maximum number of subdomain edges for any subdomain.

Proof. We have that

$$\begin{aligned}
\|E_D\boldsymbol{u}_\Gamma\|^2_{\widetilde{S}_\Gamma} &\leq 2\left(\|\boldsymbol{u}_\Gamma\|^2_{\widetilde{S}_\Gamma} + \|\boldsymbol{u}_\Gamma - E_D\boldsymbol{u}_\Gamma\|^2_{\widetilde{S}_\Gamma}\right)\\
&= 2\left(\|\boldsymbol{u}_\Gamma\|^2_{\widetilde{S}_\Gamma} + \|\overline{R}_\Gamma(\boldsymbol{u}_\Gamma - E_D\boldsymbol{u}_\Gamma)\|^2_{S_\Gamma}\right)\\
&= 2\left(\|\boldsymbol{u}_\Gamma\|^2_{\widetilde{S}_\Gamma} + \sum_{i=1}^N \|\widetilde{R}_\Gamma^{(i)}(\boldsymbol{u}_\Gamma - E_D\boldsymbol{u}_\Gamma)\|^2_{S_\Gamma^{(i)}}\right).
\end{aligned}$$

Let $\boldsymbol{u}_\Gamma^{(i)} := \widetilde{R}_\Gamma^{(i)}\boldsymbol{u}_\Gamma$. Denote by $\boldsymbol{u}_{\mathcal{E}}^{(i)}$ and $\boldsymbol{u}_{\mathcal{E}}^{(j)}$ the restrictions of $\boldsymbol{u}_\Gamma^{(i)}$ and $\boldsymbol{u}_\Gamma^{(j)}$ to the common edge $\mathcal{E}$, respectively. We have that $\widetilde{R}_\Gamma^{(i)}(\boldsymbol{u}_\Gamma - E_D\boldsymbol{u}_\Gamma) = D_i^{(j)}(\boldsymbol{u}_{\mathcal{E}}^{(i)} - \boldsymbol{u}_{\mathcal{E}}^{(j)})$ on $\mathcal{E}$. Hence,

$$\|\widetilde{R}_\Gamma^{(i)}(\boldsymbol{u}_\Gamma - E_D\boldsymbol{u}_\Gamma)\|^2_{S_\Gamma^{(i)}} = \sum_{j\in\Xi_i} \|D_i^{(j)}(\boldsymbol{u}_{\mathcal{E}}^{(i)} - \boldsymbol{u}_{\mathcal{E}}^{(j)})\|^2_{S_{\mathcal{E}}^{(i)}},$$

where Ξ_i is the set of subdomain indices sharing an edge $\mathcal{E}$ with Ω_i. Then,

$$\|E_D\boldsymbol{u}_\Gamma\|^2_{\widetilde{S}_\Gamma} \leq 2\left(\|\boldsymbol{u}_\Gamma\|^2_{\widetilde{S}_\Gamma} + \sum_{\mathcal{E}\in S_{\mathcal{E}}} \|D_i^{(j)}(\boldsymbol{u}_{\mathcal{E}}^{(i)} - \boldsymbol{u}_{\mathcal{E}}^{(j)})\|^2_{S_{\mathcal{E}}^{(i)}} + \|D_j^{(i)}(\boldsymbol{u}_{\mathcal{E}}^{(j)} - \boldsymbol{u}_{\mathcal{E}}^{(i)})\|^2_{S_{\mathcal{E}}^{(j)}}\right). \tag{7.5.1}$$

Denote by $\boldsymbol{u}_{\Pi\mathcal{E}}^{(i)}$ and $\boldsymbol{u}_{\Pi\mathcal{E}}^{(j)}$ the restriction to $\mathcal{E}$ of the primal components corresponding to $\boldsymbol{u}_{\Gamma}^{(i)}$ and $\boldsymbol{u}_{\Gamma}^{(j)}$. Since $\boldsymbol{u}_{\Pi\mathcal{E}}^{(i)} = \boldsymbol{u}_{\Pi\mathcal{E}}^{(j)}$, we have that

$$\|D_i^{(j)}(\boldsymbol{u}_{\mathcal{E}}^{(i)} - \boldsymbol{u}_{\mathcal{E}}^{(j)})\|^2_{S_{\mathcal{E}}^{(i)}} \leq 2\|D_i^{(j)}(\boldsymbol{u}_{\mathcal{E}}^{(i)} - \boldsymbol{u}_{\Pi\mathcal{E}}^{(i)})\|^2_{S_{\mathcal{E}}^{(i)}} + 2\|D_i^{(j)}(\boldsymbol{u}_{\mathcal{E}}^{(j)} - \boldsymbol{u}_{\Pi\mathcal{E}}^{(j)})\|^2_{S_{\mathcal{E}}^{(i)}},$$

and by (7.4.1),

$$\|D_i^{(j)}(\boldsymbol{u}_{\mathcal{E}}^{(i)} - \boldsymbol{u}_{\mathcal{E}}^{(j)})\|^2_{S_{\mathcal{E}}^{(i)}} + \|D_j^{(i)}(\boldsymbol{u}_{\mathcal{E}}^{(j)} - \boldsymbol{u}_{\mathcal{E}}^{(i)})\|^2_{S_{\mathcal{E}}^{(j)}} \leq$$
$$2\|\boldsymbol{u}_{\mathcal{E}}^{(i)} - \boldsymbol{u}_{\Pi\mathcal{E}}^{(i)}\|^2_{S_{\mathcal{E}}^{(i)}} + 2\|\boldsymbol{u}_{\mathcal{E}}^{(j)} - \boldsymbol{u}_{\Pi\mathcal{E}}^{(j)}\|^2_{S_{\mathcal{E}}^{(j)}}. \tag{7.5.2}$$

Therefore, by combining (7.5.1), (7.5.2), and Lemma 7.4.9, we conclude that

$$\|E_D\boldsymbol{u}_{\Gamma}\|^2_{\widetilde{S}_{\Gamma}} \leq C|\Xi|\chi^2\left(1 + \log\frac{H}{h}\right)^2\|\boldsymbol{u}_{\Gamma}\|^2_{\widetilde{S}_{\Gamma}},$$

where $|\Xi| = \max_i|\Xi_i|$. We conclude the proof of the theorem by using Lemmas 7.5.1 and 7.5.2. □

7.6 Numerical results

Numerical examples are presented in this section to confirm the bound of Theorem 7.5.3 for different types of subdomains, similar to what is done in Section 6.4. We consider a new Type 4 subdomain, with edges with both straight and fractal segments. For these new subdomains, we divide the unit square into nine squares and construct a fractal edge over each initial edge on the interface. We note that the fractal segment lengths grow by a factor of 4/3 with each mesh refinement whereas the straight line segments remain constant. For each refinement

of Type 4 subdomains, every element edge on the fractal part of the boundary is first divided into three shorter edges of 1/3 the length. The middle of these edges is then replaced by two other edges with which it forms an equilateral triangle. We call the number of partitions realized over the original straight edge the order of the fractal. See Figure 7.1.

(a) Type 1 (b) Type 4

Figure 7.1: Two domain decompositions used in numerical examples.

To solve the resulting linear systems, we use a preconditioned conjugate gradient method to a relative residual tolerance of 10^{-8} with random right-hand sides. The number of iterations and maximum eigenvalues estimates (in parenthesis) are reported for each of the experiments. The condition number estimates are obtained as mentioned in Section 1.2. We approximate the condition number by the maximum eigenvalue, since the approximate value for the minimum eigenvalue is always close to 1. We note that 1 is the minimum eigenvalue of our preconditioned linear system; see e.g. [44, Lemma 6.4], [7, Lemma 3.4].

We recall that the numerical experiments for our algorithm show an improvement in the iteration count and the condition number estimates, compared to an iterative substructuring method presented in [19] and the two-level overlapping

Schwarz method considered in Chapter 6.

Example 7.6.1. We verify the scalability of our algorithm for Type 1 and 2 subdomains over the unit square. It is clear that the condition number is independent of the number of subdomains, as shown in Table 7.1.

Table 7.1: Results for Type 1 and 2 subdomains, where the unit square is decomposed into N subdomains, with $H/h = 4$, $\alpha_i = 1$ and $\beta_i = \beta$. SE is the number of subdomain edges, TE is the total number of degrees of freedom and ΓE the number of degrees of freedom on the interface. Number of iterations and condition number estimates (in parenthesis) are reported for a relative residual tolerance of 10^{-8}.

Type	N	SE	TE	ΓE	$\beta = 10^{-3}$	$\beta = 1$	$\beta = 10^{3}$
1	64	112	3008	448	9(1.5)	8(1.5)	7(1.3)
	256	480	12160	1920	9(1.5)	9(1.5)	11(1.9)
	576	1104	27456	4416	9(1.5)	9(1.5)	10(1.8)
	1024	1984	48896	7936	9(1.5)	9(1.5)	9(1.6)
2	64	161	3008	735	10(2.0)	11(2.0)	9(1.5)
	256	705	12160	3135	10(2.0)	10(2.0)	12(2.3)
	576	1633	27456	7199	10(2.0)	10(2.0)	13(3.1)
	1024	2945	48896	12927	10(1.9)	10(1.9)	13(2.4)

Example 7.6.2. This example is used to confirm the logarithmic factor in the bound of the condition number, for increasing values of H/h, with $N = 16$ subdomains. For Type 4 subdomains, we approximate H/h by $\max_i \sqrt{|\text{dof}_i|}$; see Table 7.3. We have a growth in the condition number as expected; see Figures 7.2 and 7.3. We note that our algorithm does not require all subdomain edges to be of comparable length, since Type 2 subdomains include edges both of order H_i and h_i.

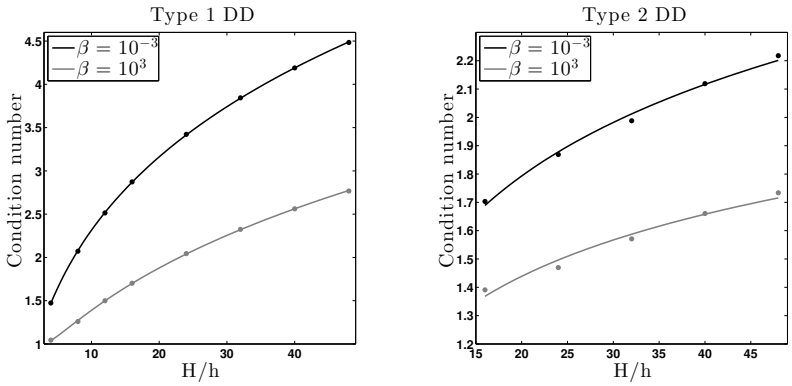

Figure 7.2: Least-squares fit to a degree 2 polynomial in $\log(H/h)$ for data of Table 7.2.

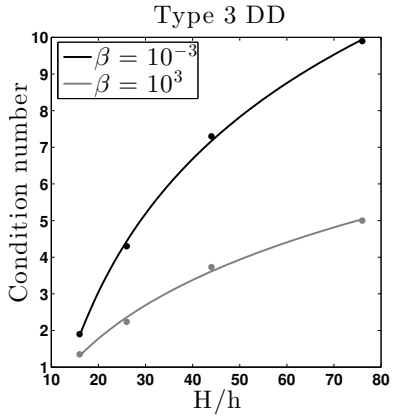

Figure 7.3: Least-squares fit to a degree 2 polynomial in $\log(H/h)$ for data of Table 7.3.

Table 7.2: Results for the unit square decomposed into 16 subdomains, with $\alpha_i = 1$, $\beta_i = \beta$. ΓE is the number of degrees of freedom on the interface, SE is 24 and 33, for Type 1 and Type 2 subdomains, respectively. See Figure 7.2.

Type	H/h	$\beta = 10^{-3}$	$\beta = 1$	$\beta = 10^{3}$	ΓE
1	16	13(2.8)	12(2.9)	8(1.7)	384
	24	14(3.4)	14(3.3)	9(2.0)	576
	32	14(3.8)	14(3.7)	10(2.3)	768
	40	16(4.2)	14(4.1)	10(2.6)	960
	48	16(4.5)	15(4.4)	10(2.8)	1152
2	16	9(1.7)	9(1.7)	8(1.4)	735
	24	10(1.9)	10(1.9)	8(1.5)	1119
	32	11(2.0)	10(2.0)	8(1.6)	1503
	40	11(2.1)	11(2.1)	8(1.7)	1887
	48	11(2.2)	11(2.2)	8(1.7)	2271

Table 7.3: Results for Type 4 subdomains, with $\alpha_i = 1$, $\beta_i = \beta$, $SE = 12$, $N = 9$. Subdomain edges are fractals. TE is the total number of degrees of freedom and ΓE is the number of degrees of freedom on the interface. The order of the fractal refers to the number of partitions realized over the original straight edge. See Figure 7.3.

Order	H/h	$\beta = 10^{-3}$	$\beta = 1$	$\beta = 10^{3}$	ΓE	TE
2	16	19(1.9)	19 (2.1)	7(1.4)	200	2821
3	26	16(4.3)	16(4.3)	10(2.2)	768	7683
4	44	18(7.3)	19 (7.3)	13(3.7)	3072	21497
5	76	22(9.9)	23(10.2)	15(5.0)	12288	58934

Example 7.6.3. This example is used to demonstrate that the performance of the algorithm need not diminish significantly when a mesh partitioner is used to decompose the mesh. Example mesh decompositions for $N = 16$, $N = 64$ and $N = 144$, shown in Figure 6.6, were obtained using the graph partitioning software METIS, see [38]. Results are shown in Table 7.4.

Table 7.4: Comparison of results for Type 1 subdomains and subdomains generated by METIS. Material properties are homogeneous with $\alpha_i = 1$, $\beta_i = \beta$. For Type 1 subdomains, $H/h = 8$. For subdomains generated by METIS, see Figure 6.6.

Type	N	$\beta = 10^{-3}$	$\beta = 1$	$\beta = 10^{3}$	ΓE
1	16	11(2.0)	11(2.0)	7(1.2)	192
	64	11(2.1)	11(2.1)	10(1.8)	896
	144	11(2.2)	11(2.1)	12(2.4)	2112
	256	11(2.1)	11(2.1)	14(3.0)	3840
	400	11(2.2)	11(2.1)	14(2.8)	6080
METIS	16	18(8.9)	18(8.8)	9(1.6)	204
	64	27(10.7)	25(10.3)	12(2.3)	963
	144	25(11.7)	25(11.7)	15(2.9)	2258
	256	25(15.0)	25(15.0)	19(4.9)	4061
	400	26(10.6)	26(10.6)	20(6.8)	6420

Example 7.6.4. This example is used to confirm that our estimate is independent of the material property values in each subdomain. Insensitivity to jumps in material properties is evident in Table 7.5. For the first set of experiments, the subdomains along the diagonal have $\alpha_i = \alpha$ and $\beta_i = \beta$, while the remaining subdomains have $\alpha_i = 1$ and $\beta_i = 1$. We also include results with random coefficients, where we generate random numbers $r_{i1}, r_{i2} \in [-3, 3]$ with a uniform distribution, and assign $\alpha_i = 10^{r_{i1}}$, $\beta_i = 10^{r_{i2}}$ for all the elements inside each subdomain Ω_i.

Table 7.5: Results for the unit square decomposed into 9 subdomains. For Type 1, $H/h = 24$, $\Gamma E = 288$, $SE = 12$. For Type 2, $H/h = 24$, $\Gamma E = 560$, $SE = 16$. For Type 3, $H/h \approx 26$, $\Gamma E = 768$, $SE = 12$ and the fractals segments have order 3.

α	β	Type 1	Type 2	Type 3
10^{-3}	10^{-3}	9(3.0)	8(1.7)	10(3.5)
10^{-3}	1	12(2.9)	9(1.8)	15(3.5)
10^{-3}	10^{3}	10(2.6)	10(2.2)	12(3.6)
1	10^{-3}	9(3.0)	8(1.7)	10(3.5)
1	1	12(3.3)	10(1.8)	16(4.3)
1	10^{3}	10(2.6)	10(2.2)	12(3.7)
10^{3}	10^{-3}	9(3.0)	8(1.7)	10(3.5)
10^{3}	1	12(3.3)	10(1.8)	16(4.3)
10^{3}	10^{3}	10(2.6)	10(2.2)	12(3.7)
α_{r_1}	β_{r_1}	11(2.8)	10(1.9)	11(4.3)
α_{r_2}	β_{r_2}	12(2.9)	11(2.3)	15(4.5)
α_{r_3}	β_{r_3}	10(3.3)	11(2.0)	12(4.3)
α_{r_4}	β_{r_4}	12(3.4)	11(2.6)	13(4.2)
α_{r_5}	β_{r_5}	9(3.0)	11(2.5)	14(4.3)

Example 7.6.5. This example is used to compare the behavior of our algorithm when there are discontinuous coefficients inside each substructure. First, the coefficients are assigned as in Figure 6.9; see Table 7.6. For this particular discontinuity pattern, results are similar for any set of random numbers. We note that our theory does not cover these cases. However, our algorithm works well even though there are discontinuities inside each subdomain. A second set of experiments is presented in Table 7.7. Here, each coefficient is assigned as in Figure 6.10. Experimental results show that the condition number deteriorates when we have discontinuities only for β_i, as shown in Table 7.7.

Table 7.6: Results for the unit square decomposed into 9 subdomains, with α_i and β_i discontinuous inside each subdomain, as shown in Figure 6.9.

Type	H/h	$\alpha = 1$, β_i disc.	$\beta = 1$, α_i disc.	α_i, β_i disc.
1	16	10(2.4)	12(2.8)	11(2.5)
	24	11(2.9)	13(3.4)	11(2.9)
	36	11(3.4)	13(4.0)	13(3.4)
2	16	9(2.5)	10(1.9)	9(2.7)
	24	10(2.7)	10(2.0)	10(2.9)
	36	11(3.1)	11(2.1)	10(3.1)
4	16	13(4.5)	15(3.2)	15(5.1)
	26	14(5.7)	15(4.1)	14(5.6)
	44	16(7.1)	16(6.1)	16(8.1)

Table 7.7: Results for the unit square decomposed into 16 Type 1 subdomains, with $H/h = 16$, α_i and β_i discontinuous inside each Ω_i and on its interface Γ_i, as shown in Figure 6.10.

Test	$\alpha = 1$, β_i disc.	$\beta = 1$, α_i disc.	α_i, β_i disc.
1	35(86)	13(2.8)	35(106)
2	52(613)	13(2.9)	37(482)
3	47(332)	13(2.8)	35(69)
4	39(119)	13(3.5)	36(64)
5	55(626)	13(2.9)	54(606)

Chapter 8

An overlapping Schwarz algorithm for Nédélec vector fields in 3D

8.1 Introduction

In this chapter, we present a new coarse space for our problem in three dimensions and some numerical results. We recall that previous studies for overlapping Schwarz methods in 3D are very restrictive about the geometry of the subdomains. To the best of our knowledge, the subdomains are usually tetrahedra or cubes, and the coarse space is the usual Nédélec space defined on the coarse grid; see, e.g., [62, 33, 35]. Results for more general subdomains were obtained in [21], where a BDDC method with deluxe scaling is analyzed.

In the next section, we introduce a new coarse space, valid for general subdomains. The two-level overlapping Schwarz algorithm with this new subspace

appears to be scalable, and independent of variations in H/h and of jumps in the coefficients across the interface, and the condition number grows quadratically as a function of H/δ, similar to the bound obtained in [62, 33].

We notice that we have tried several different approaches before, in order to obtain an scalable algorithm for irregular subdomains. The coarse space described in the following section is the only one that we have found to meet this requirement. We present some numerical results without a theoretical analysis. We note that we have some bounds for different functions that are part of a possible stable decomposition, and we hope to complete the analysis in the near future.

8.2 A coarse space

We start by defining our coarse space V_0. For each subdomain edge $\mathcal{E}$, we define a function $\boldsymbol{c}_{\mathcal{E}}$ as follows. First, we define $\lambda_e(\boldsymbol{c}_{\mathcal{E}}) = \boldsymbol{d}_{\mathcal{E}} \cdot \boldsymbol{t}_e$ for $e \subset \mathcal{E}$ and $\lambda_e(\boldsymbol{c}_{\mathcal{E}}) = 0$ for any other edge e on the wire-basket. Then, we extend these values over the faces that have $\mathcal{E}$ on its boundary. For this purpose, let $\mathcal{F}^{ij}$ be a face that has $\mathcal{E}$ on its boundary, and consider the local matrices $A^{(i)}$ and $A^{(j)}$, where we partition the degrees of freedom as

$$A^{(k)} = \begin{pmatrix} A^{(k)}_{\mathcal{C},\mathcal{C}} & A^{(k)}_{\mathcal{C},\mathcal{F}} & A^{(k)}_{\mathcal{C},\partial\mathcal{F}} \\ A^{(k)}_{\mathcal{F},\mathcal{C}} & A^{(k)}_{\mathcal{F},\mathcal{F}} & A^{(k)}_{\mathcal{F},\partial\mathcal{F}} \\ A^{(k)}_{\partial\mathcal{F},\mathcal{C}} & A^{(k)}_{\partial\mathcal{F},\mathcal{F}} & A^{(k)}_{\partial\mathcal{F},\partial\mathcal{F}} \end{pmatrix},$$

for $k \in \{i, j\}$. Here, $\mathcal{C}$ represents the degrees of freedom in the complement of the closure of the face. We then define

$$S^{(k)}_{\mathcal{F},\mathcal{F}} := A^{(k)}_{\mathcal{F},\mathcal{F}} - A^{(k)}_{\mathcal{F},\mathcal{C}} {A^{(k)}_{\mathcal{C},\mathcal{C}}}^{-1} A^{(k)}_{\mathcal{C},\mathcal{F}},$$

and

$$S^{(k)}_{\mathcal{F},\partial\mathcal{F}} := A^{(k)}_{\mathcal{F},\partial\mathcal{F}} - A^{(k)}_{\mathcal{F},\mathcal{C}} {A^{(k)}_{\mathcal{C},\mathcal{C}}}^{-1} A^{(k)}_{\mathcal{C},\partial\mathcal{F}}.$$

These two matrices are blocks of the Schur complement of $A^{(k)}$ after that all the degrees of freedom in the complement of the closure of the face are eliminated. We then define the degrees of freedom for the face as

$$\boldsymbol{u}_{\mathcal{F}} := -\left(S^{(i)}_{\mathcal{F},\mathcal{F}} + S^{(j)}_{\mathcal{F},\mathcal{F}}\right)^{-1} \left(S^{(i)}_{\mathcal{F},\partial\mathcal{F}} + S^{(j)}_{\mathcal{F},\partial\mathcal{F}}\right) \boldsymbol{u}_{\partial\mathcal{F}}.$$

We note that $\boldsymbol{u}_{\mathcal{F}}$ can be computed by solving a problem in $\Omega_i \cup \Omega_j$. Finally, we extend the values on the boundary of the subdomains harmonically into the interiors of the subdomains, given the values over each local interface Γ_i.

8.3 Numerical Results

We present some numerical results for our two-level overlapping additive algorithm. We consider a Type 1 decomposition, where the subdomains are cubes, and a METIS decomposition (see Figure 8.1).

We solve the resulting linear systems using a preconditioned conjugate gradient method and random right-hand sides, to a relative residual tolerance of 10^{-6}. The number of iterations and condition number estimates (in parenthesis) are reported for each of the experiments. These estimates are obtained as mentioned in Section

1.2.

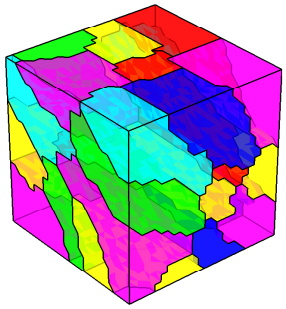

(a) Decomposition

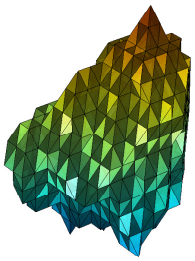

(b) Subdomain

Figure 8.1: Domain decomposition obtained by METIS for the unit cube, $N = 27$.

Example 8.3.1. We verify the scalability of our algorithm for Type 1 and METIS subdomains over the unit cube. It is clear that the condition number is independent of the number of subdomains, as shown in Table 8.1.

Table 8.1: Results for the unit cube decomposed into N subdomains, with $\alpha_i = 1$, $\beta_i = \beta$, $H/h = 8$, $H/\delta = 4$.

Type	N	$\beta = 10^{-3}$	$\beta = 1$	$\beta = 10^3$	dof	$faces$	$edges$
1	3^3	23(10.3)	24(10.5)	18(9.4)	102024	54	36
	4^3	24(10.5)	25(10.9)	19(9.2)	238688	144	108
	5^3	24(10.6)	25(10.9)	21(9.2)	462520	300	240
	6^3	24(10.3)	25(10.8)	21(9.1)	795024	540	450
METIS	3^3	26(10.5)	26(10.8)	18(7.3)	102024	101	126
	4^3	28(12.2)	28(12.3)	19(7.5)	238688	287	389
	5^3	29(12.3)	30(14.5)	22(8.4)	462520	657	951
	6^3	29(12.4)	30(14.7)	22(8.5)	795024	1210	1804

Example 8.3.2. This example is used to study the behavior of our algorithm for increasing values of H/h; see results in Table 8.2. We note that the condition number is not sensitive to the mesh parameter H/h.

Table 8.2: Results for the unit cube decomposed into 64 Type 1 and METIS subdomains, with $\alpha_i = 1$, $\beta_i = \beta$, $H/\delta = 4$.

Type	H/h	$\beta = 10^{-3}$	$\beta = 1$	$\beta = 10^{3}$	$\lvert dof \rvert$	faces	edges
1	4	22(10.2)	24(11.4)	18(9.4)	31024	144	108
	8	24(10.5)	25(10.9)	19(9.2)	238688	144	108
	12	25(10.7)	26(11.0)	20(9.3)	795024	144	108
METIS	4	29(13.5)	30(16.2)	20(8.5)	31024	291	387
	8	28(12.2)	28(12.3)	19(7.5)	238688	287	389
	12	29(13.1)	29(12.9)	20(8.7)	795024	300	418

Example 8.3.3. This example is used to study the behavior of our algorithm for increasing values of H/δ; see results in Table 8.3. Numerical results suggest a quadratic growth of the condition number as a function of H/δ.

Table 8.3: Results for the unit cube decomposed into 27 Type 1 and METIS subdomains, with $\alpha_i = 1$, $\beta_i = \beta$, $H/h = 12$.

Type	H/δ	$\beta = 10^{-3}$	$\beta = 1$	$\beta = 10^{3}$
1	3	23(9.8)	24(9.7)	18(8.5)
	4	24(10.4)	25(10.8)	19(9.9)
	6	26(12.9)	27(12.9)	19(8.6)
	12	31(24.9)	32(26.0)	21(10.4)
METIS	3	26(9.9)	26(9.9)	20(7.9)
	4	27(11.0)	27(10.9)	19(7.6)
	6	29(13.1)	30(13.8)	19(7.3)
	12	36(20.3)	38(24.4)	20(8.0)

Example 8.3.4. This example is used to study the behavior of our algorithm for discontinuous coefficients. Results are shown in Table 8.4. We include results with random coefficients, where we generate random numbers $r_{i1}, r_{i2} \in [-3, 3]$ with a uniform distribution, and assign $\alpha_i = 10^{r_{i1}}$, $\beta_i = 10^{r_{i2}}$ for all the elements inside each subdomain Ω_i.

Table 8.4: Results for the unit cube decomposed into 64 subdomains, with $H/h = 8$, $H/\delta = 4$.

α	β	Type 1	METIS
10^{-3}	10^{-3}	22(8.6)	25(9.7)
10^{-3}	1	22(8.6)	25(9.6)
10^{-3}	10^{3}	19(8.3)	20(7.1)
1	10^{-3}	23(10.4)	26(10.4)
1	1	24(10.5)	26(10.8)
1	10^{3}	21(9.4)	22(8.6)
10^{3}	10^{-3}	23(9.0)	26(10.3)
10^{3}	1	25(10.8)	27(10.2)
10^{3}	10^{3}	23(8.5)	24(8.7)
α_{r_1}	β_{r_1}	30(12.3)	30(12.2)
α_{r_2}	β_{r_2}	26(10.9)	29(11.2)
α_{r_3}	β_{r_3}	27(10.5)	28(11.1)
α_{r_4}	β_{r_4}	30(12.0)	28(11.2)
α_{r_5}	β_{r_5}	29(11.8)	29(10.2)

Bibliography

[1] D. N. Arnold, R. S. Falk, and R. Winther, *Multigrid in H(div) and H(curl)*, Numer. Math. **85** (2000), no. 2, 197–217.

[2] R. Beck, R. Hiptmair, R. H. W. Hoppe, and B. Wohlmuth, *Residual based a posteriori error estimators for eddy current computation*, ESAIM: Math. Model. Numer. Anal. **34** (2000), 159–182.

[3] B. Bojarski, *Remarks on Sobolev imbedding inequalities*, Lecture Notes in Math. **1351** (1989), 52–68.

[4] A. Bossavit, *Discretization of electromagnetic problems: The generalized finite differences approach*, Handb. Numer. Anal. **13** (2005), 105–197.

[5] D. Braess, *Finite elements: Theory, fast solvers, and applications in solid mechanics*, Cambridge University Press, 2001.

[6] S. C. Brenner and R. Scott, *The mathematical theory of finite element methods*, Texts in Applied Mathematics, Springer, 2008.

[7] S. C. Brenner and L.-Y. Sung, *BDDC and FETI-DP without matrices or vectors*, Comput. Methods Appl. Mech. Engrg. **196** (2007), 1429 – 1435.

[8] S. M. Buckley and P. Koskela, *Sobolev-Poincaré implies John*, Math. Res. Lett. **2** (1995), 577–593.

[9] J. G. Calvo, *A two-level overlapping Schwarz method for H(curl) in two dimensions for irregular subdomains*, Tech. Report TR2014-968, Courant Institute, NYU, 2014. Submitted to ETNA.

[10] ———, *A BDDC algorithm with deluxe scaling for H(curl) in two dimensions with irregular subdomains*, Tech. Report TR2014-964, Courant Institute, NYU, 2014. To appear in Math. Comp.

[11] L. Beirão da Veiga, L. F. Pavarivo, S. Scacchi, O.B. Widlund, and S. Zampini, *Isogeometric BDDC preconditioners with deluxe scaling*, SIAM J. Sci. Comput. **36** (2014), A1118–A1139.

[12] R. Dautray and J.-L. Lions, *Mathematical analysis and numerical methods for science and technology. Vol. 2*, Springer-Verlag, Berlin, 1988.

[13] ———, *Mathematical analysis and numerical methods for science and technology. Vol. 1*, Springer-Verlag, Berlin, 1990.

[14] T. A. Davis, *Direct Methods for Sparse Linear Systems (Fundamentals of Algorithms 2)*, Society for Industrial and Applied Mathematics, Philadelphia, PA, USA, 2006.

[15] C. R. Dohrmann, *A preconditioner for substructuring based on constrained energy minimization*, SIAM J. Sci. Comput. **25** (2003), 246–258.

[16] C. R. Dohrmann, A. Klawonn, and O. B. Widlund, *Domain decomposition for less regular subdomains: Overlapping Schwarz in two dimensions*, SIAM J. Numer. Anal. **46** (2008), 2153–2168.

[17] C. R. Dohrmann and O. B. Widlund, *An overlapping Schwarz algorithm for almost incompressible elasticity*, SIAM J. Numer. Anal. **47** (2009), 2897–2923.

[18] ———, *An alternative coarse space for irregular subdomains and an overlapping Schwarz algorithm for scalar elliptic problems in the plane*, SIAM J. Numer. Anal. **50** (2012), 2522–2537.

[19] ———, *An iterative substructuring algorithm for two-dimensional problems in $H(curl)$*, SIAM J. Numer. Anal. **50** (2012), 1004–1028.

[20] ———, *Some Recent Tools and a BDDC Algorithm for 3D Problems in H(curl)*, Domain Decomposition Methods in Science and Engineering XX (R. Bank, M. Holst, O. B. Widlund, and J. Xu, eds.), Lecture Notes in Computational Science and Engineering, vol. 91, Springer Berlin Heidelberg, 2013, pp. 15–25.

[21] ———, *A BDDC algorithm with deluxe scaling for three-dimensional H(curl) problems*, Comm. Pure Appl. Math (electronically published on April 28, 2015), doi: 10.1002/cpa.21574 (to appear in print).

[22] M. Dryja and O. B. Widlund, *Schwarz methods of Neumann-Neumann type for three-dimensional elliptic finite element problems*, Comm. Pure Appl. Math. **48** (1995), no. 2, 121–155.

[23] C. Farhat, M. Lesoinne, P. LeTallec, K. Pierson, and D. Rixen, *FETI-DP: a dual-primal unified FETI method. I. A faster alternative to the two-level FETI method*, Int. J. Numer. Meth. Engng. **50** (2001), no. 7, 1523–1544.

[24] C. Farhat and F.-X. Roux, *A method of finite element tearing and interconnecting and its parallel solution algorithm*, Int. J. Numer. Meth. Engng. **32** (1991), no. 6, 1205–1227.

[25] H. Federer and W. H. Fleming, *Normal and integral currents*, Ann. of Math. **72** (1960), 458–520.

[26] A. George, *Nested dissection of a regular finite element mesh*, SIAM J. Numer. Anal. **10** (1973), 345–363.

[27] J. R. Gilbert, *Some nested dissection order is nearly optimal*, Inform. Process. Lett. **26** (1988), no. 6, 325–328.

[28] J. R. Gilbert and R. E. Tarjan, *The analysis of a nested dissection algorithm*, Numer. Math. **50** (1987), no. 4, 377–404.

[29] V. Girault, *Incompressible finite element methods for Navier-Stokes equations with nonstandard boundary conditions in* $\mathbf{R}^3$, Math. Comp. **51** (1988), no. 183, 55–74.

[30] V. Girault and P.-A. Raviart, *Finite element methods for Navier-Stokes equations*, Springer Series in Computational Mathematics, vol. 5, Springer-Verlag, Berlin, 1986, Theory and algorithms.

[31] M. R. Hestenes and E. Stiefel, *Methods of conjugate gradients for solving linear systems*, J. Research Nat. Bur. Standards **49** (1952), 409–436.

[32] R. Hiptmair, *Multigrid method for Maxwell's equations*, SIAM J. Numer. Anal. **36** (1999), no. 1, 204–225.

[33] R. Hiptmair and A. Toselli, *Overlapping and multilevel Schwarz methods for vector valued elliptic problems in three dimensions*, Parallel solution of Partial Differential Equations (P. Bjørstad and M. Luskin, eds.), vol. 120 of IMA Vol. Math. Appl., Springer, 2000, pp. 181–208.

[34] R. Hiptmair and J. Xu, *Nodal auxiliary space preconditioning in $H(curl)$ and $H(div)$ spaces*, SIAM J. Numer. Anal. **45** (2007), 2483–2509.

[35] Q. Hu and J. Zou, *A nonoverlapping domain decomposition method for Maxwell's equations in three dimensions.*, SIAM J. Numerical Analysis **41** (2003), no. 5, 1682–1708.

[36] F. John, *Rotation and strain*, Comm. Pure Appl. Math. **14** (1961), 391–413.

[37] P. W. Jones, *Quasiconformal mappings and extendability of functions in Sobolev spaces*, Acta Math. **147** (1981), 71–88.

[38] G. Karypis and V. Kumar, *A fast and high quality multilevel scheme for partitioning irregular graphs*, SIAM J. Sci. Comput. **20** (1998), 359–392.

[39] A. Klawonn, O. Rheinbach, and O. B. Widlund, *An analysis of a FETI-DP algorithm on irregular subdomains in the plane*, SIAM J. Numer. Anal. **46** (2008), 2484–2504.

[40] T. V. Kolev and P. S. Vassilevski, *Parallel auxiliary space AMG for H*(curl) *problems*, J. Comput. Math. **27** (2009), no. 5, 604–623.

[41] I. V. Lashuk and P. S. Vassilevski, *The construction of the coarse de Rham complexes with improved approximation properties*, Comput. Methods Appl. Math. **14** (2014), no. 2, 257–303.

[42] J. H. Lee, *A Balancing Domain Decomposition by Constraints deluxe method for numerically thin Reissner-Mindlin plates approximated with Falk-Tu finite elements*, SIAM J. Numer. Anal. **53** (2015), no. 1, 63–81.

[43] R. Leis, *Initial-boundary value problems in mathematical physics*, B. G. Teubner, Stuttgart; John Wiley & Sons, Ltd., Chichester, 1986.

[44] J. Li and O. B. Widlund, *BDDC Algorithms for incompressible Stokes equations*, SIAM J. Numer. Anal. **44** (2006), 2432–2455.

[45] ———, *FETI-DP, BDDC, and block Cholesky methods*, Int. J. Numer. Meth. Engng. **66** (2006), 250–271.

[46] R. J. Lipton, D. J. Rose, and R. E. Tarjan, *Generalized nested dissection*, SIAM J. Numer. Anal. **16** (1979), no. 2, 346–358.

[47] J. Mandel and C. R. Dohrmann, *Convergence of a Balancing Domain Decomposition by Constraints and energy minimization*, Numer. Lin. Alg. Appl. **10** (2003), 639–659.

[48] J. Mandel, C. R. Dohrmann, and R. Tezaur, *An algebraic theory for primal and dual substructuring methods by constraints*, Appl. Numer. Math. **54** (2005), 167–193.

[49] O. Martio and J. Sarvas, *Injectivity theorems in plane and space*, Ann. Acad. Sci. Fenn. Ser. A I Math. **4** (1979), no. 2, 383–401.

[50] V. G Maz'ja, *Classes of domains and imbedding theorems for functions spaces*, Soviet Math. Dokl. **1** (1960), 882–885.

[51] C. Müller, *Foundations of the mathematical theory of electromagnetic waves*, Revised and enlarged translation from the German. Die Grundlehren der mathematischen Wissenschaften, Band 155, Springer-Verlag, New York-Heidelberg, 1969.

[52] J.-C. Nédeléc, *Mixed finite elements in* $\mathbb{R}^3$, Numer. Math. **35** (1980), 315–341.

[53] D.-S. Oh, *An overlapping Schwarz algorithm for Raviart-Thomas vector fields with discontinuous coefficients*, SIAM J. Numer. Anal. **51** (2013), 297–321.

[54] D.-S. Oh, O. B. Widlund, and C. R. Dohrmann, *A BDDC algorithm for Raviart-Thomas vector fields*, Tech. Report TR2013-951, Courant Institute, NYU, 2013.

[55] D. O'Leary and O. B. Widlund, *Capacitance matrix methods for the Helmholtz equation on general three-dimensional regions*, Math. Comp. **33** (1979), 849–879.

[56] A. Quarteroni and A. Valli, *Domain decomposition methods for partial differential equations*, Numerical mathematics and scientific computation, Clarendon Press, 1999.

[57] ———, *Numerical approximation of partial differential equations*, Springer Ser. Comput. Math., vol. 23, Springer, 2008.

[58] Y. Saad, *Iterative methods for sparse linear systems*, 2nd ed., SIAM, 2003.

[59] Y. Saad and M. H. Schultz, *GMRES: a Generalized Minimal Residual Algorithm for solving nonsymmetric linear systems*, SIAM J. Sci. and Stat. Comput. **7(3)** (1986), 856–869.

[60] H. A. Schwarz, *Über einen Grenzübergang durch alternierendes Verfahren, Vierteljahrsschrift der Naturforschenden Gesellschaft*, in Zürich, 1870, pp. 272–286.

[61] B. F. Smith, P. E. Bjørstad, and W. D. Gropp, *Domain decomposition: Parallel multilevel methods for elliptic partial differential equations*, Cambridge University Press, New York, NY, USA, 1996.

[62] A. Toselli, *Overlapping Schwarz methods for Maxwell's equations in three dimensions*, Numer. Math. **86** (2000), 733–752.

[63] ———, *Dual-primal FETI algorithms for edge finite-element approximations in 3D*, IMA J. Numer. Anal. **26** (2006), 96–130.

[64] A. Toselli and A. Klawonn, *A FETI domain decomposicion method for edge element approximations in two dimensions with discontinuous coefficients*, SIAM J. Numer. Anal. **39** (2002), 932–956.

[65] A. Toselli and X. Vasseur, *Robust and efficient FETI domain decomposition algorithms for edge element approximations*, COMPEL **24** (2005), 396–407.

[66] A. Toselli and O. B. Widlund, *Domain decomposition methods-algorithms and theory*, Springer Ser. Comput. Math., vol. 34, Springer, 2005.

[67] A. Toselli, O. B. Widlund, and B. Wohlmuth, *An iterative substructuring method for Maxwell's equations in two dimensions*, Math. Comp. **70** (2001), 935–949.

[68] L. N. Trefethen and D. Bau, *Numerical linear algebra*, SIAM, 1997.

[69] O. B. Widlund, *Accommodating irregular subdomains in domain decomposition theory*, Domain Decomposition Methods in Science and Engineering XVIII (M. Bercovier, M. J. Gander, R. Kornhuber, and O. B. Widlund, eds.), Lecture Notes in Computational Science and Engineering, vol. 70, Springer-Verlag, 2009, pp. 87–98.

[70] B. Wohlmuth, A. Toselli, and O. B. Widlund, *An iterative substructuring method for Raviart–Thomas vector fields in three dimensions*, SIAM J. Numer. Anal. **37** (2000), 1657–1676.

[71] J. Xu and Y. Zhu, *Robust Preconditioner for H(curl) Interface Problems*, Domain Decomposition Methods in Science and Engineering XIX (Yunqing Huang, Ralf Kornhuber, Olof Widlund, and Jinchao Xu, eds.), Lecture Notes in Computational Science and Engineering, vol. 78, Springer Berlin Heidelberg, 2011, pp. 173–180.